Λ POLARIZATION AT 90° IN $K^{+}\Lambda$ PHOTOPRODUCTION

Thesis by

Donald Eugene Groom

In Partial Fulfillment of the Requirements

For the Degree of

Doctor of Philosophy

California Institute of Technology

Pasadena, California

1965

(Submitted 25 May, 1965)

ACKNOWLEDGEMENTS

The debugging and data-collecting stages of this experiment were supervised by Prof. Robert L. Walker. His comments have been valuable, and working under him has been a rewarding and enjoyable experience.

The experiment was done in close collaboration with J. Howard Marshall. Except for such obvious items as power supplies and scalers, all of the electronics used were designed and built either by him or under his supervision. This was done with such thoroughness and care that we were essentially free of such traditional bandersnatches as non-zero gate pedestals, long veto time resolution in coincidence circuits, nonlinearities, and electronic failures.

The suggestion that we use a counter telescope as a kaon detector originated with Prof. A. V. Tollestrup. Its modification to the pulse height correlation scheme employed was suggested by Prof. M. L. Sands, under whose supervision the work was started. The debt to these people is obvious.

M. J. Hauser spent many hours assisting in the data-taking and other necessary tasks associated with the experiment.

For financial support, the author is indebted to the National Science Foundation, the Atomic Energy Commission, the Eastman Kodak Corporation, and the California Institute of Technology.

ABSTRACT

The polarization of Λ hyperons in the reaction $\gamma + p \rightarrow K^+ + \Lambda$ has been measured, using the Caltech synchrotron. The measurements were made at 90° in the c.m. system, at laboratory photon energies of 1100 MeV, 1200 MeV, and 1300 MeV. Protons from the asymmetric decay of the Λ were detected by counters placed symmetrically above and below the plane defined by the photon beam and the mean kaon momentum. Kaons were detected in a 16 to 18 counter range telescope. If preliminary logic was satisfied, all pulse heights from counters in the telescope were digitized and recorded on paper tape, along with relevant coincidence information. A detailed fit to the Bragg curve was made in a digital computer to establish the kaon identification. The results were $P_\Lambda = +0.34 \pm 0.09$ at 1100 MeV, $+0.30 \pm 0.07$ at 1200 MeV, and $+0.08 \pm 0.07$ at 1300 MeV, where P_Λ is measured in the $\hat{k}_\gamma \times \hat{p}_\Lambda$ direction. These data, together with those of other groups, add support to the suggestion that the effects of the third πN resonance are evident in $K\Lambda$ photoproduction.

TABLE OF CONTENTS

LIST OF FIGURES

LIST OF TABLES

To Sisyphus

1 INTRODUCTION

This thesis reports measurements of the Λ hyperon polarization in the reaction

$$\gamma + p \rightarrow K^+ + \Lambda$$

at incident photon laboratory energies of 1100, 1200, and 1300 Mev and a center of mass angle of 90^o.

Over the past several years experimenters have measured the differential cross section for this reaction from its threshold to about 300 MeV above threshold[1-5]. In contrast to the violent behavior of the cross section for other reactions such as pion photoproduction, the results are surprisingly simple. The total cross section at first rises linearly with the kaon center of mass momentum, then flattens to remain constant at 2.2 μbarns between laboratory photon energies of 1000 MeV and 1200 MeV[7]. The angular distributions are isotropic near threshold, then peak more and more forward with increasing energy. They are easily fitted by quadratics in $\cos\theta$, to the frustration of all attempts to find one kaon exchange terms, $F_{5/2}$ resonances, etc.[5]

However, the very fact that several partial waves are present (at least s and p waves) suggests that the Λ hyperons produced in association with the kaons may be polarized. Measurement of the polarization would provide one more handle in the understanding of the reaction. It was with this goal in mind that this experiment was designed.

In the center of mass system, the only independent kinematic variables available for the description of the reaction are the incoming and outgoing momenta. (We restrict ourselves to unpolarized beam and target, so that effects due to spins will cancel.) Any possible parity-conserving theory of the interaction must require that the polarization, an axial vector, be constructed of these variables. The only available candidate is their cross product, so that

$$P_\Lambda \propto \hat{k}_\gamma \times \hat{p}_\Lambda \quad .$$

Thus, the Λ polarization will be normal to the production plane and it will depend upon the center of mass production angle at least as the sine of the angle.

An equally familiar result is that the Λ decay

$$\Lambda \rightarrow \pi^- + p \qquad (\tau = 0.262 \text{ ns})$$

does not conserve parity and leads to the decay proton distribution

$$N(\theta)\, d\Omega = \frac{d\Omega}{4\pi} (1 + \alpha P_\Lambda \cos\theta) \quad .$$

Here θ is the angle between the proton momentum and the Λ polarization direction, in our case the $\hat{k}_\gamma \times \hat{p}_\Lambda$ direction.

On the basis of these considerations, the experiment was designed to measure the up-down asymmetry of the Λ decay protons, relative to the production plane defined by the incident photon beam and the outgoing kaon direction. The experimental setup used to do this is illustrated in Figure 1. A liquid hydrogen target was illuminated

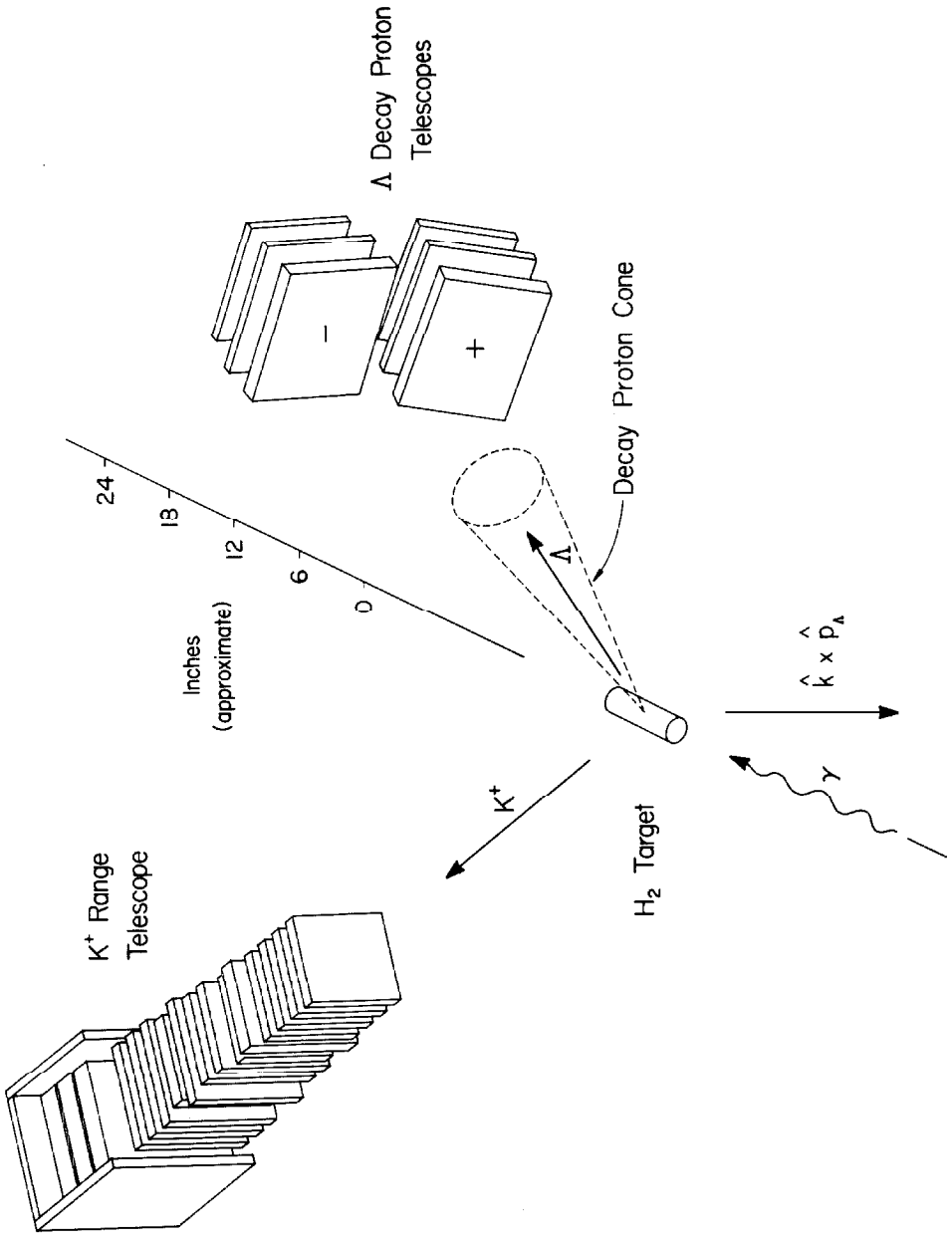

FIGURE 1. Perspective View of the Apparatus.

by a bremsstrahlung beam from the Caltech synchrotron. Kaons produced in the target were detected by a range telescope. The Λ decay protons were detected in coincidence with the kaons by simple counter telescopes placed symmetrically above and below the production plane.

Low counting rates placed a severe restriction on the number of points at which the measurement could be made. We chose to make measurements at 90° in the c.m. system, at laboratory photon angles of 1100, 1200, and 1300 MeV.

Although not of central importance in the polarization measurements, the kaon detection scheme was by far the most difficult problem encountered. It is discussed as a separate section of this thesis. Treating the telescope as a black box which detects kaons, the polarization measurements are then discussed. Detailed discussions of technicalities which are essential but less in the main stream of the thesis are relegated to appendices.

This experiment was done in close collaboration with J. Howard Marshall, and strict division of the work into two separate parts has not always been possible. This is particularly apparent in the appendices. For instance, although accidental monitoring procedures are quite important to this thesis, they are left to his. Similarly, a discussion of decay particle corrections is included here, although the results are chiefly of relevance to his cross section measurements.

2 THE K' RANGE TELESCOPE

2.1 Introduction

The identification of photoproduced K mesons has always been a difficult task. Kaon production rates are several orders of magnitude below those of potentially confusing events, and absolute rates in the typical experiment are also quite low. In 1960, when the design of this experiment was begun, a typical kaon counting rate in a magnetic spectrometer was about 6 per hour[2]. We were interested in measuring the Λ polarization, and detection of the Λ decay proton meant losing another factor of about 3 in the counting rate. For an error of ± 0.07 in the polarization, 1000 events were needed.

On the other hand, an accurate cross section determination was not important for this measurement; we were willing to accept broad resolution in angle and energy and severe, poorly known corrections such as those due to multiple scattering and nuclear interactions, if in exchange we could obtain an order of magnitude higher counting rate. These considerations led to our use of a generalization of the conventional range telescope.

2.2 Approach

An example of an elementary range telescope, consisting of three scintillation counters and two absorbers, is shown below. Counters 1 and 2 are in coincidence and counter 3 is in veto, thus defining a sample of particles whose range is between R and $R + \delta R$. Particles with different masses have different mean energy losses in 1,

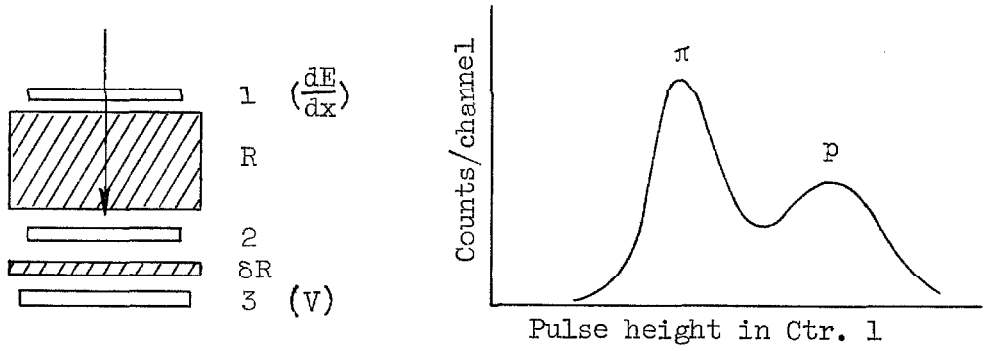

and if the peaks in the pulse height distribution are sufficiently distinct, pulse height discrimination can be used to select a pure particle sample. With increasing range, the peaks in counter 1 become progressively less distinct. If the telescope is to remain effective in particle selection, it must be made more sophisticated.

In our modification of this scheme, most of the absorber was replaced by plastic scintillators, so that detailed pulse height information was available over the particle's entire trajectory. These pulse heights were digitized and recorded for all interesting events. Later, a computer could fit them in some maximum likelihood sense to identify the particle.

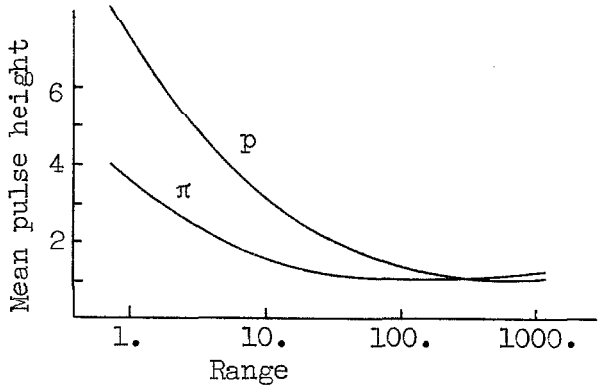

The kind of data available is illustrated in Figure 2. A particle stopped in a counter; from its pulse height in this counter and knowledge of the matter distribution in the telescope, its residual

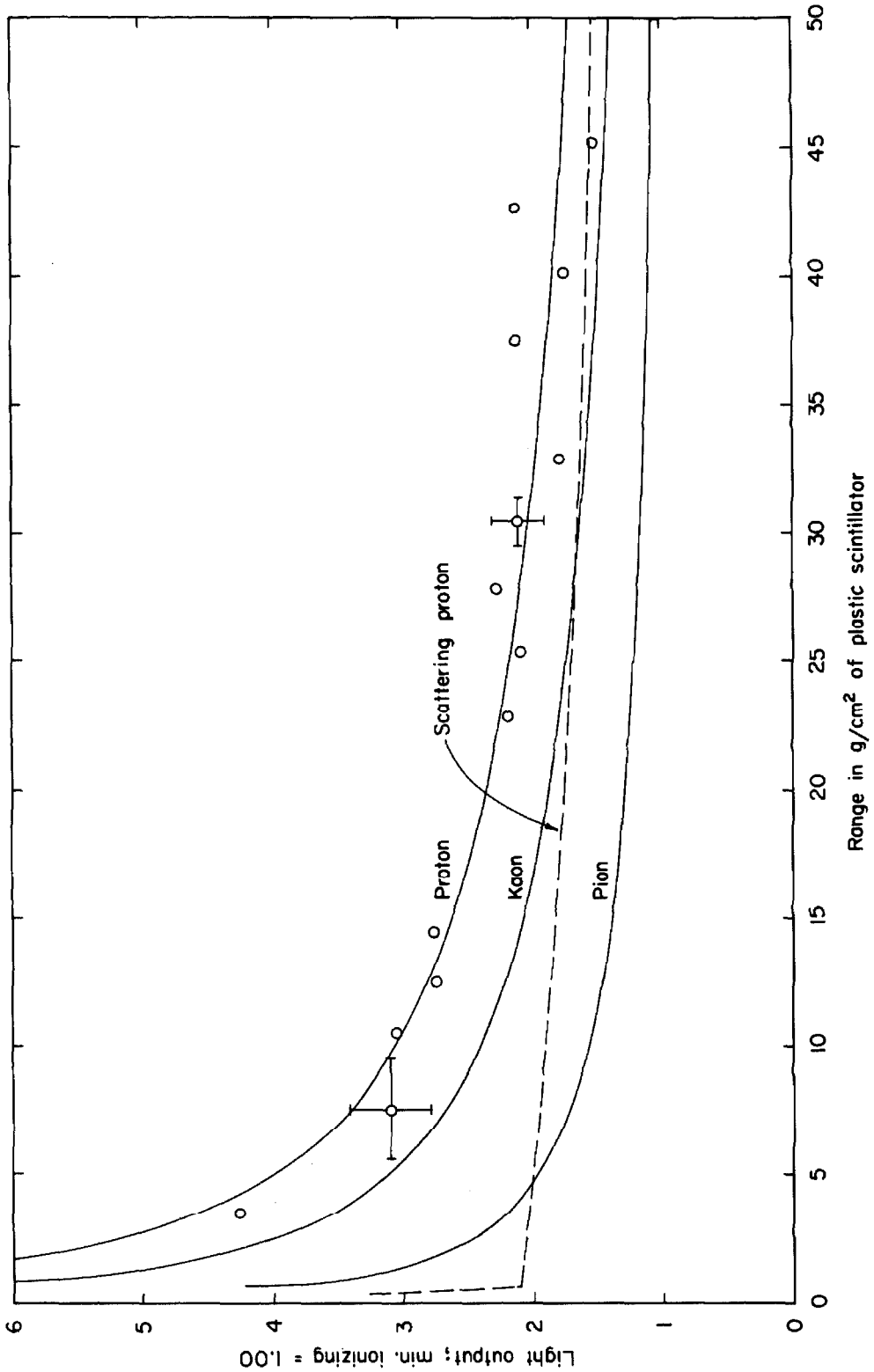

FIGURE 2. A Stopping Proton Event.

range as it traversed each other counter could be calculated. Pulse heights in these counters might then be compared with those expected for particles of various masses, as shown. If, for example, electronic bias requirements had been set in the first few counters to accept all kaons, this event could conceivably have been accepted. On the other hand, a computer, dealing with all of the information, would have no difficulty assigning it probable identification as a proton.

2.3 Apparatus

The telescope was designed to detect kaons produced at photon energies of 1100, 1200, and 1300 MeV and at a center of mass angle of 90°. The kinematics relevant to these conditions are given in Table 1.

A drawing of the telescope appears as Figure 3. In addition to the scintillation counters already mentioned, two lucite Čerenkov counters were inserted to help veto the high flux of electrons, and to a lesser extent that of pions, which passed through the system. Enough polyethylene was added to trim the range to the desired value. Particles were constrained to stop in counters δR1, δR2, and δR3. The side counters, L and R, detected a K decay particle with about 30% probability. This was not required electronically, but could be used by the computer to select an especially pure kaon sample.

At the rear of the system were two additional counters, used for calibration purposes. The logic could be modified so that E and

TABLE 1

Laboratory System Kinematics at $\theta_{c.m.} = 90^{\circ}$

Photon Energy	1100 MeV	1200 MeV	1300 MeV
θ_K	37.39°	40.17°	41.48°
T_K	179.1 MeV	233.8 MeV	288.1 MeV
$\frac{dk}{dT_K}$	1.196	1.437	1.609
θ_Λ	20.64°	23.53°	25.40°
T_Λ	249.9 MeV	295.1 MeV	340.9 MeV
ξ_m	8.71°	7.94°	7.31°
η_m	180.0°	64.9°	58.7°

K = Photon energy.

θ = Angle between momentum of particle and momentum of photon.

T = Kinetic energy of particle.

ξ_m = Maximum angle between Λ momentum and its decay proton momentum.

η_m = Maximum angle between Λ momentum and its decay pion momentum.

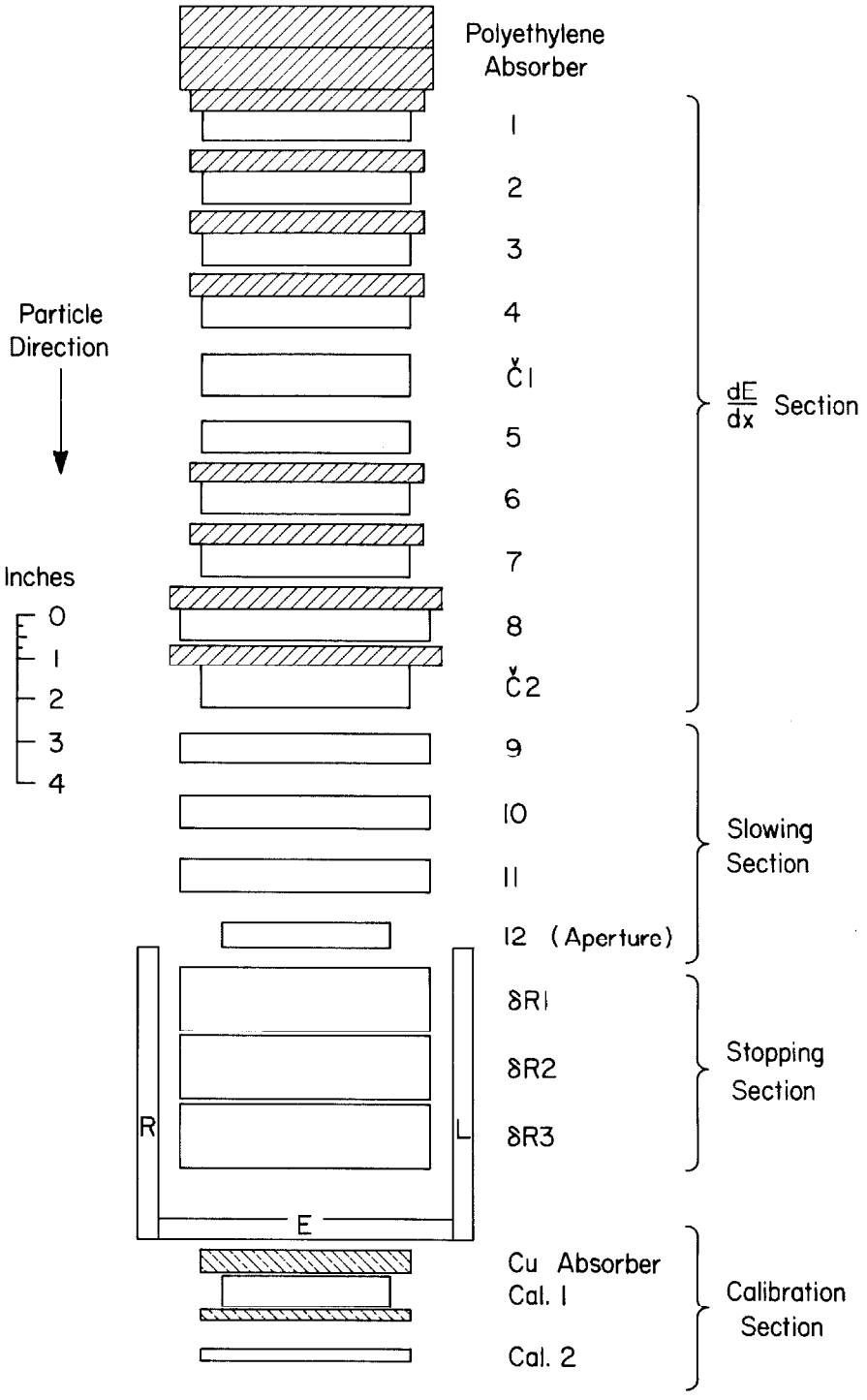

FIGURE 3. The K^+ Range Telescope.

Cal. 1 were required, while Cal. 2 was in veto. The absorbers were chosen so that well defined peaks produced by particles of known range were then produced in all counters in the K telescope, and a pulse height calibration was possible. L and R were moved into the telescope for the calibration runs.

The counter immediately in front of the stopping section was the smallest in the system, and thus defined the acceptance aperture. It was 4" square, and subtended a solid angle of 0.007 sr. as seen from the liquid hydrogen target. The target was 6" long, in order that at the planned laboratory running angles of 35^{o} - 40^{o} it would have a projected size equal to that of the aperture. This resulted in a nearly triangular angular resolution function whose full width at half maximum was 4.2^{o}. Other counters in the system were made large enough that multiple scattering did not result in appreciable particle loss, although the scattering did somewhat smear the angular distribution.

The thickness of the stopping section was chosen to permit an acceptance band of 35 MeV in the kaon kinetic energy. The spread of photon energies introduced by this range spread was equal to that introduced by the angular aperture. The energy band, of course, could have been subdivided further in the analysis, but this was not done. The photon energy resolution functions are given in Figure 4[8]. The increase in width with energy reflects the increase in the derivative of photon energy with respect to both kaon angle and kaon energy.

The telescope configuration shown in Figure 3 is for the

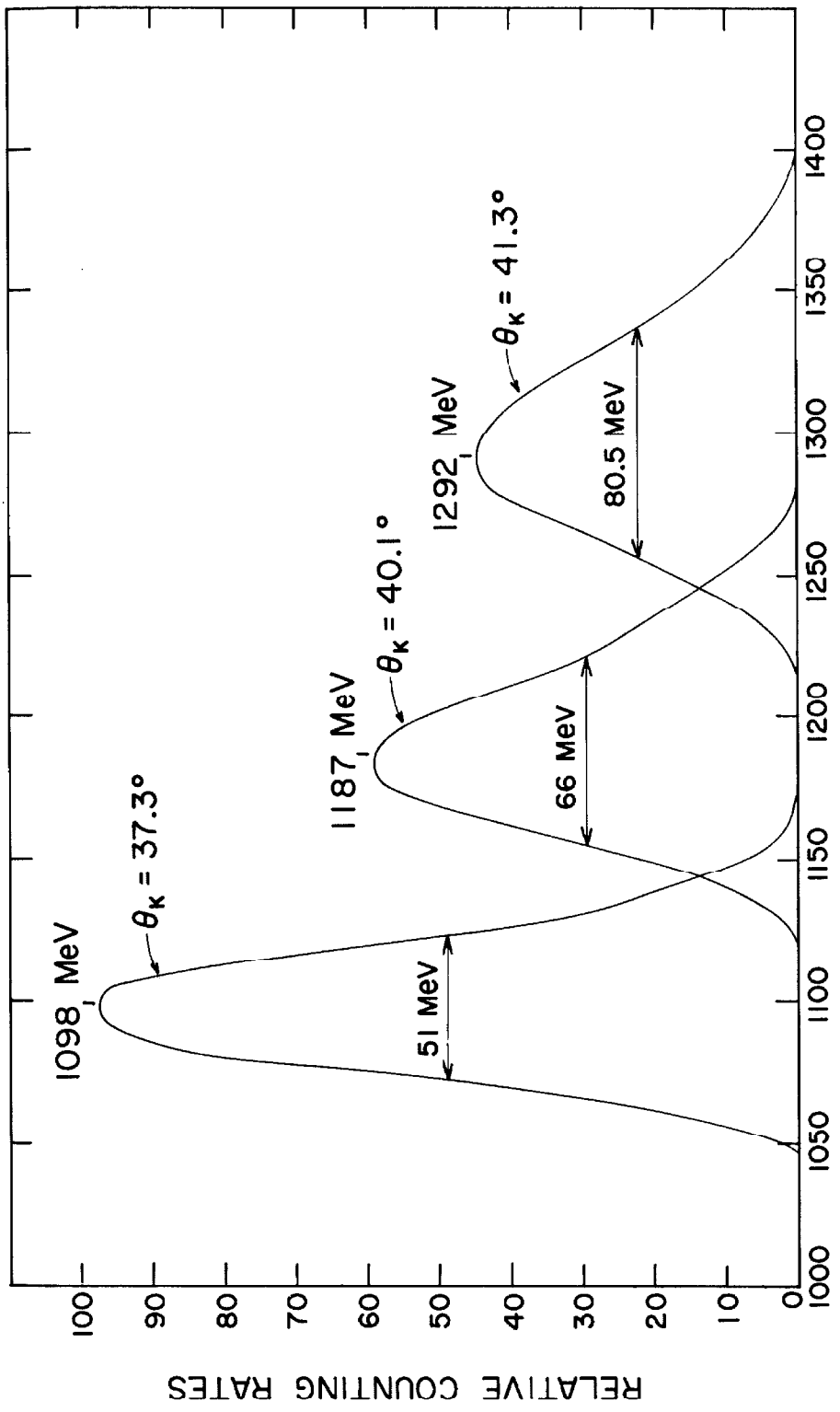

FIGURE 4. Photon Energy Resolution.

1200 MeV point. At 1300 MeV, more absorber was added. At 1100 MeV, Č1 was placed in front of counter 1, counters 9 and 10 were removed, and absorber changes were made.

The Λ decay proton was detected in coincidence with the kaon by one of two counter telescopes which were mounted symmetrically above and below the plane defined by the beam line and center of the K^+ telescope aperture. Each consisted of a lucite Čerenkov counter followed by two plastic scintillators. The second of these was smaller and hence defined the aperture, which subtended a solid angle of about 0.025 sr. centered at 21° to 25° from the beam line.

All counters in the system were observed by single RCA 6810-A phototubes.

The relative orientation of the counter arrays may be seen in Figures 1 and 5.

2.4 Electronic Selection and Data Recording

Standard electronic techniques[9] involving a sequence of fast and slow logic were used to eliminate all events which were not kaon candidates.

The fast preselection scheme is illustrated in Figure 5. In the telescope, the front counter and the aperture counter were in a 5 ns. coincidence which could be vetoed by pulses from either of the Čerenkov counters between them. The output signal (the "gate" signal) was used to open 35 ns. linear gates on all scintillators in the telescope.

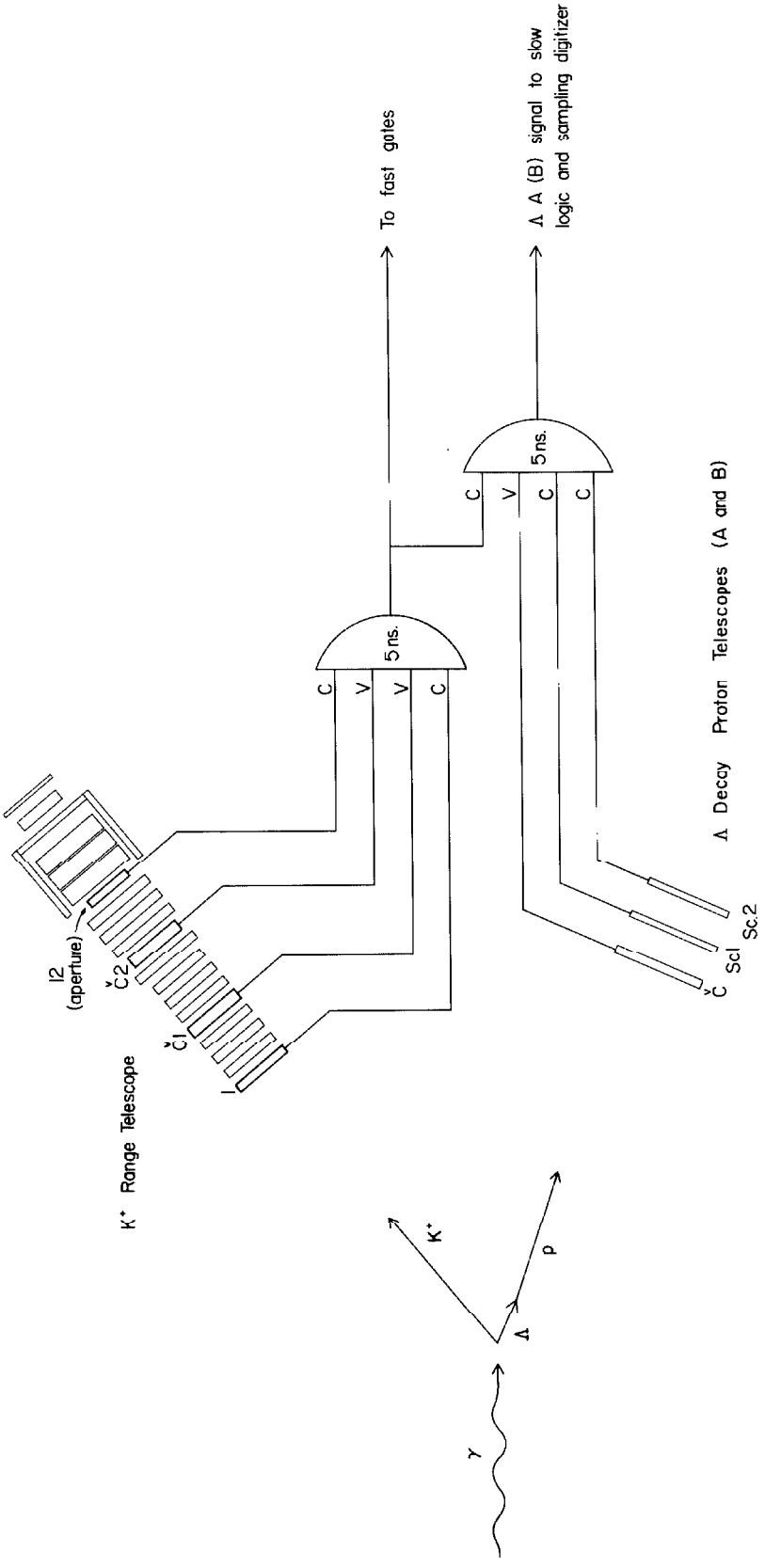

FIGURE 5. Fast Preselection.

A signal was also formed when, in coincidence with the gate signal, a particle went through a Λ decay proton telescope without triggering its Čerenkov counter. This signal, signifying the direction of the Λ decay proton, was used by the slow logic and was recorded for later use by the computer.

In addition, several other delayed fast coincidences, not shown, were formed to monitor various accidental rates.

The slow logic is sketched in Figure 6. Discriminators were used to set pulse height "windows" on the first 8 scintillators. Typically, limits were set about 35% away from the extremes of the expected pulse height spread. At least a small pulse was required of δR1 to ensure the particle's entry in the stopping section, and E was in veto. A signal indicating a coincidence in at least one of the two Λ decay proton telescopes was also required.

As already has been indicated, the logic could be changed for calibration purposes. The signal $(\delta R1)(E)(Cal.1)(\overline{Cal.2})$ could be required in place of $(\Lambda A \text{ or } \Lambda B)(\overline{E})$. The windows on the front section were set wide enough to accommodate protons satisfying this logic, so that the change only meant changing several switches.

When the slow logic was satisfied, a 25 dimensional pulse height analyzer[10] was triggered. Pulses, accepted in parallel, were stored in analog form. They were then sequentially digitized and stored in a digital memory. The ΛA and ΛB pulses also set certain bits of memory. The event could then be read out either onto paper tape or directly to the computer. The direct computer

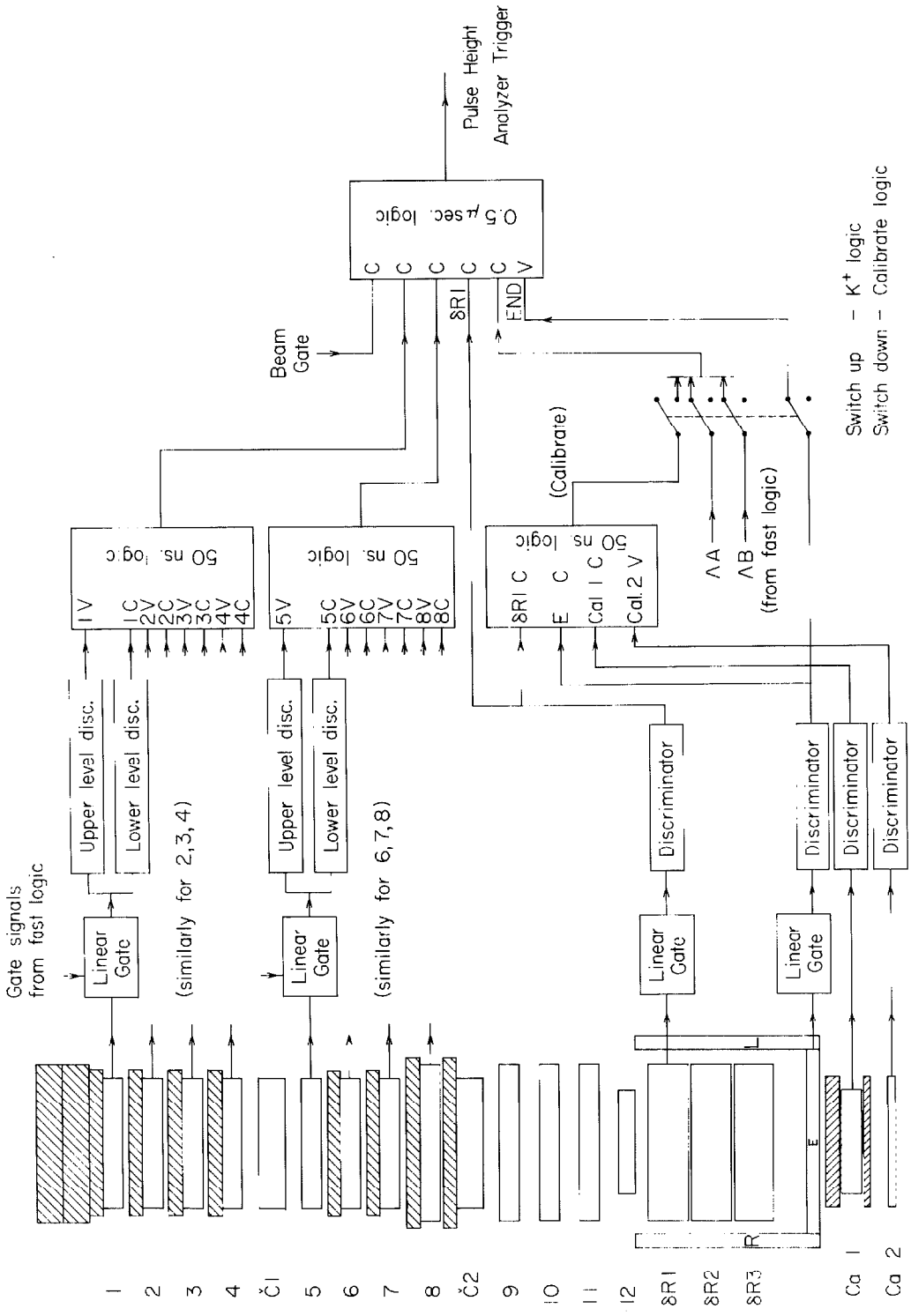

FIGURE 6. Slow Logic.

link, although occasionally used, did not turn out to be very useful for this experiment. In either case, a Burroughs 220 computer was used in the subsequent analysis.

The overall integral linearity of the system was ± 1%. Pulses were digitized to two decimal digits. The data could be punched in the 1 sec. interval between beam dumps, but we were limited to one event per dump. This introduced dead time corrections of about 6% in the K rates.

Examples of the counting rates experienced at the operating points are given in Table 2. Of the events which satisfy certain liberal computer-imposed kaon criteria, a fraction $\underline{b}$ are not kaons. Quantities related to this fraction are also listed in the table, and will be discussed later.

The $\Lambda A + \Lambda B$ rate is consistent with the expected accidental rate. Thus the fraction of such events which result in pulse height analyzer triggers is also the fraction of gated events satisfying the slow logic. As will become apparent, the background rate of the experiment followed the $\Lambda A + \Lambda B$ rate. To make the experiment work at all, it was necessary to expend a great deal of effort making this coincidence as "clean" as possible. As much absorber as could be tolerated was placed in front of the Λ decay proton telescopes. The coincidence circuit input biases were set as high as was possible without reducing the proton efficiency, and pulses were "clipped" at the phototubes so that the time resolution could be optimized.

The $\check{C}1$ and $\check{C}2$ veto requirement effectively halved the gate

TABLE 2

Representative Counting Rates

Photon Energy	1100 MeV	1200 MeV	1300 MeV
Gates/BIP (a)	1125.	460.	204.
$(\Lambda A + \Lambda B)$/BIP	11.01	6.16	2.46
Pulse height analyzer Triggers/BIP	1.14	1.04	0.35
K^+/BIP (b)	.0493	.0427	.0423
b	0.378	0.164	0.063
Gates/b	2980.	2810.	3130.
$(\Lambda A + \Lambda B)$/b	29.3	37.5	38.9

(a) 1 BIP $\approx 1.2 \cdot 10^{13}$ MeV of bremsstrahlung beam. Conditions during the experiment were such that 1 BIP was accumulated in approximately 1 sec. of beam time, or 10 sec. of real time.

(b) Observed rate. Without the ΛA or ΛB requirement, it would have been about three times larger.

rate. Thus, for the 1100 MeV point, about 40,000 real coincidences occurred between the front and aperture counter for each kaon. The Čerenkov veto reduced this to 20,000, and the Λ decay proton requirement reduced it further to 200 per kaon. Of these, 20 events satisfied the slow logic and were recorded. To provide the remaining factor of 100 or 200 which would reduce this to an acceptable background was the chore of the computer.

2.5 Pulse Height Distribution in a Single Counter

Let $f(L, L_o)$ be the probability frequency function of pulse heights observed in a plastic scintillator for an incident beam of particles of specified energy and mass. Here L is the observed pulse height, and L_o is the mean of the distribution. The mean depends upon the range R and mass m of the particles. For a traversing particle, in fact, it is a function only of R/m.

The mean light output is nearly proportional to the mean energy loss except at high ionization. In the analysis of this experiment, we have used the approximations[11]

$$\frac{dL}{dx} = \frac{C}{a} \ln \left(1 + a \frac{dE}{dx}\right)$$

$$a \simeq 0.025 \ (\mathrm{MeV/g/cm^2})^{-1}$$

to correct for the known nonlinearity. Data collected in the course of this experiment suggests that a value of 0.007 to 0.015 for a would have been more appropriate, but this turns out to be a minor consideration.

If particles of range R are incident on a counter of thickness t, we have

$$L_o = \int_b^R \frac{dL}{dx}\, dx \qquad (b = (R - t) \text{ or } 0, \text{ whichever is greater})$$

and in the special case $R >> t$,

$$L_o = \left.\frac{dL}{dx}\right|_{R-t/2} \cdot t$$

For sufficiently energetic particles, the function $f(L, L_o)$ could be satisfactorily represented by folding together two frequency functions:

a) The Symon function[12], which takes into account energy loss fluctuations in the scintillator.

b) An approximately normal function which takes into account electron statistics in the photomultiplier observing the scintillator.

For counters near the front of the system, the resulting distribution had a slight positive skewness and a standard deviation of 8 - 10%, depending on the position and the particular phototube.

For more highly ionizing particles, both of the above functions became narrow and smaller effects, such as phototube gain instability and the sensitivity of L_o to the particle's position in the counter, became more important. The resultant dependence of the resolution upon L_o is indicated in Figure 7. These results must be regarded as approximate, however, since all contributions varied from

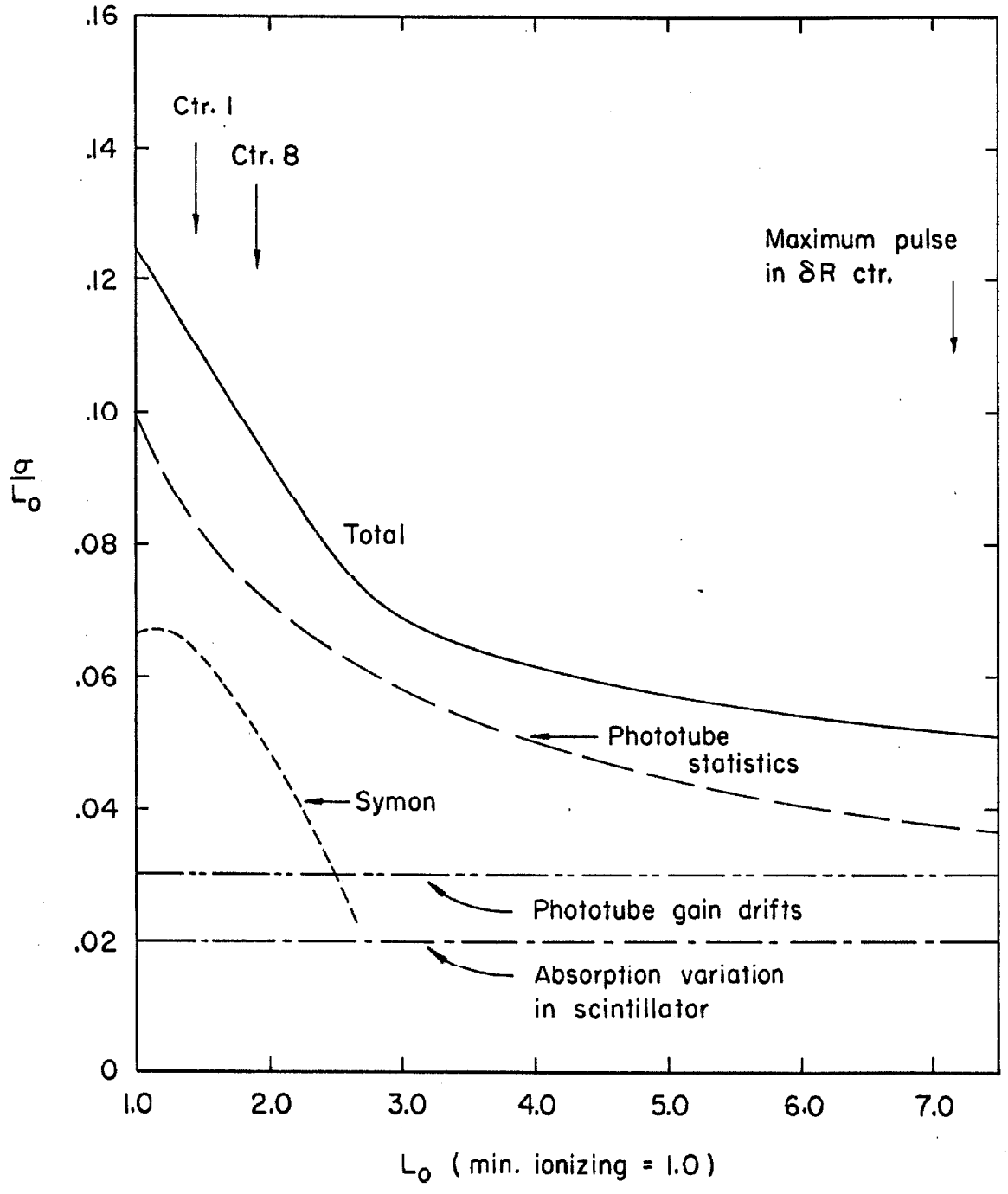

FIGURE 7. Light Output Dependence of Counter Resolution.

counter to counter. For instance, calibration data indicated phototube drifts of the order of 3% during times in which data were taken, but individuals in the sample varied a factor of two about this figure.

2.6 The Analysis Problem

Since the distribution functions are relatively well known, we might set up the identification problem by the standard likelihood techniques. We may write

$$w(R, m) = \log \mathfrak{L} = \sum_{i=1}^{n} \log f_i(L_i, L_{io})$$

where the subscripts refer to the i^{th} counter, and w is the logarithm of the likelihood function $\mathfrak{L}$. We may find R^* and m^* such that w is maximized, or find $w(R_j^*, m_j)$ for a given set of masses m_j to see which is the most likely, or set a bias on $w(R_K^*, m_K)$ to exclude events due to particles whose mass is not m_K.

We have examined these approaches and tried several in detail. They have one feature in common: None is able to cope with the data.

The reason is to be found in the data. This technique can easily eliminate the bulk of the normal, stopping protons and pions which constitute most of the data left to the computer. But for the most part, this has already been done by the electronics, which has admitted exactly those events which by scattering, charge exchange, or other interaction look very much like kaons.

Consider, for example, a proton whose range would have been

twice that of the expected kaon, but which by scattering in $\delta R3$ avoids being vetoed by E. Its mean light output as a function of apparent range is indicated in Figure 2. Since the L_{io} depend only upon R_i/m, the proton is indistinguishable from the expected kaon as it passes through the front counters. The incorrect slope of L_o with range is lost in the width of the f_i.

The elimination of such an event is further impeded by the fact that the normal kaon decays. This hopelessly clouds interpretation of the pulses from the δR counters themselves, which would otherwise be the richest in information.

Information does exist, however. An event such as this scattering proton produces very low pulse heights in the last few counters before entering the stopping section. And, if the scattering took place after $\delta R1$, the pulse in $\delta R1$ would also be anomalously low. A stopped kaon could not decay in such a way as to produce this anomaly.

So the problem reduces to questions of weighting and of permitting various possibilities. Counters near the stopping section must be weighted more heavily than those near the front. If the decay particle from a kaon decaying in $\delta R2$ entered $\delta R1$, the $\delta R1$ pulse should not be used; otherwise, it should.

These considerations led to the development of an empirical method rather hand-tailored to the problem. The telescope was somewhat arbitrarily divided into two parts for purposes of analysis: a front $(\frac{dE}{dx})$ section, and a rear section in which particles slowed

and stopped. Data from the rear section were used only to establish a range and that the event was a reasonable stopping, decaying kaon. Then, given this range, a fit of statistical significance could be made to the $\frac{dE}{dx}$ section.

Since the Burroughs 220 is a fairly slow computer, a premium was placed on the simplicity of the forms used. The most serious approximation made was that the widths of the f_i were proportional to the L_{io}. For the $\frac{dE}{dx}$ section, the variation of the width was lost within its uncertainty. For the slowing and stopping sections, the approximation had the effect of changing certain weightings which were not well known in any case.

2.7 Rear Section Fit

Under the assumption that an event was a stopping kaon, a penetration depth δ into the stopping section was computed under several different hypotheses, as follows:

a) The kaon decayed after the linear gate had closed so that no decay particle was observed. In this case, an upper limit δ_U could be set on the penetration depth by assuming that all of the pulse in the last counter to show a pulse was due to the stopping kaon. The range so calculated in this counter was constrained to be less than the counter thickness.

b) The maximum possible decay particle contribution was present. In this case the contribution was subtracted, in

one or two counters as was appropriate, before computing δ as in a). This established a lower limit δ_L for the penetration depth.

c) A sequence of counters near the end of the particle's range were not affected by the decay products, which permitted us to "extrapolate" a penetration depth.

From the light output in the i^{th} counter, a penetration depth $\delta(L_i)$ may be calculated. The uncertainty ΔR in the determination is simply related to the width σ of the pulse height distribution:

$$\Delta R = \frac{\sigma}{\frac{d}{dR} L_o}$$

We may take $L_o \sim \frac{dL}{dx} \cdot t$. Since $\frac{d^2L}{dx^2}$ changes rapidly with x, we may approximate $\sigma \propto L_o$. Then

$$(\Delta R)^{-1} \propto \zeta = \frac{d}{dx} (\log \frac{dL}{dx})$$

Now, using the data from the slowing section and n counters of the stopping section, we may define the penetration depth as the weighted average

$$\delta_n = \frac{\sum \zeta_i^2 \delta(L_i)}{\sum \zeta_i^2}$$

where the measured pulse height L_i is taken as the best estimator of L_{io}. The function ζ varies extremely rapidly with R, so that the final 3 or 4 pulse heights

effectively determine δ_n.

This process yielded a sequence of estimates

$$\delta_o, \delta_1, \ldots, \delta_j$$

where the j^{th} counter was the last to show a pulse. In addition, any δ_k not satisfying

$$\delta_L < \delta_k < \delta_U$$

was neglected.

Some of the δ's in the sequence $\delta_L, \delta_o, \ldots, \delta_U$ were seriously in error due to the effect of decay particles, but the sequence also contained good estimates.

A quantity U_K was then computed for the event:

$$U_j = \frac{1}{N}\left[\sum_{\substack{\text{Slowing}\\ \text{Section}}} \left(\frac{L_i - L_{io}^{(j)}}{0.1\, L_{io}^{(j)}}\right)^2 + \sum_{\substack{\text{Stopping}\\ \text{Section}}} \begin{cases} \left(\dfrac{L_i - L_{io}^{(j)}}{0.1\, L_{io}^{(j)}}\right)^2 & \text{if } L_i < L_{io}^{(j)} \\ 0 & \text{if } L_i > L_{io}^{(j)} \end{cases}\right]$$

U_K = Smallest of the U_j .

Here $L_{io}^{(j)}$ is the mean light output expected in the i^{th} counter under the penetration depth hypothesis δ_j, and N is the number of pulse heights used. In writing $\sigma = 0.1\, L_o$, we have again used the approximation discussed in the previous section.

The selection procedure thus discarded the worst estimates of δ. It should be emphasized that there is nothing special about

this particular procedure; indeed, a more reasonable approach might be to search for a minimum in $U(\delta)$ for $\delta_L < \delta < \delta_U$. The procedure used developed historically, and since it was satisfactory the cumbersome job of rewriting the programs for the above approach was not undertaken.

The "free" admission of pulses for which $L > L_o$ in the stopping section effectively permitted K decay products to exist. If these products entered the slowing section, the event was presumed lost. Corrections to the counting rate due to this and other effects of the decay products have been calculated by a Monte Carlo method.

U_K is similar to χ^2 divided by the number of degrees of freedom. A more detailed statement about its distribution must be made empirically. The experimental distribution is shown in Figure 8a. The entire telescope was also mocked up in a Monte Carlo calculation; the spectrum of U_K obtained by this method is given in Figure 8b. The width of the Monte Carlo spectrum is presumably wider due to a slightly pessimistic estimate of counter resolution.

In the Monte Carlo case, $3.0 > U_K > 2.0$ for 0.3% of the events. For no event was U_K greater than 3.0. A sampling of the 1200 MeV data placed (2.6 ± 1.0)% of the events showing a side counter pulse in this region. They are part of a long, featureless "tail" such as that evident in Figure 8a. Their distribution will be more apparent after the discussion of the front section fits. Since they were fit by no stopping particle hypothesis, we feel confident in identifying them

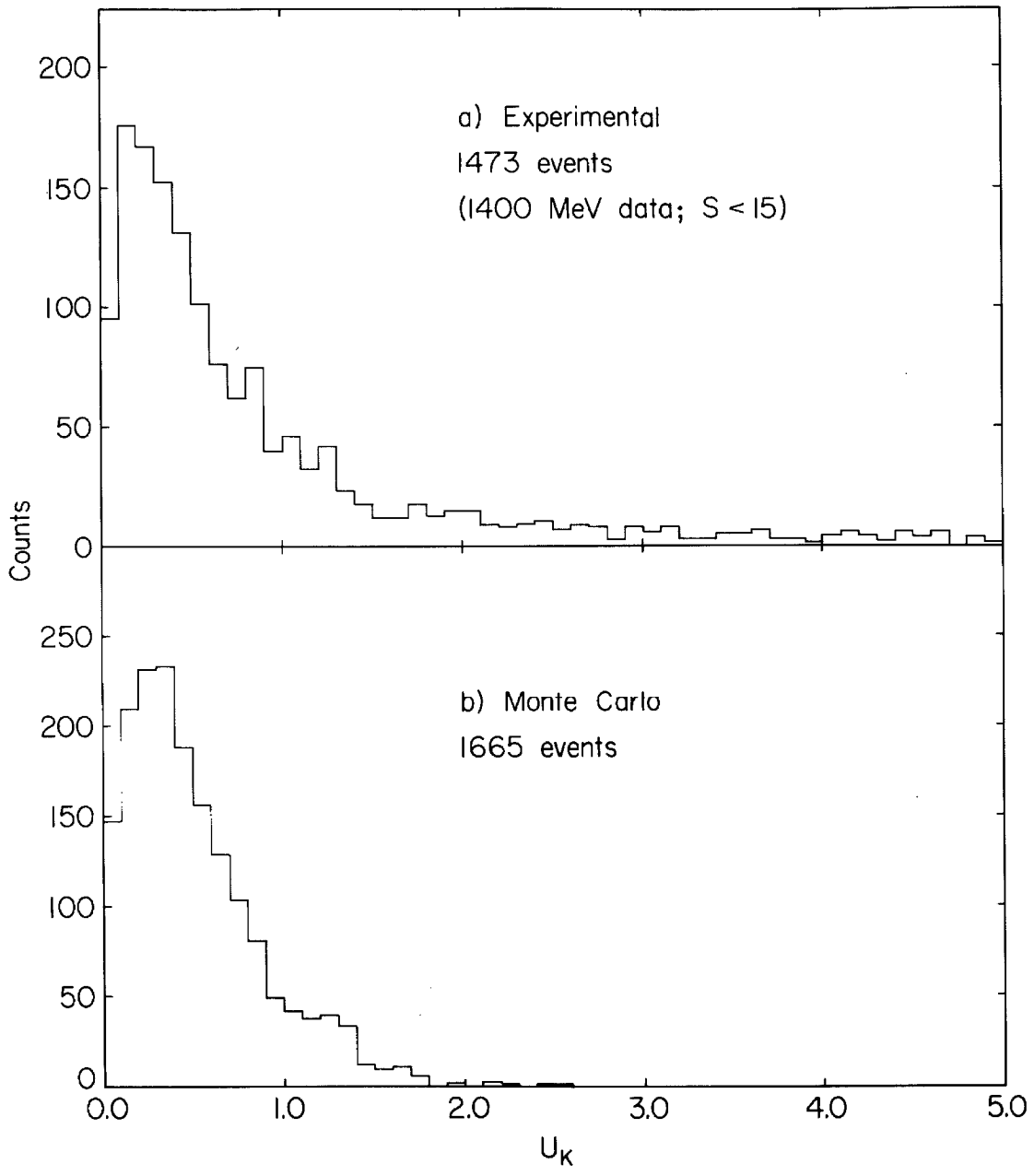

FIGURE 8. Experimental and Monte Carlo U Spectra.

with the scattering and interaction events discussed earlier. If this interpretation is correct, 0.99 ± 0.01 of the kaon events are retained when U_K was biased at 2.0. We took this bias as our criterion for "reasonable" kaon events.

For the Monte Carlo events, the analysis procedure reconstructed the true penetration depth δ with a standard deviation of about 11%. This, coupled with the result that the distribution of δ for real events was satisfactorily flat, led us to believe that the other goal of the rear section fit, the establishment of a range, was met.

2.8 Front Section Fit

For the $\frac{dE}{dx}$ section of the telescope, we defined the function

$$S = \sum_{\frac{dE}{dx}\ \text{section}} \left(\frac{L_i - L_{io}}{0.1\, L_{io}} \right)^2$$

where the L_i are the observed pulse heights and L_{io} is the mean pulse height expected in the i^{th} counter for a particle of given mass and the penetration depth estimated by the rear section fit.

If L_i were normally distributed about L_{io} with standard deviation r/L_{io}, $(\frac{0.1}{r})^2 S$ would be χ^2 distributed with N degrees of freedom, where N is the number of counters in the $\frac{dE}{dx}$ section. We expected $(\frac{0.1}{r}) \approx 1$. Deviations in the shape of the S distribution from that of the χ^2 distribution were also to be expected. In particular, the slight skewness of the f_i would lead to more events of

higher S than would occur if the L_i were normally distributed. We therefore expected the distribution of S to possess a slightly larger positive skewness than the χ^2 distribution.

The correlation between S and U is illustrated in Figure 9. Solid dots indicate events in which side counter pulses were present. In this case eight counters were used in the $\frac{dE}{dx}$ section, and as expected, the S distribution shows a maximum at about 6. Except for small U, no clustering in S is evident. Side counter pulses are absent in events with large U and large S.

With the bremsstrahlung end point energy chosen below the kinematic threshold, the clustering at small U and $S \sim 6$ vanishes (Figure 10). The background events have about the same distribution, but are less frequent.

The S distribution of background events for which $U < 2$ is illustrated in Figure 11. As with the data of Figure 10, these data were obtained while running the machine below kinematic threshold. The distribution is consistent with the function

$$B(S) = \text{const} \cdot S/10 \qquad S < 10$$

$$= \text{const} \qquad S > 10 ,$$

as shown. We have used this function in subsequent fitting; results were not very sensitive to its form.

The S spectra obtained for one of the data points are illustrated in Figure 12. Shown are spectra for all kaons fitted, those kaons with the side counter pulse present, and stopping protons

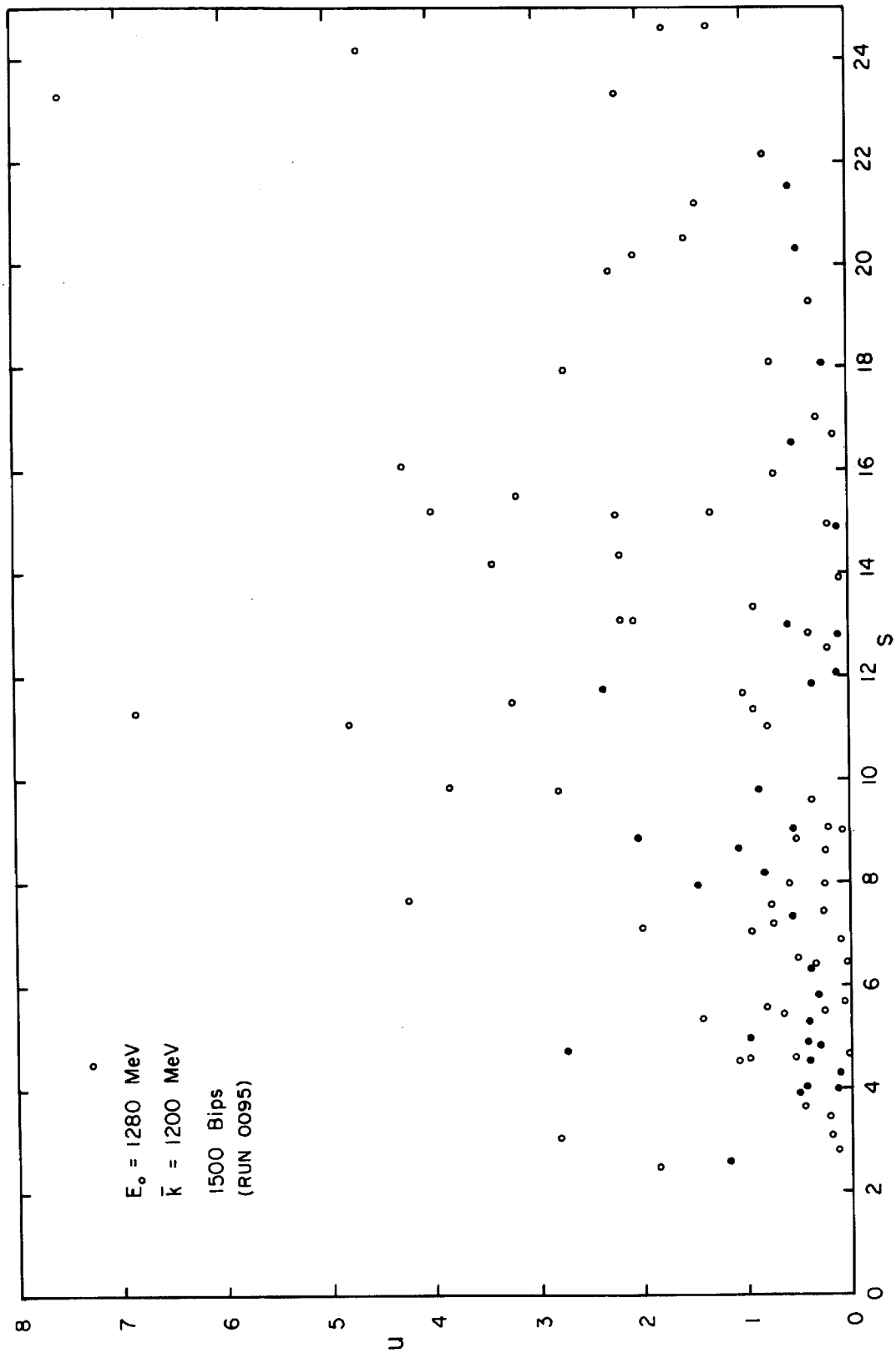

FIGURE 9. Correlation between S and U above Kinematic Threshold. (1200 MeV Configuration)

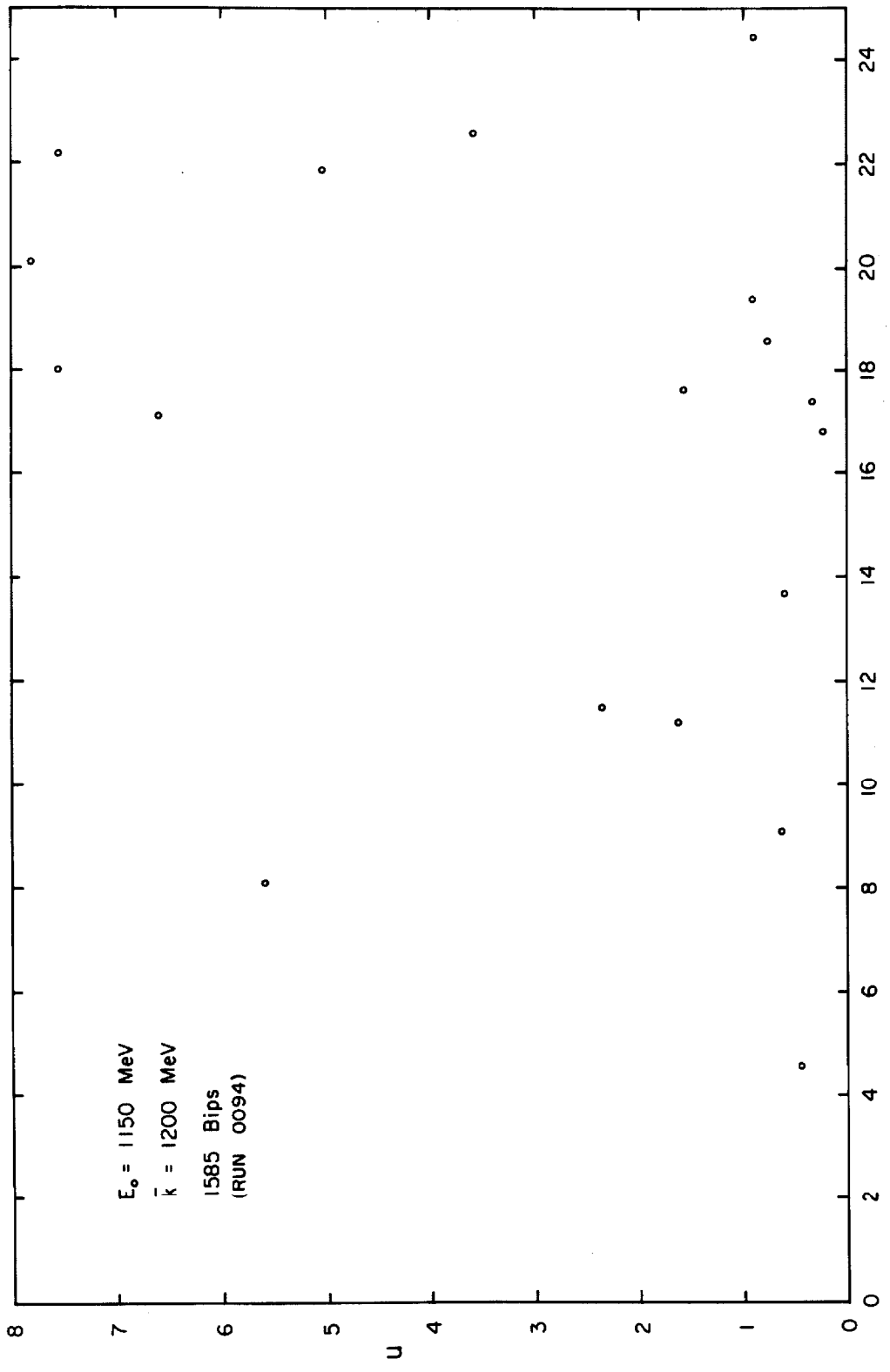

FIGURE 10. Correlation between S and U below Kinematic Threshold. (1200 MeV Configuration)

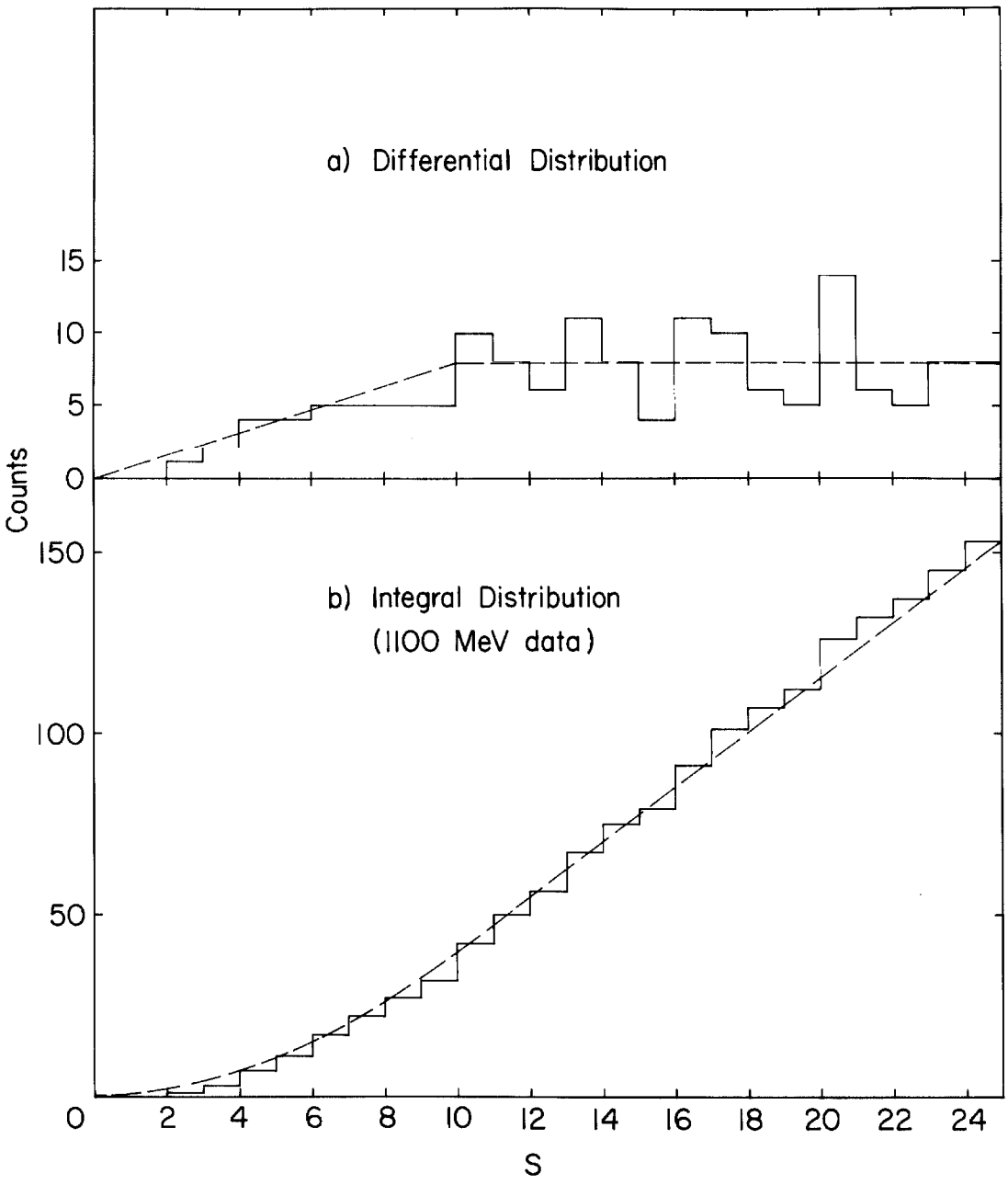

FIGURE 11. S Spectrum of "Kaon" Events Taken Below Kinematic Threshold.

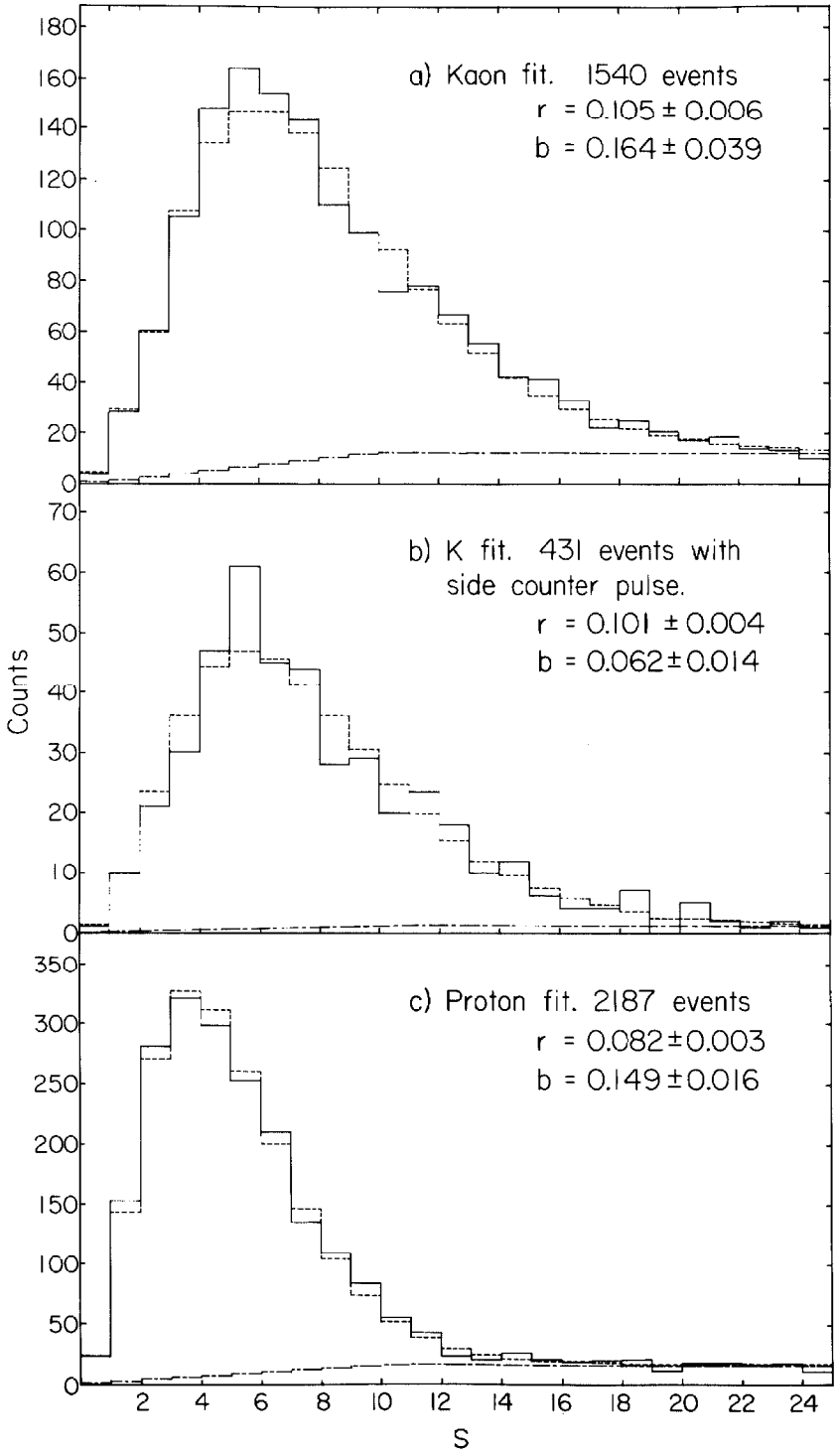

FIGURE 12. S Spectra from the 1200 MeV Data.

found in the same data. In the case of the protons, the definition of S was as above except that a proton mass was used. The rear section fit differed also in that decay particles were not admitted.

The observed S spectrum should be a superposition of two distributions:

a) A fraction (1 - b) of the events are particles of the desired type. From them, $(\frac{0.1}{r})^2 S$ is roughly χ^2 distributed with as many degrees of freedom as there are $\frac{dE}{dx}$ counters.

b) A fraction b of the events are background, with S distributed as discussed above.

We have approximated the distribution of S with the function

$$N(S) = (1 - b)k_n\left((\frac{0.1}{r})^2 S\right) + b\,B(S)$$

where

$$k_n(x) = \frac{x^{(\frac{n}{2} - 1)}\ e^{(-\frac{x}{2})}}{2^{n/2}\ (n/2)}$$, the χ^2 distribution of x with n degrees of freedom.

B(S) = the background distribution as above, normalized to unit area below some cutoff in S.

In view of our observation that the non-background distribution is more skew than $k_N\left((\frac{0.1}{r})^2 S\right)$, when N front counters are used, we may expect that $n < N$ will give a better fit than $n = N$. We have therefore treated n as a continuous parameter.

The data have been fitted with the functions N(S) by standard

maximum likelihood techniques, with r, b, and n as parameters. For purposes of fitting, the data were grouped into bins of width $\Delta S = 1$. The integral of N(S) as given above was differenced to calculate the expected mean, and Poisson statistics were assumed. The dotted curves of Figure 12 were calculated by this method. The solutions for r and b are given in the Figure; $n = 7.5$ was used, with $N = 8$. The value $n = N - 0.5 \pm 0.5$ was typical. The smaller value of r in the proton case reflects the proton's greater light output in the counters.

In view of the assumptions that went into the functional form for the S distribution, it is a somewhat surprising result that the fits thus obtained are statistically very good ones. A goodness of fit criterion is somewhat hard to define for the Poisson statistics used, but the parameter which would asymptotically approach χ^2 was typically 15 to 20 with 25 degrees of freedom.

A further check that the fit is sensible can be made by calculating Y, the total number of kaons, from a truncated S distribution. Let N_S counts fall below S. Then, using the fitting parameters, we may write

$$Y_S = f(S;r,b,n)N_S .$$

Y_S should be a constant within statistics. The results of such a test are given in Figure 13 for the kaon example of Figure 12a. The typical error indicated on N_{25} is statistical, while the error on Y_{25} includes that in the determination of b.

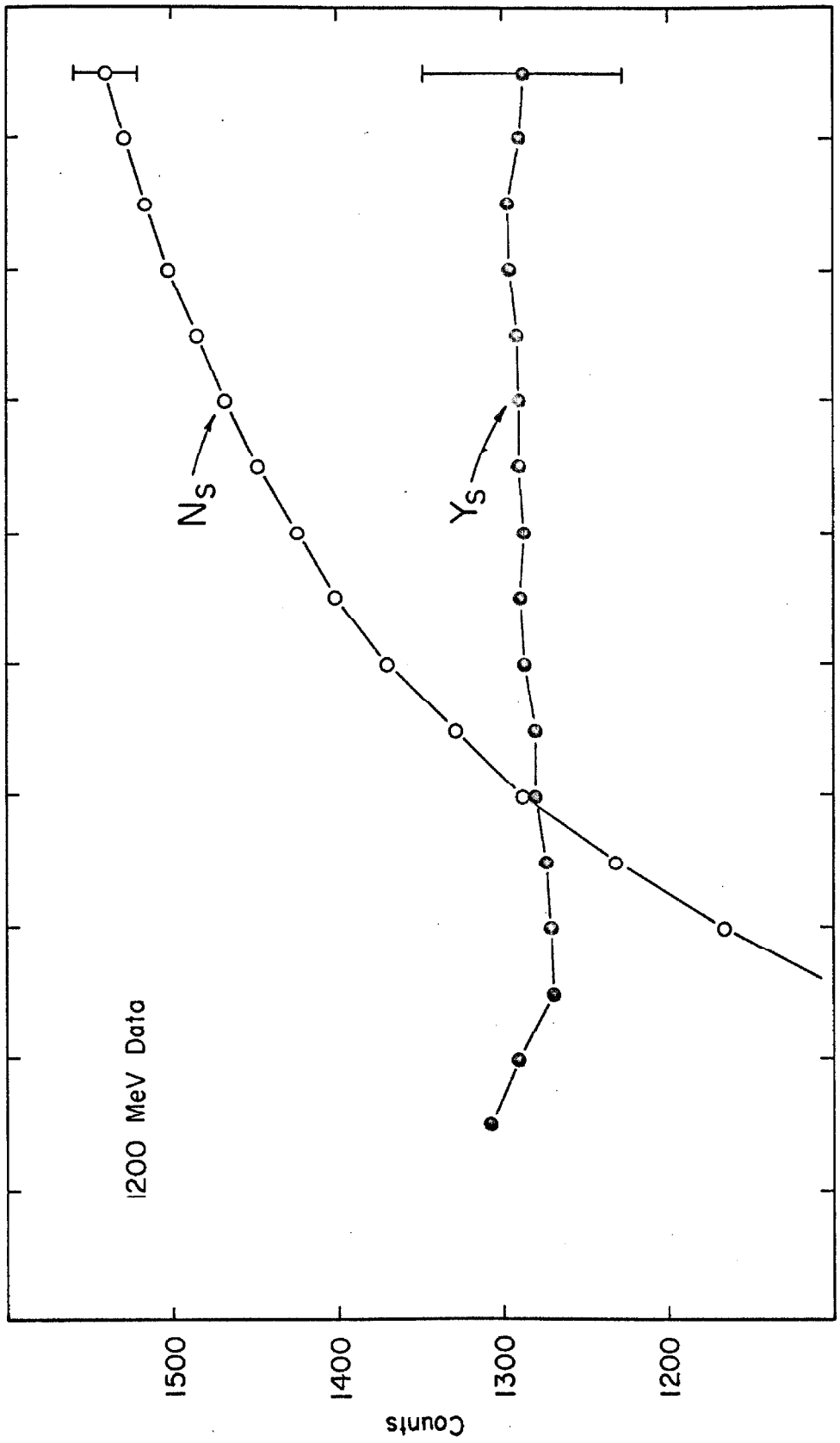

FIGURE 13. The Effect of S Spectrum Truncation on Kaon Counting Rate.

Whether or not we wish to regard b as the background of the experiment is a matter of taste. The S distribution has been truncated at 25 since it was apparent that practically no kaons would lie outside this region. This has been borne out in the fitting procedure. The truncation could just as easily have been made elsewhere, with the same result for the area under the particle peak. It might sound better to say that the background is 10 % than that it is 16%, but the result is the same.

The statistics of the data are not good enough to support a further examination of the S distribution. However, we have been able to define a region which contains virtually all the kaon events, and to estimate the fraction of background events included within the region.

2.9 Calibration

A simplified version of the algorithm discussed above was used in the pulse height calibration procedure. As was mentioned earlier, it was possible, by the use of the auxiliary counters Cal. 1 and Cal. 2 and slightly modified logic, to define a particle beam of known range. This range and its width δR were chosen so that $\delta R \frac{d}{dR} L_{io}$ was small compared with the expected standard deviation of the L_i. With the logic in this mode, about half of the particles accepted were protons. A large fraction of the remainder were interaction events, since the Čerenkov counters and pulse height limits eliminated most electrons and pions.

The computer identified the protons and calculated the parameters of their distribution in various counters by an iterative procedure. A table of expected mean pulse heights was first constructed. Taking these means as the L_{io}, S was computed for each event. The event was rejected if S was greater than 17 (a limit somewhat arbitrarily chosen). If accepted, its contributions to the first three moments of the distribution were accumulated. Upon completion of this procedure for all of the data, the set of means so constructed was reduced to that expected of a minimum ionizing particle, printed, stored, and filed away as a new table of expected mean pulse heights. If the r. m. s. deviation in the $\frac{dE}{dx}$ section of the new means from the previous set was greater than a certain amount, the process could be iterated. It was found that if the deviation was less than about 3%, subsequent iterations would agree.

The apparatus was linear to 1%, so gain calibrations were also made to this accuracy. With resolutions of the order of 10%, about 100 protons, or 200 events, were needed. These could be recorded in a few minutes. Such calibration runs were made every few hours during the experiment. Several were taken during each kaon run; a weighted average of their results was used in the kaon analysis.

An additional check on the entire procedure was made by doing the same thing with pions. Čerenkov vetos were removed, as were the lower limits on pulse height imposed by the slow logic. A run was taken which included both protons and pions. The above procedure was used to calibrate on the protons in the data. Then the mass was

changed to the pion mass. The program used a different set of events, and the calibration results found had an r.m.s. deviation of 2.6% from the proton results. In view of the electron contamination accompanying the pions and the uncertainty in the $\frac{dE}{dx} - \frac{dL}{dx}$ relationship, this was regarded as satisfactory.

Although each calibration produced results which were statistically significant to 1%, the calibrations made a few hours apart usually disagreed by 2 to 4%. Gains appeared to wander by this amount about values which were constant over many months. It also appeared to be an individual matter, as some phototubes were stable to 1% while others consistently fluctuated by 5%.

2.10 Background

The effectiveness with which the electronic preselection and computer analysis held back the flood of competing events is perhaps best illustrated by Figures 14 and 15. Figure 14 is similar to Figure 9, except that it is taken from the 1100 MeV data where, as may be noted from Table 2, b is much greater. The data of Figure 15 were taken under identical conditions except that the ΛA or ΛB signal was not required. It represents about 0.01 the running time of that of Figure 14. 65 kaons should appear in Figure 14, and since there is no Λ decay proton efficiency correction, 3 should appear in Figure 15.

It had originally been hoped that the telescope might be operated without the Λ decay proton requirement. It is evident from Figure 14, however, that operation was marginal at 1100 MeV

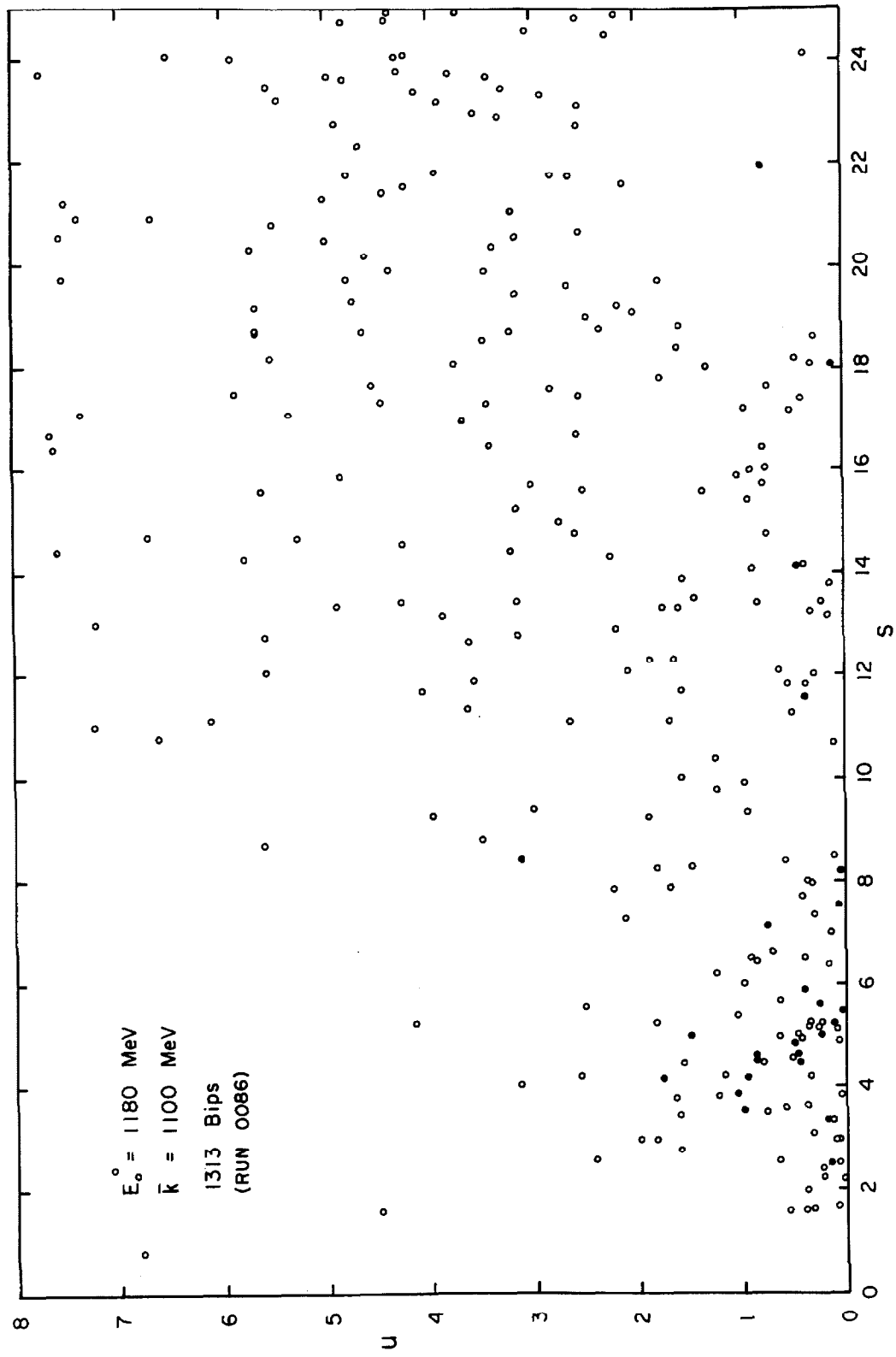

FIGURE 14. Correlation between S and U above Kinematic Threshold. (1100 MeV Configuration)

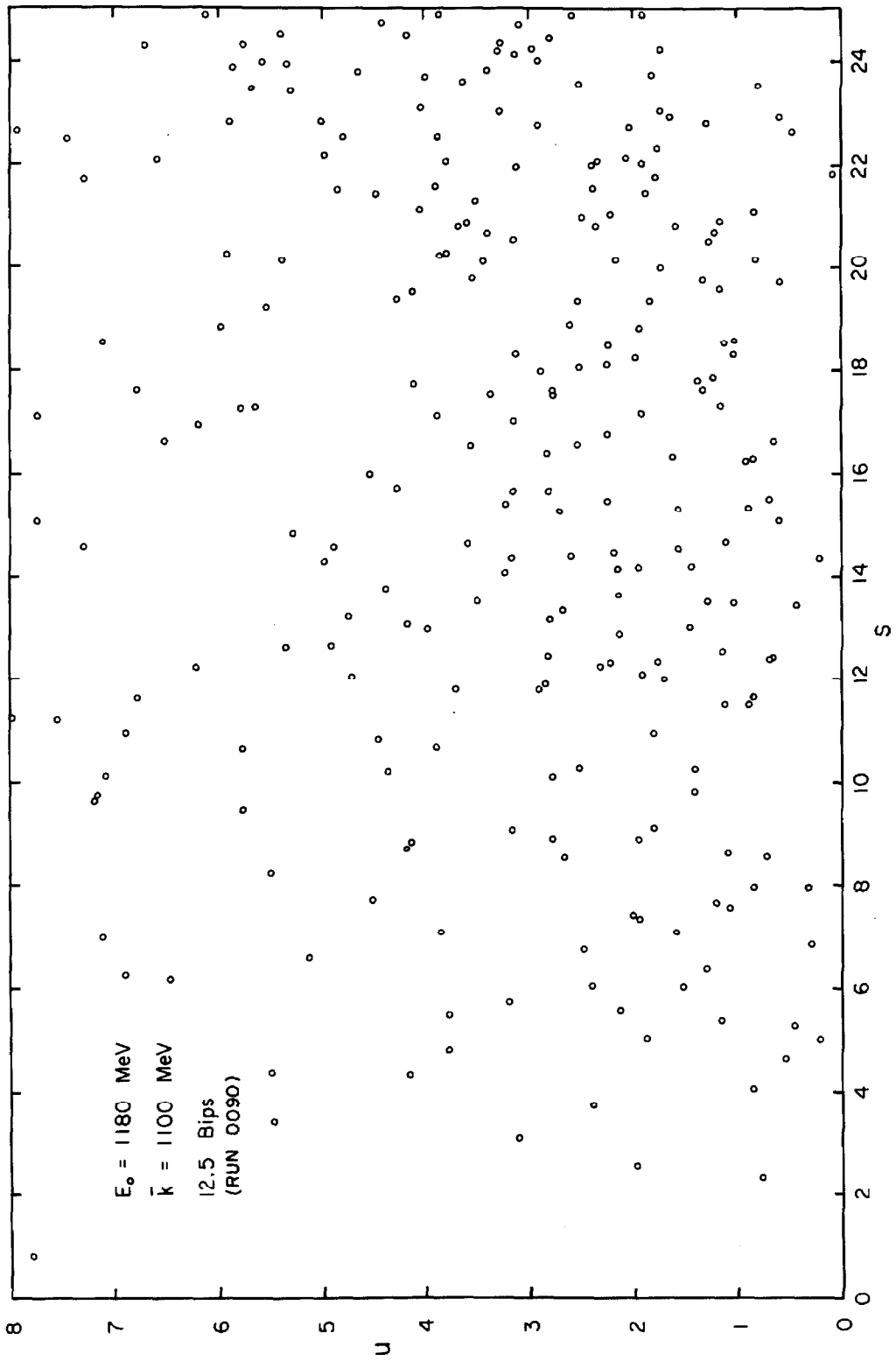

FIGURE 15. Correlation between S and U above Kinematic Threshold. (1100 MeV Configuration, but with no Λ requirement.)

even with the Λ information. Our error in the estimation of the importance of this background was the only serious discrepancy between the plan and execution of the experiment, except for a similar miscalculation of the time required for the experimental program. The error is sufficiently important that the nature of the background should be examined in some detail.

The run of Figure 15 consisted of 1300 events, whose analysis breakdown is as follows:

Some counter saturated the pulse height analyzer	120
Not fit by stopping K or p hypothesis	428
Fit by proton hypothesis only (i.e. $U_p < 2$, $S_p < 25$)	666
Fit by kaon hypothesis only (i.e. $U_K < 2$, $S_K < 25$)	51
Fit by either kaon or proton hypothesis	35
	1300

The 86 events fit by the kaon hypothesis distribute in S as the below threshold events of Figure 11. The 35 events also satisfying proton criteria yield a higher average S; only four occur with $S < 12$. These figures imply that about 5% of the normal stopping protons occur in the region $U_K < 2$, $S_K < 25$, and about 0.6% in the region $U_K < 2$, $S_K < 12$. We conclude on the basis of such data that 30% - 50% of the observed background events were stopping protons.

But why was the scheme so ineffectual in eliminating protons? The fraction accepted is ten times that expected even with the U_K criterion removed. Oddly enough, the answer lies entirely with the range determination made from the data of the slowing and stopping sections. Throughout this section, pulse heights from a stopping proton were larger than those expected of a kaon. A small U_K could often be obtained, however, by using δ_L, the lower limit on the penetration depth. This was the case for all 35 ambiguous events of the above example. δ_L typically differed from the proton's true penetration depth δ_t by 1.7 - 2.0 g/cm^2. The kaon pulse heights calculated for the front section were thus about 10% closer to the proton peak:

$$\frac{L_{io}(\delta_L, m_K) - L_{io}(\delta_t, m_K)}{L_{io}(\delta_t, m_p) - L_{io}(\delta_t, m_K)} \approx 0.1$$

This was sufficient to raise the proton acceptance fraction by a factor of about 10.* The precise size of the effect is difficult to estimate because of its extreme sensitivity to δ, but it is large enough to account for the high proton acceptance.

Pion events evidently did not contribute to the remaining background. Their pulse height separation from the kaons was quite good, and many were vetoed by the Čerenkov counters. An interacting pion, with lower initial pulse heights, was even more

---

*The problem of the proton's distribution in S_K is treated in detail in section 4.4.

obviously non-kaon like. Monte Carlo pion events were quickly discarded by the analysis program.

There remains a background rate, about 20 times larger than the kaon rate at the 1100 MeV point, which is apparently not caused by single stopping particles. Our experiments to understand the nature of this background have been largely inconclusive. The data of Table 2 (p. 18) indicate that its rate accurately followed the gate rate. More precisely, it followed the $\Lambda A + \Lambda B$ rate (mostly an accidental rate) since removal of the ΛB or ΛA requirement increased the background rate by the factor (Gate rate)/($\Lambda A + \Lambda B$). With $\check{C}1$ and $\check{C}2$ veto requirements removed, both the gate rate and the background rate were doubled.

The first observation merely says that a fixed fraction of the gate signals were produced by events which would fall into the kaon region. The second suggests that electron showers contribute. Inspection of individual events appears to corroborate this. In many events, there was very little correlation from one counter to another; occasionally counters were even "skipped." Given enough shower events, some satisfying kaon criteria would be found.

Many of the events which were inspected accurately conformed to the scattering proton hypothesis mentioned earlier. Further evidence for this interpretation was provided by the frequent occurrence in such events of a large pulse in a side counter, which indicated the passage of a highly ionizing particle. Again, given complete freedom in choosing a kaon decay hypothesis, a large

fraction of such proton scattering events satisfied kaon criteria.

So in general, the discrimination against background fell short of the mark because a set of kaon criteria liberal enough to admit arbitrary kaon decays could be satisfied by several other frequent kinds of events. The coupling which sometimes occurred between the front and rear section fits was particularly insidious. Perhaps an even more sophisticated use of the pulse height information could have been made. Although several ideas presented themselves, one feels that a point of diminishing returns was reached.

It was realized in advance that the background was a largely unknown factor, and that the Λ requirement could be used, if necessary. The requirement did mean that the K^+ telescope could not also be used as a means of quickly gathering a great deal of cross section data. But the main object of the experiment was the Λ polarization measurement, and since the Λ decay signature was in any case necessary for this measurement, the kaon beam defined by the telescope was satisfactory.

2.11 Results and Conclusions

The evidence that this apparatus correctly defines a kaon beam may be summarized with three observations:

a) The differential cross sections deduced from the data were consistent with those found in other experiments, within statistics and the uncertainties involved.

b) Below kinematic threshold, the counting rate was consistent

with zero. With increasing bremsstrahlung end point energy, the counting rate increased as predicted.

c) The expected fraction of kaon events exhibited side counter pulses caused by the kaon decay products.

The cross section data are presented in Figure 16[8], and excitation curves in Figure 17[8]. In addition to the background subtraction discussed above, the usual corrections for nuclear absorption, decay in flight, electronic dead time, etc. have been made. For the polarization measurement, only the background is important. Since the remainder of the data reduction has been extensively treated by J. H. Marshall[8], it will not be further discussed here.

A summary of the results pertinent to the polarization measurement is given in Table 3. The uncertainty in mean photon energy is based upon a 2.5% uncertainty in our range and the range-energy relationship, while the resolution δk is based upon the data of Figure 4. We have also tabulated the observed efficiency of the side counters in detecting kaon decay products. This efficiency is to be compared with the predicted efficiency of 0.278 ± 0.023, which was computed by combining a Monte Carlo geometrical efficiency calculation with the known branching ratio data.

In retrospect, many of the problems encountered in the course of this experiment might have been anticipated from the results of simpler experiments. In practice, however, the problems as well as the results appeared only with the complete system. The programs

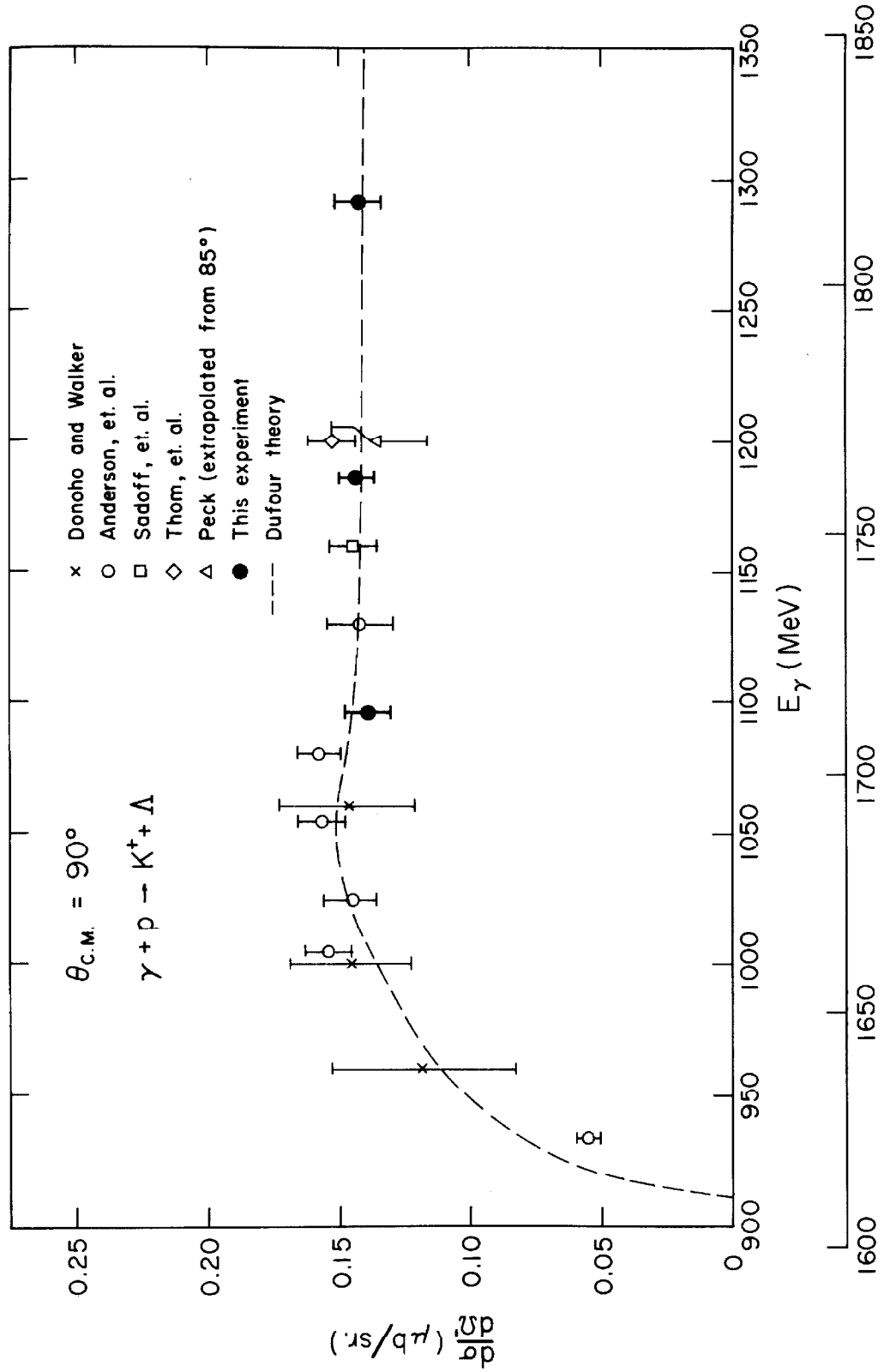

FIGURE 16. $K^+\Lambda$ Photoproduction Cross Section at $\theta_{c.m.} = 90°$

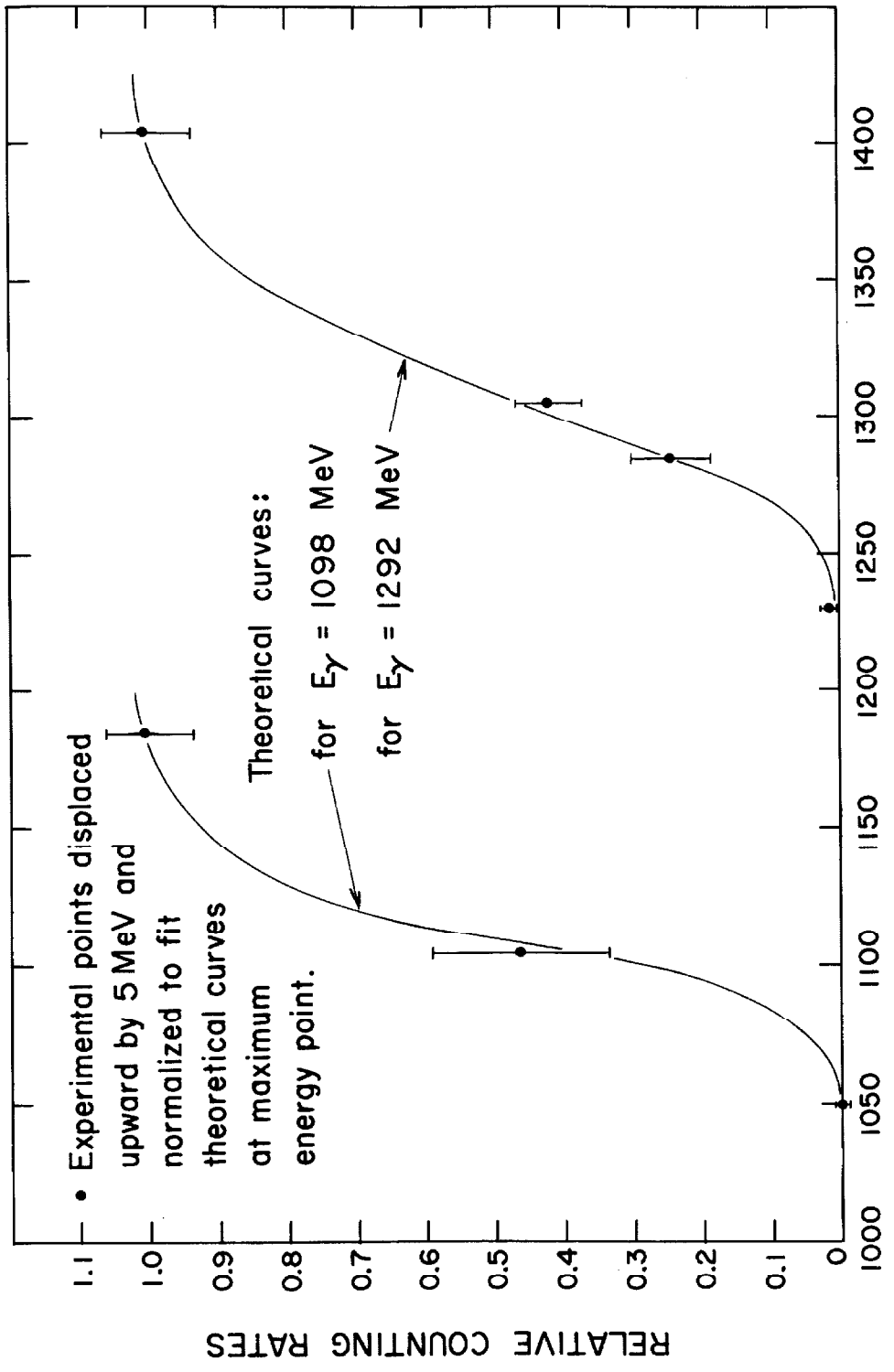

FIGURE 17. Kaon Excitation Functions.

TABLE 3

Summary of K^+ Detection Results

Nominal Photon Energy	1100 MeV	1200 MeV	1300 MeV
$\bar{k}$	1098 ± 5.3 MeV	1187 ± 8.5 MeV	1292 ± 11.6 MeV
δk (a)	25.5 MeV	33.0 MeV	40.3 MeV
Nominal $\theta_{c.m.}$	90°	90°	90°
$\theta_{c.m.}$	89.9°	90.2°	89.8°
$\delta\theta_{c.m.}$ (a)	5.1°	4.6°	4.3°
Total counts (all K-like events)	1385	1540	1522
b	0.378 ± .036	0.164 ± .039	0.063 ± .052
r (b)	0.095 ± .005	0.104 ± .005	0.113 ± .005
n	6.5	7.5	7.5
Y (c)	862 ± 54	1287 ± 68	1426 ± 89
Y_D (d)	253 ± 18	402 ± 27	397 ± 25
Y_D/Y (e)	0.293 ± .028	0.311 ± .027	0.278 ± .021

(a) Half width of the resolution function at half maximum.

(b) The error quoted for r is closely correlated to the width in n. When N is held fixed, the error in r is typically ± 0.002.

(c) Total number of kaons.

(d) Total number of kaons exhibiting side counter pulses.

(e) The predicted ratio is 0.278 ± 0.023.

were as indispensable as the hardware. For instance, we have discussed the serious kaon beam contamination from normal stopping protons. The extent of the contamination depended upon the details of the fitting procedure, even for a Monte Carlo calculation. In turn, the fitting procedure evolved in many steps, in the attempt to separate kaons from several kinds of background. The extent and character of the background were not known in advance. Since programs were written in machine language and in general occupied most of the computer memory, these steps came slowly.

Another example is that of phototube gain instability. When this experiment was begun, it was possible to take a pulse height spectrum in a single counter with 5% channel widths. The information that phototubes exhibit 2% to 5% gain instabilities under "steady state" synchrotron operating conditions was not available to us until the calibration scheme had been debugged and operated for some time.

On the other hand, a more experienced experimenter (including this one, in the future) might well shy away from an approach such as this, in which rare events were sought in a medium where interaction was the rule rather than the exception. To do this in conjunction with a necessarily complex analysis scheme was to invite difficulty.

But the technique was successful. There is information in pulse heights, and it may be used. One of the more satisfying illustrations of this was the S spectrum, which was even simpler than one might expect. And finally, the method did permit the rapid accumulation of the Λ polarization information.

3 Λ POLARIZATION

3.1 General Considerations

Given the kaon detection scheme described in section 2 of this thesis, the remaining problems in the Λ polarization measurement are chiefly those associated with assuring the symmetric placement and operation of the two Λ decay proton telescopes.

As may be seen from Table 1 (p. 9), the protons from the Λ decay are confined to a narrow cone of half angle ξ_m about the Λ direction. The solid angle mapping from the center of mass to laboratory frames is such that the distribution in the cone is sharply peaked to the maximum angle available. For instance, at the 1200 MeV point, where $\xi_{lll} = 7.9^o$, 50% of the decay protons appear outside the 6.7^o cone.

In the Λ c.m. system, the decay proton distribution is given by

$$N(\theta)\, d\Omega = \frac{d\Omega}{4\pi} (1 + \alpha P_\Lambda \cos\theta)$$

where θ is the polar angle in a coordinate system in which $\hat{k} \times \hat{p}_\Lambda$ is along the z axis. From the measurements of Cronin and Overseth[13],

$$\alpha = 0.62 \pm 0.07.$$

The apertures of the Λ decay proton telescopes map into "caps" on the unit sphere in this system; we integrate $N(\theta)$ over these caps to obtain

$$P_{\pm} = \frac{1}{2} F(1 \pm \alpha P G)$$

where $P_+(P_-)$ is the probability of the proton being detected by + (-) telescope. (We avoid the usual "up-down" notation because $\hat{k} \times \hat{p}_\Lambda$ points downward. See Figure 1.) Then if n_K kaons pass through the telescope and a fraction β of the Λ particles decay in the charged mode*, the number of counts observed in the + (-) telescope is

$$N_{\pm} = \frac{1}{2} n_K \beta F(1 \pm \alpha P G) .$$

From this and from the binomial statistics involved, we obtain

$$\alpha P = \frac{1}{G} A_{+-} \pm \frac{1}{\sqrt{\beta n_K}} \frac{1}{G\sqrt{F}} \sqrt{1 - A_{+-}^2}$$

where

$$A_{+-} = \frac{N_+ - N_-}{N_+ + N_-} .$$

Machine running time is proportional to n_K, and $\sqrt{1 - A_{+-}^2} \approx 1$ for reasonable values of G and P. Hence to optimize the polarization measurement, counters must be designed so that the quantity $\frac{1}{G\sqrt{F}}$ is minimized. For rectangular counters which are about as wide as the base of the Λ decay cone, this

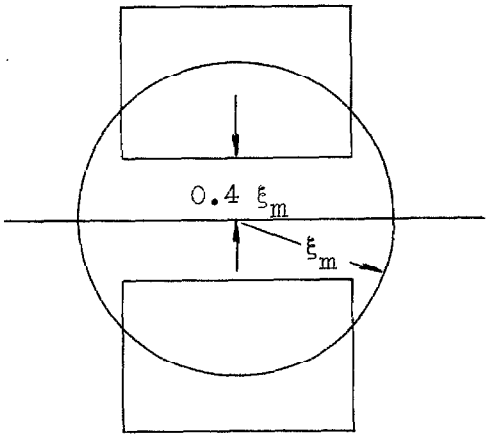

*$\beta = 0.677 \pm 0.010$ [14]

function goes through a flat minimum when the counter edges are about $0.4\xi_m$ from the production plane.

This convenient result arises from the fact that for protons emitted near the production plane, $\theta \approx 90^o$, and hence no polarization information is obtained from their observation. The larger number of events, however, leads to a larger statistical error. On the other hand, for $\xi \sim \xi_m$ there are so few events that the error is again large.

For purposes of analyzing this experiment, F and G have been computed not only by integrating over the caps mentioned, but also over the target length, the K^+ telescope aperture, and the K^+ telescope energy acceptance. The 6-fold integrals were done by Simpson's method.

Let $N = N_+ + N_-$ be the measured number of events. Then

$$N = \beta n_K F$$

and

$$P_\Lambda = \frac{1}{aG} A_{+-} \pm \frac{1}{\sqrt{N}} \frac{1}{aG} \sqrt{1 - A_{+-}^2}$$

Under the operating conditions of the experiment,

$$\frac{1}{aG} \approx 2.2 .$$

The behavior of the Λ decay pions is similar to that of the protons, except that the cone half angle is from 59^o to 180^o in the range of the experiment. A counter so placed as to detect a large

fraction of the protons will thus detect practically no pions. With the apparatus used in this experiment, the pions passed through a counter about 0.06 as frequently as the protons, and were detected with about 50% efficiency*. In addition, in two thirds of these cases the proton was detected in the other Λ decay proton telescope; such events were discarded. θ was near 90° for the other third. Corrections to the asymmetry because of pion detection are thus negligible.

3.2 Electronic Asymmetries

A bias would obviously be introduced into the asymmetry if one of the Λ decay proton telescopes were more efficient than the other as a proton detector. Such a difference could exist for a number of reasons, most of which would be associated with incorrect setup of the coincidence circuit parameters. In addition, accidental veto rates could differ for the two telescopes for reasons of electronics or of different particle flux.

Efficiency differences which were constant in time and those not associated with particle flux differences between the two telescopes were eliminated by frequently interchanging the telescopes during the running.

Let A and B label the counter telescopes, and + and -

---

*Kaon events were accompanied by triggers from both proton telescopes $(2.0 \pm 0.5)\%$ of the time in a large sample of data. The expected accidental rate was 0.4%; the expected πp coincidence rate was 4%.

label their positions. Also define

$f_{A(B)}$ = Fraction of running time with telescope A(B) in + position.

$e_{A(B)}$ = Detection efficiency of telescope A(B).

$N_{A(B)}$ = Observed events in telescope A(B).

$N_{+(-)}$ = Observed counts in telescope +(-).

$$e = \frac{e_A - e_B}{e_A + e_B} .$$

$$f = \frac{f_A - f_B}{f_A + f_B} .$$

We then obtain

$$A_{+-} = \frac{N_+ - N_-}{N_+ + N_-} = \frac{ef + aPG}{1 + efaPG}$$

And similarly,

$$A_{AB} = \frac{N_A - N_B}{N_A + N_B} = \frac{e + faPG}{1 + efaPG}$$

We may thus choose $f \approx 0$ to eliminate any electronic asymmetry in A_{+-}.

As a check on the procedure, A_{AB} and A_{+-} were computed for several kinds of recorded events:

a) All ΛA and ΛB triggers.

b) Rejected events. Events satisfying the slow logic, but which could be fit by no stopping particle hypothesis.

c) Stopping protons. Events fit by a stopping proton hypothesis, with $S \leq 15$.

d) Kaon events. All events in the $S_K < 15$, $U_K < 2$ region.

The asymmetries for these various cases are given in Table 4. Because input pulse height biases on the Λ decay proton telescope coincidence circuits were run as high as possible, it would be surprising if the telescopes had identical efficiencies for near-minimum ionizing particles. Presumably the bulk of the triggers are due to near-minimum ionizing accidentals, so we should expect to see an AB asymmetry in all but the kaon case. Most of the data are consistent with

$$e = -0.03$$

or

$$ef = -0.005 .$$

The most flagrant exception is the 1100 MeV proton case. The other 1100 MeV accidental asymmetries are based upon exactly the same data, so that even systematic effects should be the same if the ΛA and ΛB triggers really come from the same source. One possibility is that they do not, but even so, A_{+-} should vanish. Either we are dealing with a statistical accident, or the efficiencies have varied while the data was being taken. We will discuss related problems in section 3.5.

In the kaon case, e should be even smaller than the value quoted above. Since the data are more or less self consistent, we feel justified in placing an upper limit of ± 0.01 on the systematic electronic asymmetry's contribution to A_{+-}.

Because of the high counting rates, 3 - 5% of the potential

TABLE 4

Measured AB and + - Asymmetries

	Photon Energy		1100 MeV	1200 MeV	1300 MeV
	f		0.166	0.175	0.127
a)	All ΛA, ΛB triggers	A_{AB}	-0.030 ± .002	-0.042 ± .002	-0.030 ± .003
		A_{+-}	+0.005 ± .002	+0.001 ± .002	-0.001 ± .003
b)	Rejected events	A_{AB}	-0.002 ± .010	-0.029 ± .007	-0.036 ± .011
		A_{+-}	+0.005 ± .010	-0.007 ± .007	+0.011 ± .011
c)	Protons	A_{AB}	+0.045 ± .013	-0.013 ± .022	-0.052 ± .038
		A_{+-}	+0.030 ± .014	-0.004 ± .022	-0.010 ± .038
d)	Kaons	A_{AB}	-0.028 ± .030	+0.016 ± .027	-0.061 ± .028
		A_{+-}	+0.128 ± .030	+0.130 ± .027	+0.047 ± .028

ΛA (ΛB) triggers were accidentally vetoed by the proton telescope Čerenkov counters. The veto rates were reasonably constant while the experiment was running at a given energy, and they were roughly identical for the two telescopes. Therefore no corrections were made to the data for this effect.

A final source of efficiency error would arise if one telescope position were subject to a higher background particle flux than the other. This would result in an accidental veto rate which was always larger, e.g., for the telescope in the + position, but with a difference which might always be within the statistics of the rate measurement. That A_{+-} is consistent with zero for the non-kaon events is evidence that this is not the case.

3.3 "Geometric" Asymmetries

If both Λ decay proton telescopes were displaced vertically from their nominal position by 0.1", the asymmetry A_{+-} would change by 0.02 and the polarization by 0.05. There existed several effects which were equivalent to displacements or position uncertainties potentially of this order, and which therefore must be understood before meaning may be attached to the Λ decay asymmetries listed in Table 4.

Immediately behind the proton telescopes a precision rule (the "Λ rule") was mounted vertically. As a matter of convenience, all displacements and errors were reduced to those of the intersection of the production plane with this rule.

The telescopes were positioned with respect to a nominal intersection point of the production plane with the Λ rule. To establish this plane, a photographic plate was exposed in the beam, and the maximum intensity point located photometrically. The image was mapped to a collimator some distance away to define a beam line. By means of a transit, the intersection of the plane containing these two points and a crosshair on the center of the K^+ telescope aperture counter was located on the Λ rule. An examination of the errors involved in the procedure and in locating the counter led to an uncertainty of 0.019" in the intercept. The procedure was repeated four times with different configurations of the apparatus; when reduced so that they could be compared, the results agreed with an r.m.s. deviation of 0.016".

However, the beam intensity maximum was not located at the mean of the intensity profile. Rather, the vertical beam profile was roughly as indicated in the drawing at the left. The details of the profile could be understood as the result of collimating a bremsstrahlung beam which was produced by electrons striking a rather large portion of the radiator. The collimation was represented by a function $C(x, y)$, and the beam profile by $B(k, r-r_o)$; then the vertical intensity mean was given by

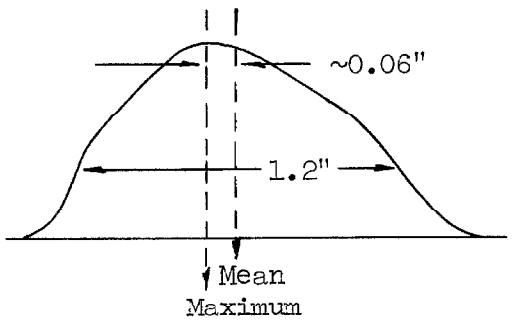

$$\bar{y} = \int B(k, r-r_o)\, C(x, y)\, y\, dx\, dy\ .$$

The softening of the collimator edge shadow, the result of the finite source size, was taken into account by "rounding" the edges of $C(x, y)$. $\vec{r}_o$ is the position of the beam maximum with respect to the collimator center. The results of such integrations were used to relate the position of the maximum intensity and collimator edges, as measured on photographic plates, to the position of the mean beam intensity.

The intensity maximum could be located to $\pm$ 0.007", and the collimator edges to $\pm$ 0.010". Additional uncertainties arose over the form of $C(x, y)$, but the error on the resultant correction, at the target, was about $\pm$ 0.015".

The beam position was usually constant throughout a run, but varied from day to day. Plates were therefore exposed every few hours during the running of the experiment. From the plate analysis results, corrections were made to the plane intercept separately for each run. The displacement, as measured at the target, was usually of the order of 0.060" $\pm$ 0.015"; this mapped into 0.100" $\pm$ 0.025" on the Λ rule.

An additional displacement arose because of the detailed use of pulse height information by the K^+ telescope. Identical particle beams passing through different parts of a plastic scintillator give rise to different mean pulse heights, because of the position dependence of light self-absorption and collection efficiency. In the counters used in this experiment, this variation was a strong function only of the distance from the light pipe through which the light reached the photomultiplier. It was characterized by a sharp drop of

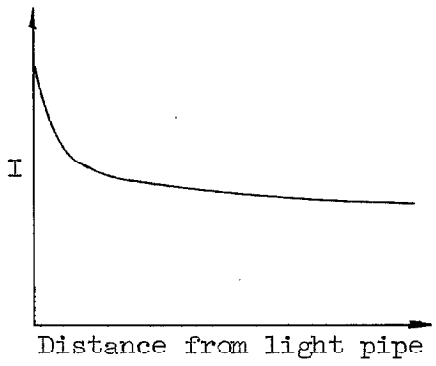

about 20% in the first half inch or so, followed by a gradual decrease of 1% - 2%/inch to the end of the counter. Usually such effects were not important, since only mid-sections of counters were used, where the total variation was small. Phototubes on consecutive counters were mounted on alternate ends of the counters, so that the situation was symmetric. But by definition, the entire area of the aperture counter was used. Since the kaon detection efficiency was sensitive to pulse height errors, it fell off near the light pipe. The counter was mounted vertically. Hence the mean center of the kaon beam defined by the telescope was moved, and the production plane rotated.*

Kaiser and deVilliers[15] have observed that the distribution of mean intensity along a coordinate x measured away from the light pipe can be fit by

$$I(x) = I_1 e^{-\mu_1 x} + I_2 e^{-\mu_2 x}$$

Our measurements on a piece of scintillator cut from the same sheet as was the aperture counter indicate a result which can be fit by this form, although our values of μ_1 and μ_2 differ from those of Kaiser

---

*There are several obvious and elementary ways to avoid the entire difficulty. However, the effect did not occur to us until a large fraction of the data had been taken.

and deVilliers. The smaller μ can be fit from our data; the other bracketed.

The variation of kaon detection efficiency with aperture counter pulse height was determined empirically, by re-analyzing a data sample with various aperture counter gains. This yielded an efficiency $E(I(x))$. The mean center of the aperture counter was then

$$\bar{x} = \int x E(I(x))\, dx \Big/ \int E(I(x))\, dx$$

This led to a displacement*

$$\delta x = -0.051" \pm 0.010"$$

which reflected into a change

$$\delta y = +0.028" \pm 0.006"$$

on the Λ rule. The quoted error brackets the uncertainties in $I(x)$ and $E(I)$.

A summary of the errors inherent in these measurements and corrections is given below. The resultant error reflects

Source of Error	Estimate of Size (on Λ rule)
Production Plane Survey	0.019"
Beam mean position	0.025"
Aperture mean position	0.006"
Total	0.032"

*The calculation also indicated an efficiency loss of 2.9% for kaon detection because of this mechanism.

into an error of ± 0.007 in the $+-$ asymmetry. We have previously estimated that systematic electronic errors could have been as large as ± 0.01. The combined result reflects a possible systematic error of ± 0.03 in the Λ polarization.

Each time the Λ decay proton telescopes were interchanged, the positions of their aperture counters with respect to the Λ rule were measured. Such measurements were reproduceable to $\pm 0.005"$, although a variation of about $0.035"$ occurred.

For each run, the position of each proton telescope was known, although in general their placement was not exactly symmetric. In an obvious generalization of the notation of section 2.1, we may write, for the i^{th} run,

$$N_+^i = \frac{1}{2} n_K^i \beta F_+^i (1 + \alpha P G_+^i)$$

$$N_-^i = \frac{1}{2} n_K^i \beta F_-^i (1 - \alpha P G_-^i)$$

for this case. We may also note that

$$n_K^i \propto B^i$$

where B^i is the integrated beam intensity during the i^{th} run. Furthermore, we define

$$\overline{G} = \frac{\sum B^i (F_+^i G_+^i + F_-^i G_-^i)}{\sum B^i (F_+^i + F_-^i)}$$

$$\delta F = \frac{\sum B^i (F_+^i - F_-^i)}{\sum B^i (F_+^i + F_-^i)}$$

$$\delta(FG) = \frac{\sum B^i (F_+^i G_+^i - F_-^i G_-^i)}{\sum B^i (F_+^i G_+^i + F_+^i G_+^i)}$$

$$N_{+(-)} = \sum N^i_{+(-)} \quad .$$

Then

$$aP\bar{G} = \frac{A_{+-} - \delta F}{1 - \delta(\bar{F}G) A_{+-}}$$

This procedure was used to combine the data from different runs. δF was usually of the order of 0.012, while $\delta(FG) A_{+-}$ was negligible.

3.4 Background Corrections

A fraction b of N observed events are the non-kaon background; we have already presented evidence that such events are detected symmetrically by the proton telescopes. Then we may write

$$N_{\pm} = \frac{N}{2}\left[(1 - b)(1 \pm aPG) + b\right]$$

And proceeding as in section 2.1,

$$aPG = \frac{1}{1 - b}\left[A_{+-} \pm \frac{1}{\sqrt{N}}\sqrt{1 - A_{+-}^2}\right]$$

In the K^+ telescope discussion, it was noted that the kaon counting rate Y could be computed from the observed S distribution, truncated at an arbitrary value S:

$$Y_S = f(S; r, b, n) N_S$$

The independence of Y_S of S was taken as evidence that the fitting function was satisfactory. The equivalent operation can be performed in making the background correction to the asymmetry. We define

$$b_S = b \int_o^S B(S')\, dS'$$

and rewrite the background correction as

$$\alpha PG = \frac{1}{1 - b_S} \left[A_{+-} \pm \frac{1}{\sqrt{N_S}} \sqrt{1 - A_{+-}^2} \right]$$

The correction as applied to the 1200 MeV data is shown in Figure 18.

In the asymmetry case, however, something was to be gained by the truncation. It was not necessary to include the high S tail, which consisted for the most part of background events, and it was certainly safer not to do so. We have chosen to truncate at S = 15, since for smaller S a significant number of kaons are lost.

3.5 Polarization Results

A summary of the analysis so far discussed, together with final results, is presented in Table 5. Also included are relevant parameters from Table 3. Our results, together with those of groups at Cornell and Frascati, are plotted in Figure 19.

One irregularity present in the data should be discussed. The kaon +- asymmetry data and counting rate data for the 1200 MeV point are given in Figure 20, broken up by runs. In both cases the raw numbers for $S < 15$ are shown, with no corrections. Solid circles indicate telescope A in the + position; open circles B.

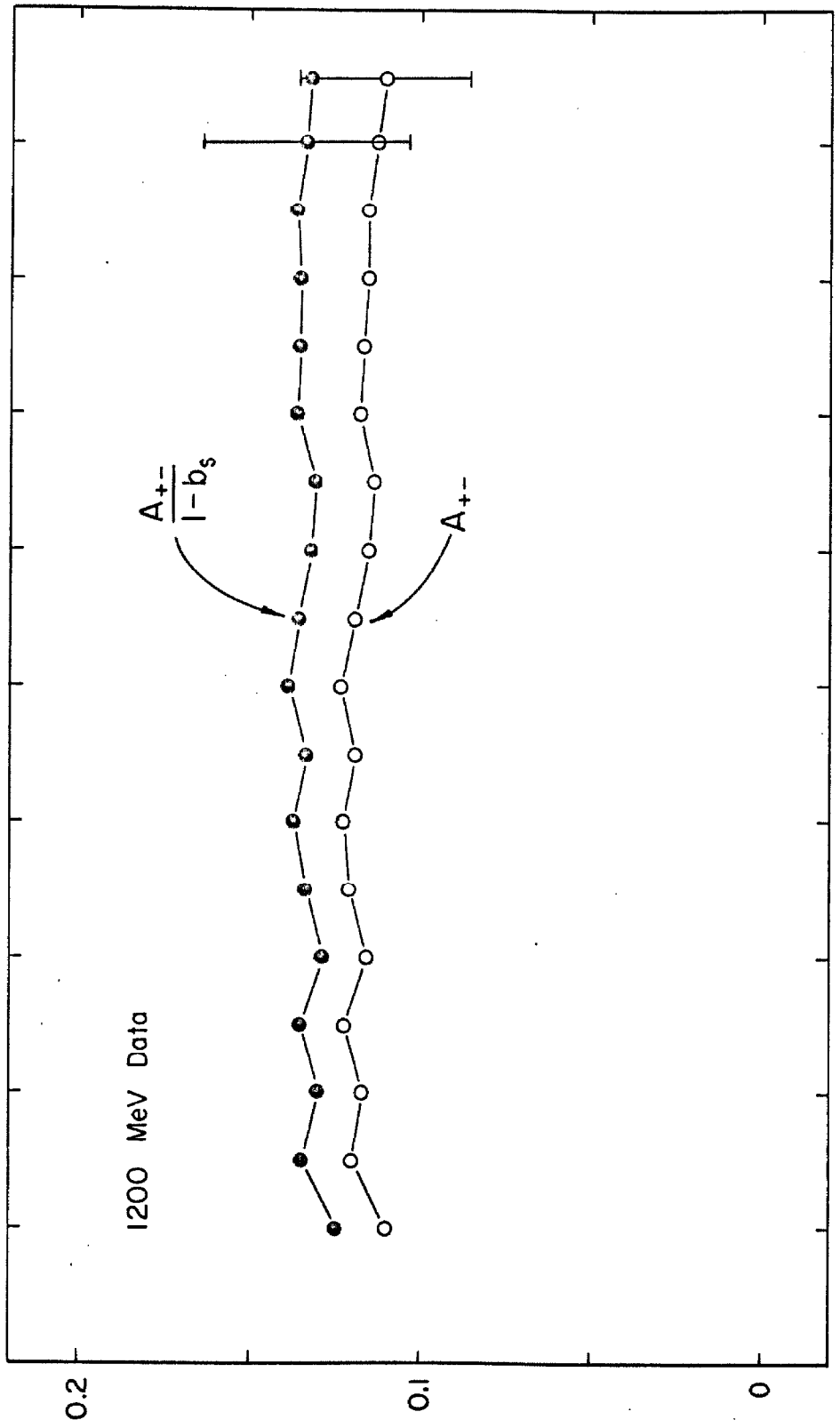

FIGURE 18. The Effect of S Spectrum Truncation on Kaon Asymmetry.

TABLE 5

The Polarization of Photoproduced Λ Particles at $\theta_{c.m.} = 90^{\circ}$

Nominal Photon Energy	1100 MeV	1200 MeV	1300 MeV
$\bar{k}$	1098 $\pm$ 5.3 Mev	1187 $\pm$ 8.5 MeV	1292 $\pm$ 11.6 MeV
δk (a)	25.5 MeV	33.0 MeV	40.3 MeV
$\theta_{c.m.}$	89.9°	90.2°	89.8°
$\delta\theta_{c.m.}$ (a)	5.1°	4.6°	4.3°
F	0.366	0.451	0.512
G	0.777	0.731	0.703
A_{+-} (raw data)	0.127 $\pm$ .031	0.130 $\pm$ .027	0.051 $\pm$ .027
A_{+-} (with geometric corrections)	0.118 $\pm$ .031	0.119 $\pm$ .027	0.034 $\pm$ .027
$(1 - b_{15})$ (kaon fraction)	0.720 $\pm$ .030	0.888 $\pm$ .031	0.955 $\pm$ 0.038
A_{+-} (with all corrections)	0.162 $\pm$ .043	0.134 $\pm$ .030	0.036 $\pm$ 0.028
αP_{Λ}	0.209 $\pm$ .055	0.183 $\pm$ .042	0.051 $\pm$ 0.040
P_{Λ} (b)	+0.337 $\pm$ .089	+0.296 $\pm$ .067	+0.082 $\pm$ 0.065

(a) Half width of the resolution function at half maximum.

(b) Only statistical errors are included. In addition, the estimated systematic error is $\pm$ 0.03, and the value of α used[13] was $\alpha = 0.62 \pm 0.07$.

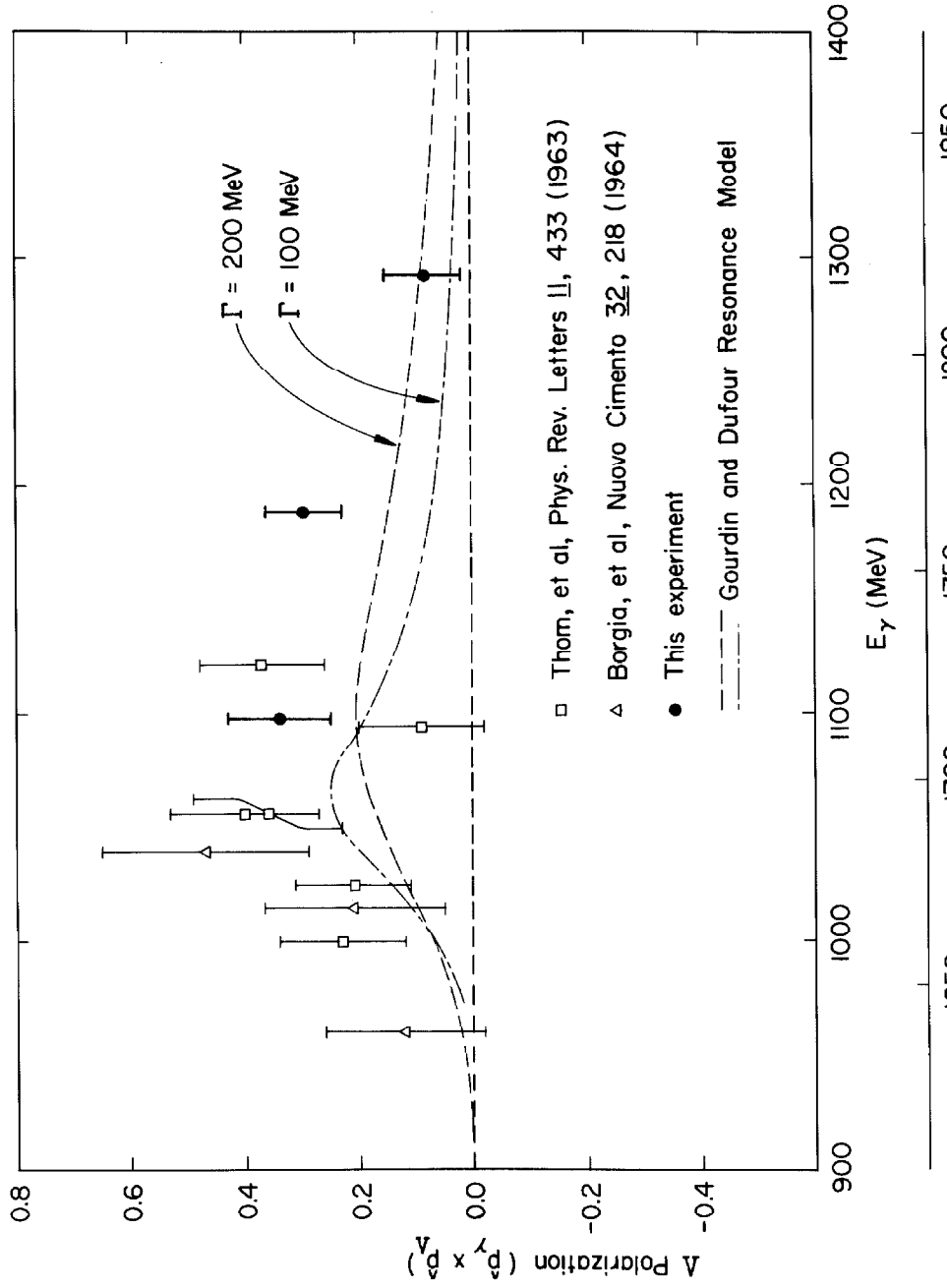

FIGURE 19. The Polarization of Photoproduced Λ Hyperons $\theta_{c.m.} = 90^{o}$.

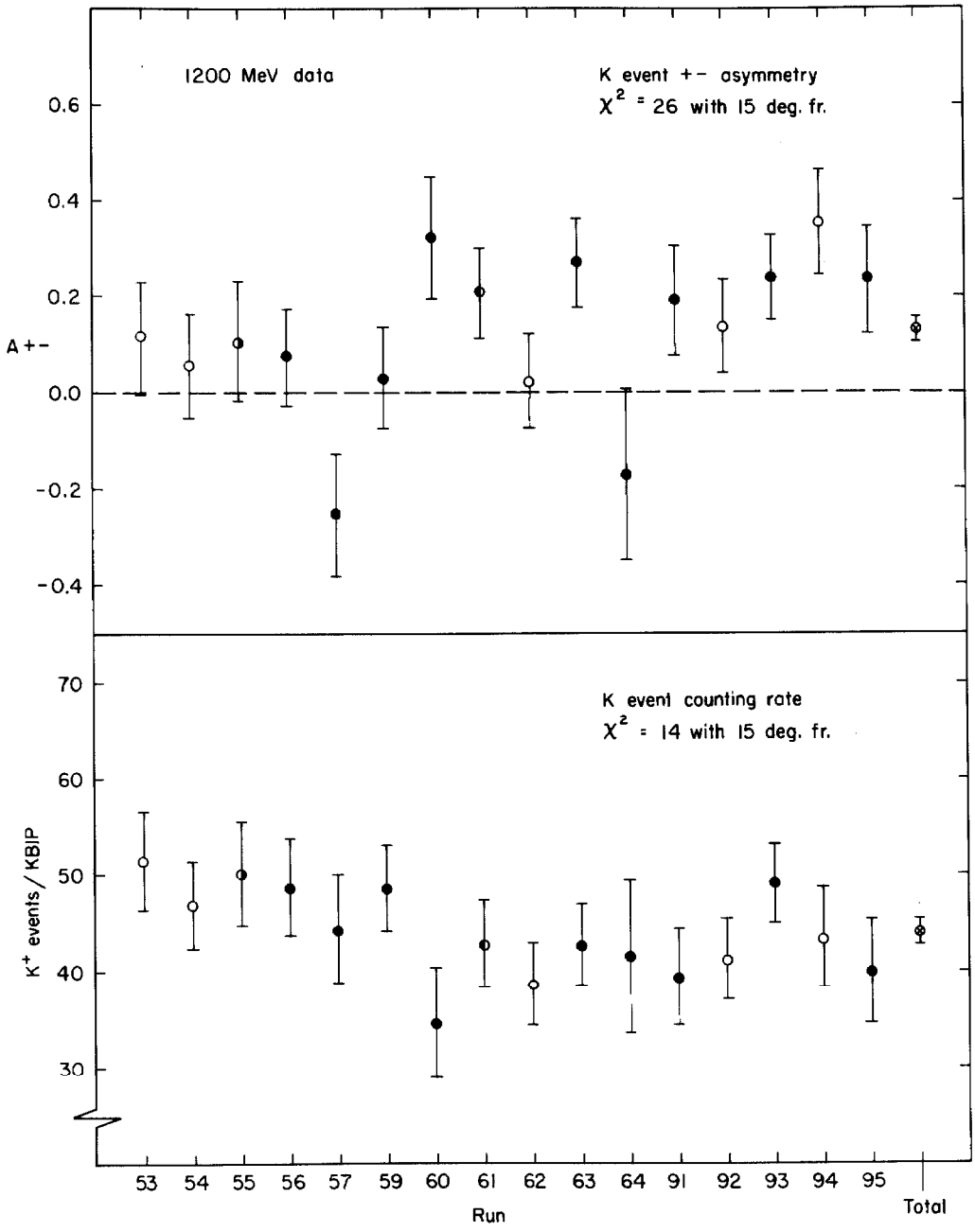

FIGURE 20. Run Dependence of Kaon + - Asymmetry and Counting Rate.

Each point is based upon 60 - 100 events, so that nearly normal statistics obtain, as indicated by the bars. For comparison purposes, the AB asymmetries observed for several types of non-kaon events are plotted in Figure 21. The striking feature of the kaon A_{+-} data is the large scatter of the points. Statistically, such a scatter should occur less than 3% of the time. Similar results were obtained for the other data points.

No satisfactory explanation for the scatter has been found. Most mechanisms which suggest themselves would produce an observable effect either in the counting rate or in the various background asymmetries, and all of these appear to be well behaved. If the errors were 20% - 30% larger, the scatter would be reasonable; however, there is no a priori reason to do this. Evidently sources of fluctuation exist which we have not discovered.

3.6 Discussion

The results of this experiment, particularly when combined with those of other groups, indicate a quite large (~ 0.35) polarization in the vicinity of $E_\gamma = 1100$ MeV. There is also some evidence, based chiefly upon a single point at 1300 MeV, that at higher energies the polarization decreases. Thus, although no enhancement of the cross section occurs at this energy, a bump in the polarization, centered at 1050 MeV or a total energy of 1690 MeV, is strongly suggested.

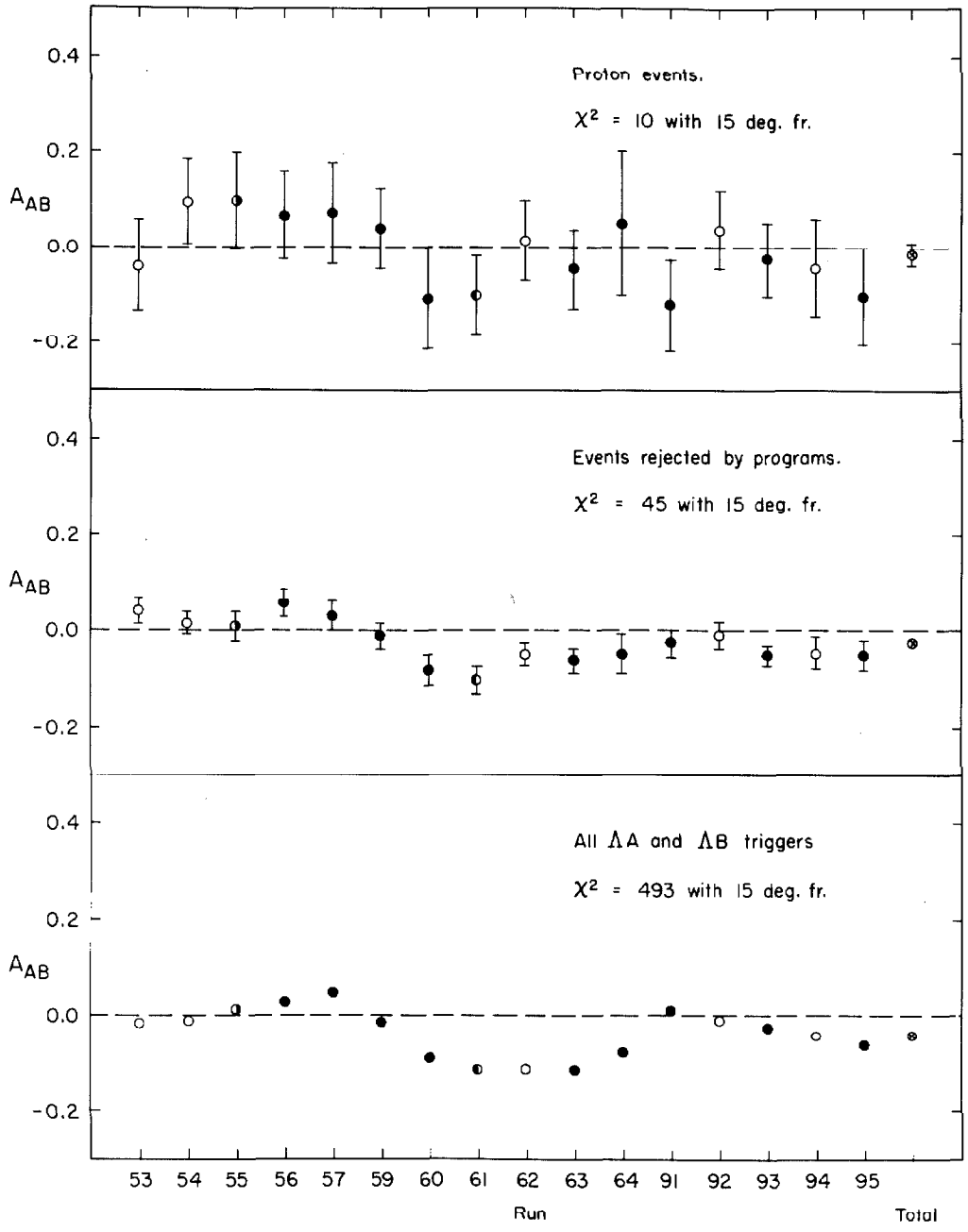

FIGURE 21. Run Dependence of Accidental AB Asymmetries.

Effects of the third resonance* are to be expected in K photoproduction for several reasons. The cross section data for the pionic production

$$\pi^- + p \rightarrow K^o + \Lambda$$

exhibit a broad, pronounced bump in this region. The angular distributions are fit by quadratics in $\cos\theta$ except at the resonant energy, where a cubic term is also necessary[17]. At this energy, the polarization as a function of angle changes sign twice, which is to be expected as the result of an $F_{5/2}$ state interfering with an S state. And finally, the decay

$$N^*_{1/2}(5/2^+, 1688) \rightarrow K + \Lambda$$

evidently has been observed directly[18]. Perhaps the absence of an enhancement of the photoproduction cross section should be more surprising than is the bump in the polarization. Indeed, there is some evidence that the total cross section has decreased at higher energies[19].

The only theoretical attempts to understand the photoproduction results have been the phenomonological resonance models of various authors[20-24]. In all of these models, the amplitude is approximated as the sum of terms arising from single particle and resonance

---

*$N^*_{1/2}(5/2^+, 1688)$. Although most authors assume the $F_{5/2}$ assignment for the third resonance, the πN scattering data also indicate D waves in this region[16].

contributions. C. Peck[6] has examined and experimented with several of these models in some detail, with the conclusion that they have little relevance to the data in the sense that little can be learned from them. For this reason, we have made very little effort to apply them to the polarization data in any detailed way. On the other hand, their statements concerning the polarization should at least be examined; by default they are the best available.

In the context of these models, single particle exchanges result in relatively real contributions to the amplitude, as do resonance exchanges if the energy in question is far from the resonance energy. In the vicinity of a resonance, a relatively imaginary contribution appears, and hence polarization of the hyperon is possible. Kuo[20] and Beauchamp and Holladay[21], for instance, discuss a model in which the polarization arises through the interference of a somewhat mysterious $p_{1/2}(1700)$ resonance with other states.* They make a definite polarization prediction; unfortunately, the sign is wrong.

Hatsukade and Schnitzer[22] and Gourdin and Dufour[24] discuss a model in which the polarization arises through interference of the $N^*_{1/2}(5/2^+, 1688)$ with other states. We have been unable to reproduce Hatsukade and Schnitzer's numerical results, using their parameters. Dufour's results[27] are plotted in Figure 19, for two

---

*This resonance was introduced by Kanazawa in a model for pionic $K\Lambda$ production.[25] An alternative explanation of this data is given, e.g., by Rimpault.[26]

widths of the resonance. The SU(3) prediction for the Λ's magnetic moment, $\mu_\Lambda = \frac{1}{2}\mu_n$, was used; other parameters are based upon a least squares fit to all of the presently available cross section data, including Peck's recent data.[5] The cross section at 90°, plotted in Figure 16, was computed with the same parameters (Γ=100 MeV).

These fits are impressive; however, there are two obvious objections to the model. One is evident in Figure 22. Two best fits to the 1200 MeV data are plotted. In one case, the $N^*_{1/2}(5/2^+, 1688)$ resonance is included and in the other case it is not. The qualitatively wrong behavior at forward angles is inherent, if the theory is to yield a non-zero polarization. We have our choice of fitting one or the other. The other objection is the model's inability to predict the cross section at higher energies. Apparently it achieves its fit to the data by a delicate balance of cancellation of various amplitudes. Outside the region fitted, the predicted cross section essentially blows up.

Aside from their comment on particular resonance models, the data do suggest that the existence of polarization is related to the third resonance. If so, it is probably largely the result of interference of the $F_{5/2}$ state with the $S_{1/2}$ amplitude. The angular distribution should exhibit two zeros other than those of $\sin\theta$, with large polarizations of opposite sign at $\sim 35^\circ$ and $\sim 140^\circ$. Even a fairly rough measurement of the angular distribution of the polarization near the resonance energy would serve to confirm or disprove this. In addition, the "bump" nature of the energy distribution

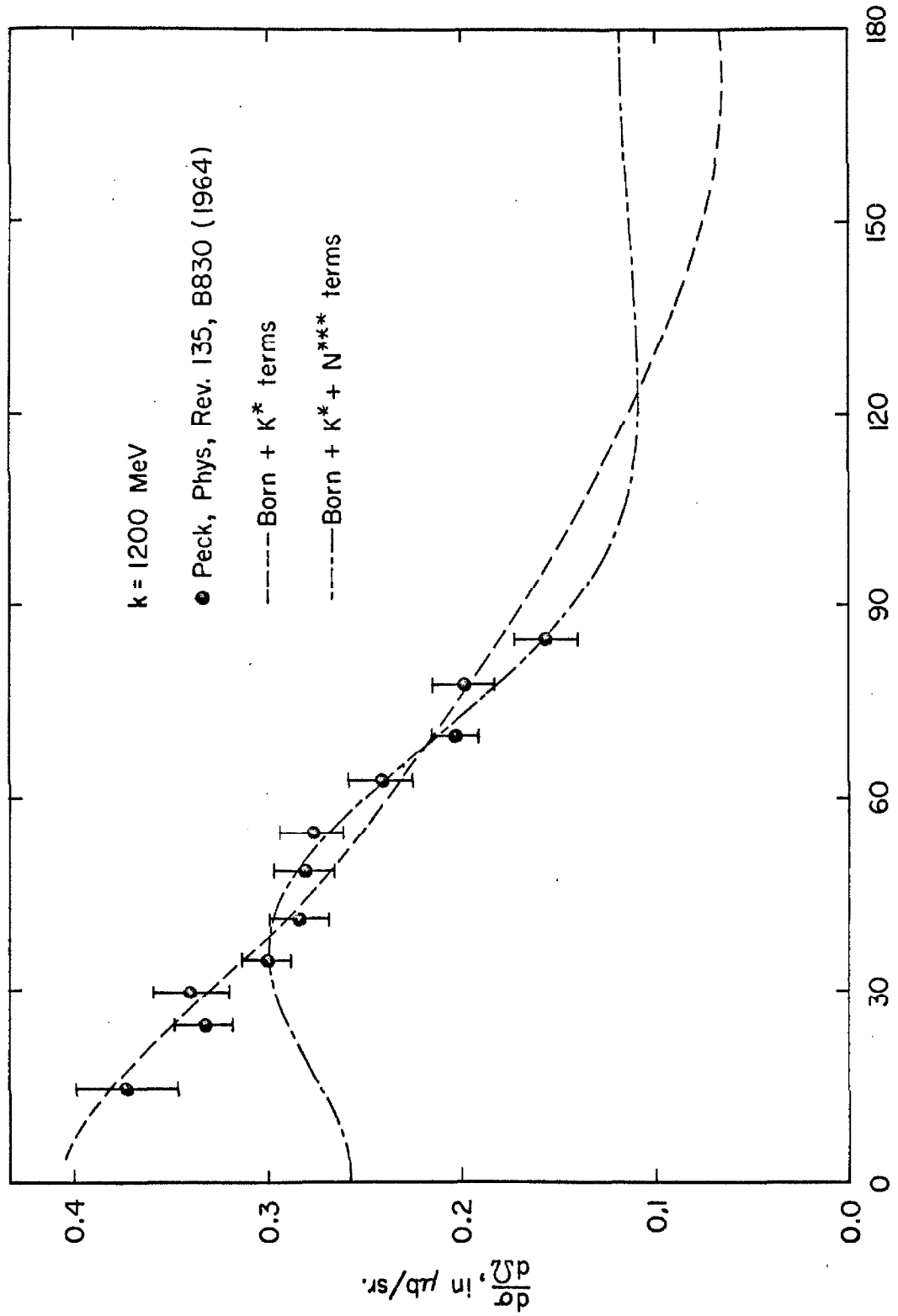

FIGURE 22. Dufour Model Fits to the 1200 MeV Cross Section Data.

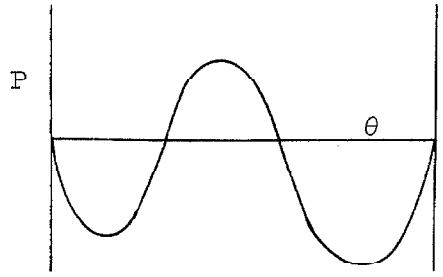

should be confirmed or disproved. Measurements at ($\theta = 35^{o}$, k = 1050 MeV), ($\theta = 90^{o}$, k = 1250 MeV), and ($\theta = 90^{o}$, k = 1350 MeV), which are not unreasonable from an experimental point of view, should serve to settle both of these points.

3.7 Conclusions

The results of this experiment corroborate the evidence of others that photoproduced Λ hyperons exhibit a large polarization in the 1100 MeV region, and suggest that at higher energies the polarization decreases. The only effect of this result is to add some strength to the growing body of evidence that the effects of the third πN resonance are apparent in reactions with a $K\Lambda$ final state.

The range telescope technique used was satisfactory and was rather interesting in its own right, but was probably an unduly complicated kaon detection method. Some of the techniques learned, such as the use of pulse height correlation in the front counters and the use of an on-line computer, will have more general application, but the range telescope as such probably will not.

4 APPENDICES

4.1 Experimental Setup Details

The experiment was done in the south beam of the Caltech electron synchrotron. As with most other experiments done in the laboratory, the particles were produced in a liquid hydrogen target through which passed a bremsstrahlung beam. This beam was produced at a radiator internal to the synchrotron, and after passing through the target it was absorbed by an ionization chamber. The output of this chamber was integrated to provide a monitor of target exposure.

In Figure 1 we have already shown the counter arrays used in the experiment. The relationship of these arrays to the associated hardware is illustrated in Figures 23 and 24.

The beam passed through a rectangular collimator which was placed approximately halfway between the radiator and hydrogen target. The resulting beam was about 1.0" high and 0.8" wide at the target, with a distribution such that the r.m.s. deviation from the mean was about 0.3" in the vertical direction. Various scraping walls and sweeping magnets were used to decrease the number of charged particles, mostly electrons, present in the beam because of interactions with matter along its path.

The liquid hydrogen was contained in a cylinder which was 6" long and 2" in diameter. The end caps were of 0.005" Mylar. The vacuum chamber in which it was mounted had long "snouts" along the

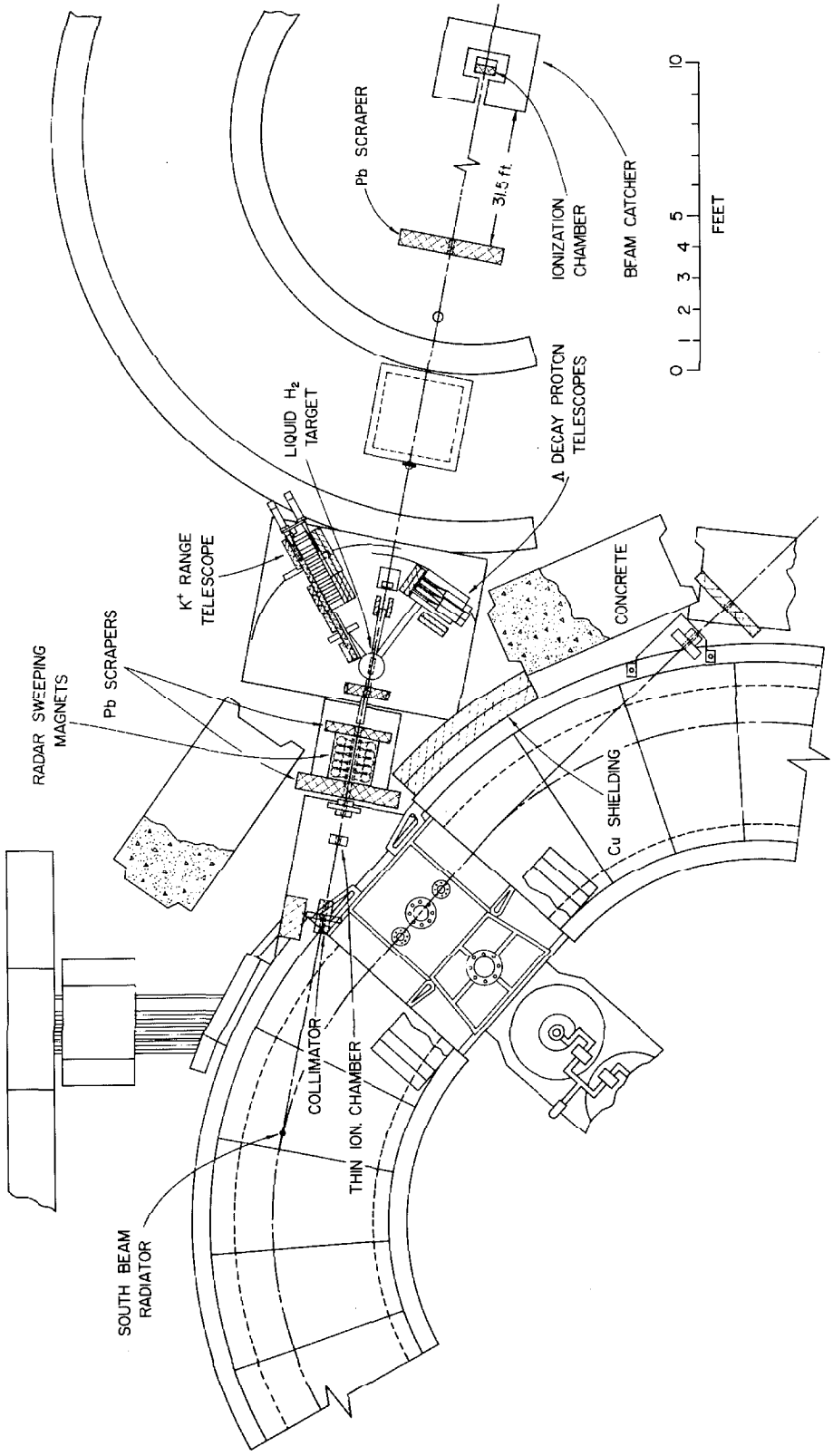

FIGURE 23. South Beam Experimental Area.

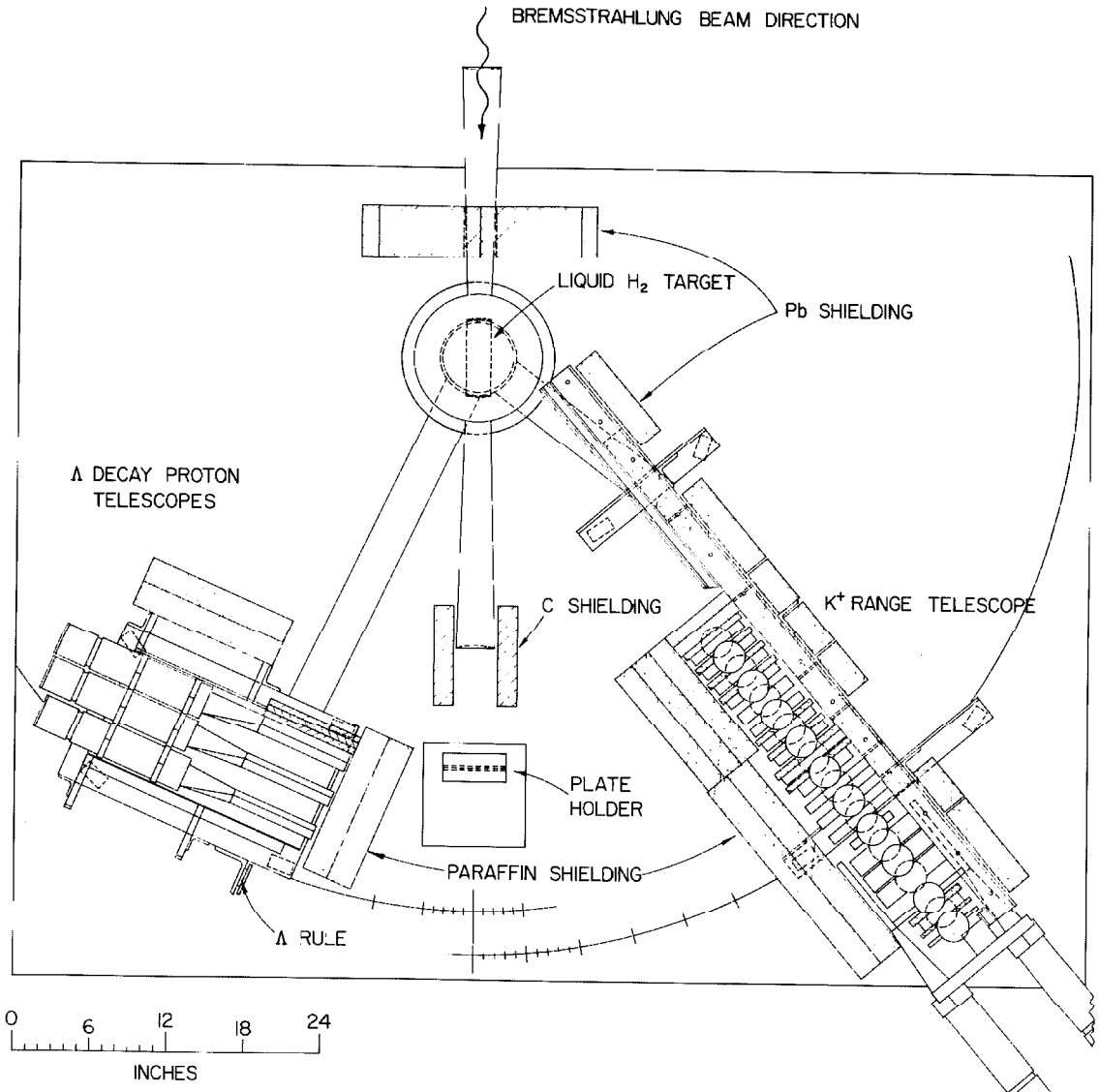

FIGURE 24. Details of the Counter Arrays.

beam line, so that it was geometrically possible to shield counters from particles produced by the beam in passing through the windows.

This target, along with most of the other apparatus peculiar to this experiment, was mounted on a large table which may be seen in the Figures. This table was 21-1/2" beneath the beam line. It consisted of 3/8" sheet of steel, with reinforcing struts underneath, upon which had been poured a "lake" of non-viscous epoxy to achieve a flat, even surface. Protractors, by means of which the counter arrays could be set to the proper angles, were scribed into its surface.

K mesons were detected in a range telescope. This telescope, like the simpler telescopes for the detection of the Λ decay protons, was mounted on a moveable cart so that it could pivot about the target. All counters but the two side counters were viewed by phototubes mounted vertically, alternately above and below the counters.

Protons from Λ decays were detected in counter telescopes which were placed symmetrically above and below the production plane defined by the photon beam and the range telescope. Each consisted of a lucite Čerenkov counter, followed by two scintillators.

The dimensions of all counters used are listed in Table 6. The notation is that of Figures 3 and 5.

The method used to mount 28 of the 30 counters used turned out to be so useful as to deserve description. Two split ring brackets were attached to the 2-5/8" o.d. Shelby tubing which contained the phototube and secured the counter head. To the counter carts were

TABLE 6

Counter Specifications

Counter	Height[a]	Width	Thickness	Material
1	5.0"	5.0"	0.75"	NE 102[b]
2	5.0	5.0	0.75	NE 102
3	5.0	5.0	0.75	NE 102
4	5.0	5.0	0.75	NE 102
$\check{C}1$	6.0	5.0	1.00	UVT Lucite
5	5.0	5.0	0.75	NE 102
6	6.0	5.0	0.75	NE 102
7	6.0	5.0	0.75	NE 102
8	6.0	6.0	0.75	NE 102
$\check{C}2$	6.0	5.0	1.00	UVT Lucite
9	6.0	6.0	0.75	NE 102
10	6.0	6.0	0.75	NE 102
11	6.0	6.0	0.75	NE 102
Aperture	4.0	4.0	0.75	Pilot B[c]
δR1	7.0	6.0	1.50	NE 102
δR2	7.0	6.0	1.50	NE 102
δR3	7.0	6.0	1.50	NE 102
E	8.0	7.0	0.50	NE 102
Cal.1	5.0	4.0	0.75	Pilot B
Cal.2	7.0	5.0	0.25	?(Scintillator)
L	8.0	7.0	0.50	NE 102
R	8.0	7.0	0.50	NE 102
Each Λ decay proton telescope: $\check{C}$	6.0	7.5	1.00	UVT Lucite
Each Λ decay proton telescope: Sc.1	6.0	7.5	0.50	SC 700[d]
Each Λ decay proton telescope: Sc.2	5.5	7.0	0.50	SC 700

(a) Height with respect to the laboratory. The orientation with respect to the phototube may be obtained from Figure 24.

(b) Nuclear Enterprises Ltd., Plastic Scintillator NE 102.

(c) Pilot Chemicals, Inc., Pilot Scintillator B.

(d) Isotopes, Inc., SC 700 Scintillator Plastic.

attached pairs of rails. A counter was placed on the rails and a screw tightened if desired. Counters could be moved, removed, or accurately positioned very easily. The scheme is illustrated in the drawing below.

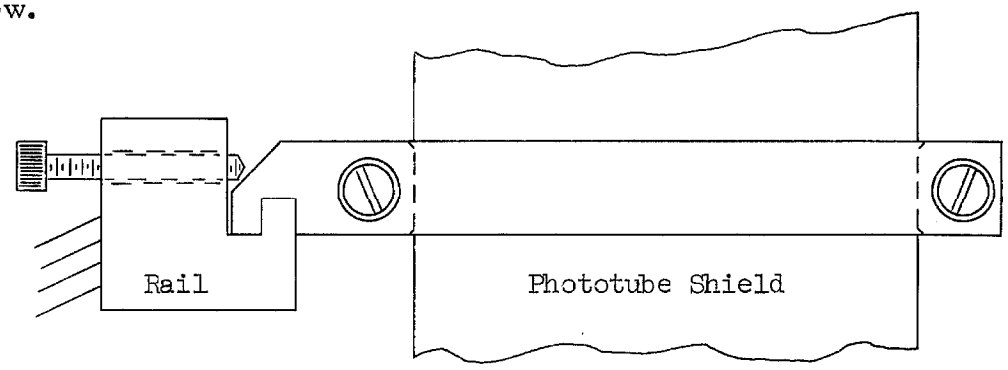

During the earlier stages of the experiment, optical contact between phototube and counter light pipe was made with Celvacene Medium* vacuum grease. It was found that after a year or so the grease fractionated into two components. The low viscosity component wet the region between the counter wrapping and counter, which destroyed the internal reflection characteristics of the counter. Later, seals were made with Shell Epon 828, a transparent epoxy, which was quite satisfactory. Such joints could be broken without destroying either phototube or counter by adroit use of a razor blade and hammer.

Except for scraper walls and a wall on the upstream side of the K^+ telescope, lead was not used as shielding. Paraffin was measurably more effective, evidently because extra-target background sources produced low-energy electrons and photons in such

---

*Consolidated Electrodynamics Corp.

ratio that showers on lead walls counterbalanced its superior absorption properties.

Behind the Λ decay proton telescopes was mounted a Starrett 4 ft. precision rule. This rule was used as the reference for all measurements made on the system.

A plate holder was mounted downstream from the target in such a way that a fiducial plate could be accurately re-positioned in the beam, and photographic plates exposed behind it. The fiducial plate consisted of 0.010" tungsten wire inbedded in a lucite sheet and arranged as shown at left. The symmetry of the pattern was such that from a scanning microphotometer trace of the photographic plate, made in either direction along an x or y coordinate, the orientation of the tracing with respect to the laboratory could be reconstructed.

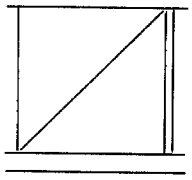

4.2 Range Telescope Design Considerations

4.2.1 Geometry

If a counter telescope is bilaterally symmetric with respect to a polar angle θ_o, then its angular resolution characteristics are determined by two apertures. Let them be half widths a and b, where b > a, and have separation ℓ. Then to first order in angle $\eta = \theta - \theta_o$,

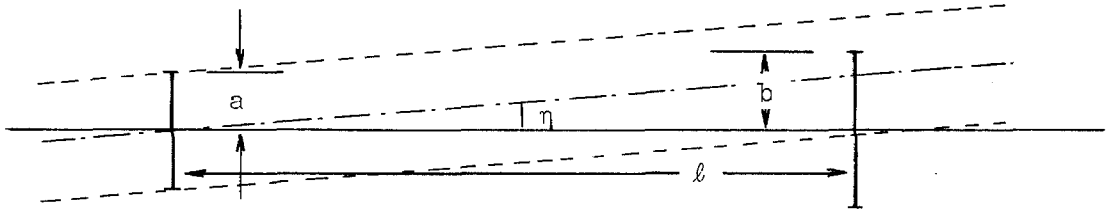

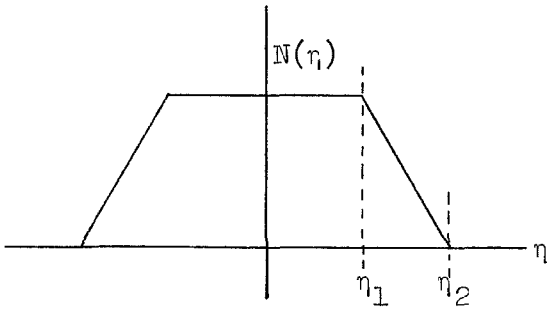

the resolution function is a trapezoid. Its area (or the counting rate) is proportional to ab/ℓ, and the break points of the function fall at $\eta_1 = \frac{b}{\ell} - \frac{a}{\ell}$ and $\eta_2 = \frac{b}{\ell} + \frac{a}{\ell}$. It easily follows that the angular resolution is optimized (e.g. $<\eta^2>$ minimized) at constant counting rate if a = b and ℓ is chosen as large as possible. The latter was accomplished in this experiment by making the front aperture the target itself and the rear aperture the last counter of the slowing section. Since all of the running was to be done near the same laboratory angle (40^o), the first condition could also be satisfied by choosing the target length d such that d sin θ_o was equal to the aperture counter width.

Some dimension is arbitrary, so the target length was chosen

as 6". This meant that the aperture was 4" wide. The target-aperture separation was originally chosen as 36", but an increase of beam intensity permitted us to increase the resolution by changing the separation to 49". Considerations of the up-down Λ decay asymmetry measurement led us to choose the width of the aperture in the azimuthal direction as 4" also.

4.2.2 Multiple Scattering

The trapezoidal or nearly triangular resolution function is smeared as the result of multiple scattering in the matter between the target and rear aperture. Most of this matter consists of the other counters and absorber. If these scatterers are sufficiently wide, as many particles scatter into the aperture as scatter out and the total number of counts in the aperture is unaffected.

In this section we calculate the effect of multiple scattering upon the resolution and estimate the particle loss due to the finite width of scatterers. We assume that the multiple scattering distribution can be approximated by a normal distribution. Following Rossi[28] (eqn. 2.16.7), the projected mean square angle of deflection of a particle of momentum p in traversing a thickness t of material is taken as

$$a^2 = \frac{1}{2}\left(\frac{E_s}{\beta cp}\right)^2 \frac{t}{X_o} \equiv \frac{1}{2}\theta_s^2 t$$

where

$$E_s = 21 \text{ MeV}$$

and X_o is a radiation length in the material. In the case of plastic

scintillator NE 102,

$$X_o = 43.1 \text{ g/cm}^2 .$$

The telescope may be approximated as a series of thin scatterers. Let α_i^2 be the projected mean square scattering angle of a particle

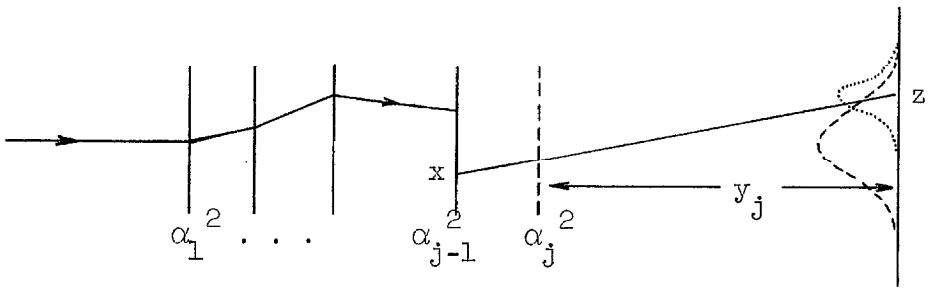

in the i^{th} scatterer, and let y_i be the distance from it to the aperture. Then the particle distribution on the plane of the aperture is normal with a second moment

$$Y^2 = \sum y_i^2 \alpha_i^2 .$$

We may prove this statement as follows. Let the scatterers $j, j+1, \ldots, n$ be removed. Assume that the scatterers $1, 2, \ldots, j-1$ produce a normal distribution of mean square width Y_{j-1}^2 on the plane of the aperture. Now consider a beam of particles which emerge from a point x on the $j\text{-}1^{th}$ scatterer and are incident at a point z on the aperture plane. The effect of adding the j^{th} scatterer is to normally distribute this beam with mean square width $\alpha_j^2 y_j^2$ about z. This is true of any point x, so it is true for all particles which would have been incident at z in the absence of the j^{th} scatterer. z was

arbitrary. Thus, the net effect of adding the j^{th} scatterer is to fold its contribution into the total distribution:

$$Y_j^2 = Y_{j-1}^2 + a_j^2 y_j^2$$

Then by induction, we obtain the result stated above.

As an example, let us calculate the spatial distribution of an initially collimated beam as it emerges from an absorber of thickness x. Let us assume that energy loss in the absorber is negligible. We break up the absorber into planes of thickness $\Delta = \frac{x}{n}$; then

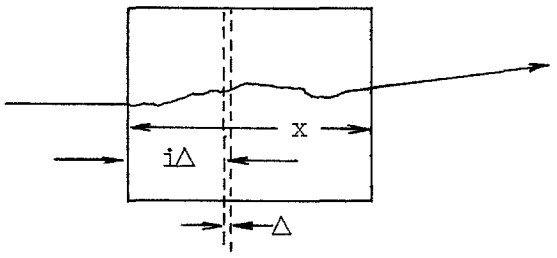

$$a_i^2 = \frac{1}{2}\theta_s^2 \Delta$$

$$y_i = (n - i)\Delta$$

and

$$Y^2 = \frac{1}{6}\theta_s^2 x(1 + \frac{1}{n})(1 + \frac{1}{2n}) \xrightarrow[n \to \infty]{} \frac{1}{6}\theta_s^2 x,$$

which agrees with Rossi's[28] result (eqn. 2.17.12).

We obtain a value of 1.60 cm. for Y for the telescope in the 1200 MeV configuration, assuming a kaon beam stopping at the center of δR2. As might be expected, Y grows more or less linearily with depth; it is 1.43 cm. at counter 11.

The resolution and efficiency corrections may now be calculated. First, let us consider the counters between the target and rear aperture as sufficiently wide that no particles are lost. Let us assume

that the front aperture is of width 2a, the rear one of width 2b, and that they are a distance ℓ apart. A particle beam passing through a

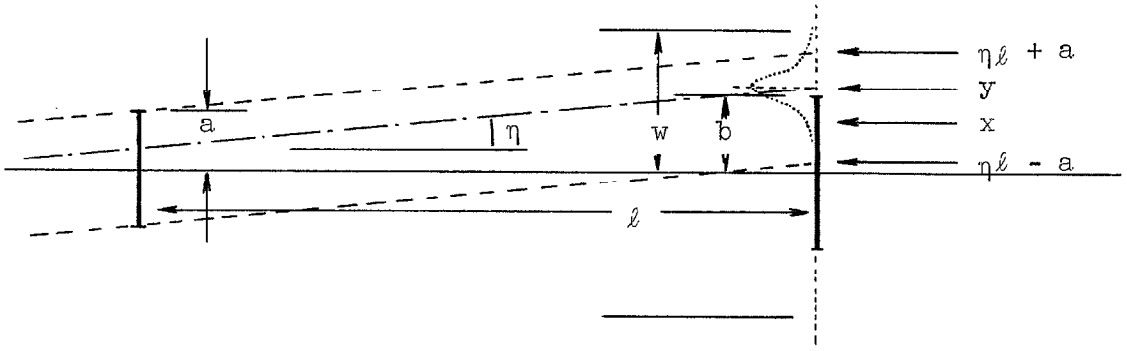

point on the front aperture at an angle η with the central angle gives rise to a distribution of width Y centered at a point y on the plane of the rear aperture. A fraction

$$\int_{-b}^{b} \frac{1}{\sqrt{2\pi}\,Y} e^{-\frac{(x-y)^2}{2Y^2}} dx$$

of the particles pass through the rear aperture. Integrating over all possible positions on the front aperture, we then obtain

$$N(\eta) = \int_{\eta\ell - a}^{\eta\ell + a} \int_{-b}^{b} \frac{1}{\sqrt{2\pi}\,Y} e^{-\frac{(x-y)^2}{2Y^2}} dx\, dy\,.$$

Here the normalization is such that $\int N(\eta)\, d\eta = 4ab/\ell$.

It is convenient to define the function

$$F(x) = \frac{1}{\sqrt{2\pi}} e^{-x^2/2} - x\int_{x}^{\infty} \frac{1}{\sqrt{2\pi}} e^{-z^2/2} dz,$$

and to note that

$$F(-x) = x + F(x)$$

Then the above integral is simply

$$N(\eta) = Y \left\{ F\left(\frac{\eta\ell + a + b}{Y}\right) + F\left(\frac{\eta\ell - a - b}{Y}\right) - F\left(\frac{\eta\ell + a - b}{Y}\right) - F\left(\frac{\eta\ell - a + b}{Y}\right) \right\}$$

This function is interesting in that it is an analytic representation for a trapezoid with rounded corners.

For our purposes here, only the case $a = b$ is of interest:

$$N(\eta) = Y \left\{ F\left(\frac{\eta\ell + 2a}{Y}\right) - 2F\left(\frac{\eta\ell}{Y}\right) + F\left(\frac{\eta\ell - 2a}{Y}\right) \right\}$$

This function is plotted in Figure 25 for the case $Y = 0.4a$. We see that the half width at half maximum is about 16% greater than in the $Y = 0$ case. For $Y = 1.60$ cm. and $2a = 4"$, the width of the resolution function is 13% greater than in the $Y = 0$ case.

So far, we have assumed that for any y, particles were normally distributed about y with width Y, and hence with some probability would pass through the aperture. But if a particle's traverse position is beyond a counter edge, it cannot scatter back into the system. It is difficult to take this into account exactly, but a reasonable approximation can be made by introducing a cutoff at $\pm w$ in the y integration. w is to be roughly identified with the half width of counters near the

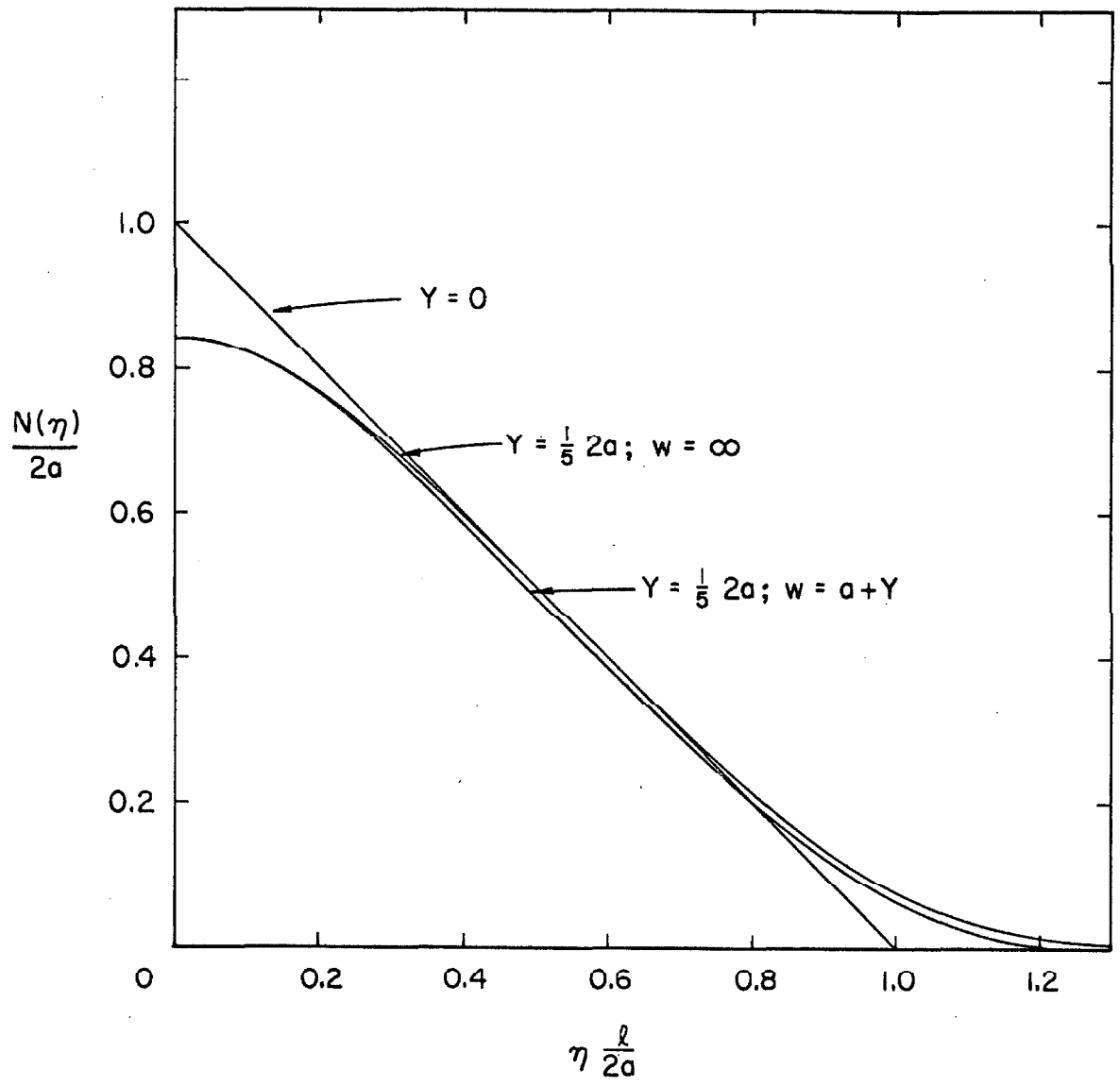

FIGURE 25. The Effect of Multiple Scattering upon a Triangular Resolution Function.

rear of the system. The integral is as before, except that y runs from the greater of $-w$ and $\eta\ell - a$ to the lesser of w and $\eta\ell + a$.

The result is plotted in Figure 25 for the case $Y = \frac{1}{5}\,2a$, $w - a = Y$. The integral under the curve is 3% less than in the $w - a \gg Y$ case.

On the basis of such considerations, it was clear that as long as counters immediately in front of the aperture satisfied the condition $w - a \geq Y$, the multiple scattering loss would be within acceptable bounds. We chose $w - a = 1''$ $(1.6\,Y)$ on all sides. The area loss in $N(\eta)$ is 1%. The same thing happens in the azimuthal direction, so our net multiple scattering efficiency loss is of the order of 2%.

4.2.3 Electronic Selection Requirements

As originally planned, pions and protons, which were 500 to 1000 times more abundant than kaons in the telescope, were to be largely eliminated by electronic selection. This was necessary so that the pulse height analyzer triggering rates would be reasonable. A factor of 50 to 100 would be quite sufficient for this purpose. The discrimination was to have been achieved by means of bias "windows" on counters in the front section of the telescope.

It was necessary to decide upon the number of counters to be used for this discrimination and to estimate the efficiencies for kaon acceptance and unwanted particle rejection. Let $P_K(L)$ be the expected integral pulse height distribution for kaons. For n identical $\frac{dE}{dx}$ counters, a fraction $\left[1 - P_K(L)\right]^n$ are lost if an upper limit of L is set on the pulse height. On the other hand, a fraction $\left[P_p(L)\right]^n$

protons, from a distribution $P_p(L)$, are accepted. The observed pulse height spectra were empirically fitted by smooth distributions to obtain approximations to the true $P_K(L)$ and $P_p(L)$, and efficiencies were calculated by this method. Results of such a calculation for a configuration similar to that used at 1300 MeV are illustrated in Figure 26.

Because approximations were made as to the form of the pulse height distributions and the counters were taken as identical, the results were not intended to be very accurate. But it was evident that with 7 to 9 $\frac{dE}{dx}$ counters, a workable level of discrimination could be obtained. Provision was thus made for windows on 8 front counters. It was also evident from these considerations that proton contamination would be more severe than pion contamination.

The procedure of setting fixed biases on the pulse heights of each counter works only for particles of fixed range. The variation of mean pulse height with range can be eliminated to first order by discriminating on a signal to which has been added a small fraction of the light output of the stopping section:[29]

$$L_i' = L_i + a_i \sum_{\substack{\text{Stopping} \\ \text{Section}}} L_j$$

The a_i can be chosen so that L_i' is relatively independent of the particle's range. Provision for this "δR feedback" scheme was therefore also built into the electronics.

The weak point of this entire scheme concerned stability. It

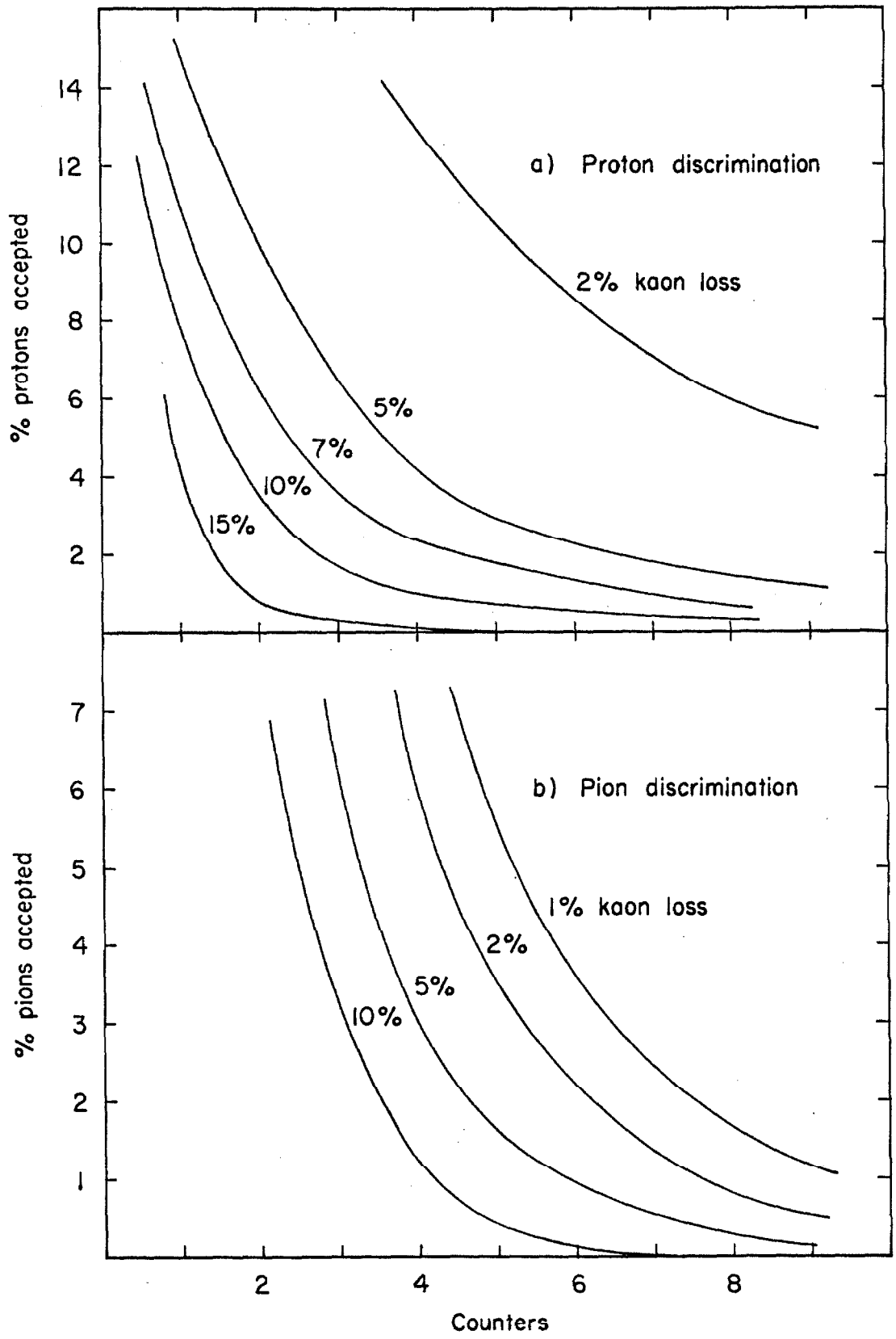

FIGURE 26. Discrimination Levels Achieved by n Counters.

was not surprising that the derivative of kaon detection efficiency with bias setting was quite large except for settings very far from the kaon peak, and the electronics was built with sufficient stability to handle the problem. However, we did not know in advance that phototubes were, by these standards, very unstable devices. With biases set close enough to the kaon peak to ensure good proton and pion discriminations, normal phototube gain drifts introduced large and incalculable kaon efficiency corrections.

These problems turned out to be minor compared to the computer's discrimination problem, which arose because of large background rates. The solution to both was to require the Λ decay proton signature. With the electronic discrimination requirements very much relaxed, very wide bias windows could be used. In practice, the windows cut counting rates by a factor of 10 rather than a factor of 100.

4.2.4 Other Considerations

The thickness of the stopping section was chosen by imposing the requirement

$$\left.\frac{\partial k}{\partial \theta}\right|_{\theta_o} \Delta\theta = \left.\frac{\partial k}{\partial T_K}\right|_{T_{Ko}} \Delta T_K$$

which permitted the energy resolution to be minimized for a fixed counting rate. To the approximations that the angular resolution function is triangular and that $\frac{\partial k}{\partial \theta}$ and $\frac{\partial k}{\partial T_K}$ are constants over the

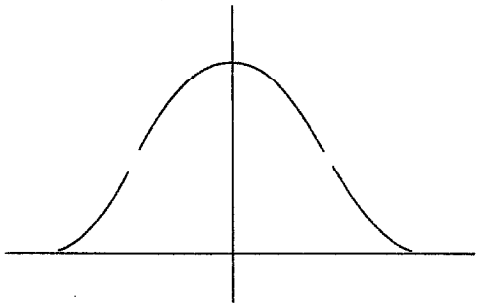

acceptance range, the photon energy resolution function was then piecewise parabolic, as illustrated at left, with a full width at half maximum of $\frac{\partial k}{\partial T}_K \Delta T_K$. The required stopping section thickness was 12 g/cm^2, or 4.5" of scintillator. For reasons having to do with phototube placement, it was broken into 3 counters, each 1.5" thick.

For the lowest energy point (k =1100 MeV), the telescope was to be almost entirely scintillator. Therefore, 0.75" was chosen as a counter thickness. This left room for two counters between the front and stopping sections. At higher energies, two more were added, for a total of 15 scintillators to the end of the stopping section.

The side counters were redundant, as far as the logic was concerned, but it was felt that they would provide useful information. There was no attempt to optimize their detection efficiency; they were just large scintillator slabs which occupied about $\frac{4\pi}{3}$ sr. as seen from the stopping section.

4.3 Λ Decay Proton Telescope Design Considerations

The statistical problem associated with the two-counter Λ decay asymmetry measurement may be phrased as follows: Suppose a large urn contains a fraction $\frac{1+p}{2}$ of "up" (+) protons and a fraction $\frac{1-p}{2}$ of "down" (-) protons. What is the probability that if N protons are chosen at random from the urn that N_+ of them are "up" protons? This is the usual binomial distribution problem, with the solution

$$P(N_+ \,|N) = \binom{N}{N_+}\left(\frac{1+p}{2}\right)^{N_+}\left(\frac{1-p}{2}\right)^{N_-} .$$

Either from the characteristic function or from a maximum likelihood approach we may obtain the moments

$$\mu_1 = N\left(\frac{1+p}{2}\right)$$

and

$$\mu_2 = N\left(\frac{1+p}{2}\right)\left(\frac{1-p}{2}\right).$$

We are more interested in the distribution of the quantity $m = N_+ - N_-$, which can be written as

$$P\left(N_+ = \frac{m+N}{2} \,|N\right) = \binom{N}{\frac{N+m}{2}}\left(\frac{1+p}{2}\right)^{\frac{N+m}{2}}\left(\frac{1-p}{2}\right)^{\frac{N-m}{2}} .$$

Calculating the moments as above we obtain

$$\frac{N_+ - N_-}{N_+ + N_-} \equiv A_{+-} = p \pm \frac{1}{\sqrt{N}}\sqrt{1-p^2}$$

In the notation of section 3.1, $p = \alpha PG$, and $N = Fn_K$. The above expression becomes

$$P = \frac{1}{\alpha G} A_{+-} \pm \frac{1}{\alpha\sqrt{n}} \frac{1}{G\sqrt{F}} \sqrt{1 - A_{+-}^2} \quad .$$

Since G is the average value of $\cos\theta$ in one hemisphere, we have

$$1 \geq G \geq \frac{1}{2} .$$

We also know that $\alpha \approx 0.62$.[13] P is expected to be 0.4 or less, so that

$$1 \geq \sqrt{1 - A_{+-}^2} \geq 0.97 \quad .$$

Thus, $\sqrt{1 - A_{+-}^2}$ may be taken as 1 for all practical purposes. n_K is proportional to machine running time. Then to obtain a polarization measurement with a given statistical error in the shortest possible time, counter geometry must be chosen so that the quantity $\frac{1}{G\sqrt{F}}$ is minimized.

In addition, the geometry should be chosen so that the sensitivity of the result to errors in counter position is small. Let us choose a coordinate system with its z axis along the Λ momentum direction and its y axis normal to the production plane. Then if counters are placed symmetrically about the y axis in the xy plane, it is clear that to first order errors due to displacements in x vanish. But if both counters are displaced a distance δy along the y axis, we obtain

$$A_{+-}' = A_{+-} + \delta y \frac{1}{F}\left(\frac{\partial F}{\partial y} - \alpha^2 P^2 \frac{G}{F} \frac{\partial(FG)}{\partial y}\right) \quad .$$

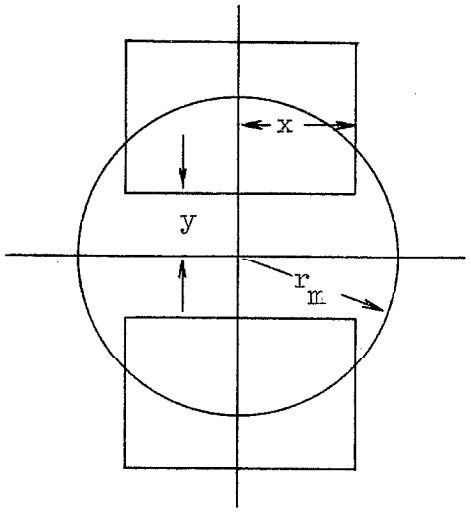

The second term in the brackets turns out to be small relative to the first. In addition to working near the minimum of $\frac{1}{G\sqrt{F}}$, it would be convenient if $\frac{1}{F}\frac{\partial F}{\partial y}$ were small also.

These quantities have been computed for the central kinematics case (i.e. without integrating over the kinematic acceptance region, target length, etc.) as functions of counter size in two directions. It was found that the results for different operating points more or less scale into each other if the dimensions are divided by r_m, the radius of the base of the Λ decay cone. The statistical error was minimized for

$$\begin{cases} x/r_m = 1.0 \\ y/r_m \approx 0.3 \, . \end{cases}$$

The results were flat enough that conditions were quite adequate for

$$\begin{cases} x/r_m \geq 0.5 \\ y/r_m \leq 0.6 \, . \end{cases}$$

The quantity $\frac{1}{F}\frac{\partial F}{\partial y}$ was minimized for

$$\begin{cases} x/r_m = 0 \\ y/r_m = 0 \, , \end{cases}$$

but again, things were reasonable for

$$\begin{cases} x/r_m \leq 0.8 \\ y/r_m \leq 0.3 \ . \end{cases}$$

With these numbers as guides to the correct vicinity for operation, calculations were made in which F and G were also averaged over the range of acceptance of the system -- i.e. the K^+ telescope aperture size and energy acceptance region and the target length. The integrals over these variables were done by a Simpson's method. The degradation of the system's analyzing power with increasing size of the K^+ telescope aperture in the azimuthal direction was examined; a 4" or 5" high aperture was found to be adequate.

It was also desirable to make the decay proton telescope counters as small as possible, because of the expected high counting rate problem. In addition, it was desirable that the same counters be used for all of the operating points. When all of this was put together, the result was a proton telescope aperture 7" wide, 5.5" high, and 40" from the target.

The Λ particle normally travelled about 6 cm. before decaying. This meant a correction of about 1% for G, which was neglected.

An illustration of the above calculation is given in Figure 27. Here we have taken the counter size and position as above and computed the relevant quantities as functions of y for our 1200 MeV operating conditions. The operating point was chosen at $y/r_m = 0.4$. Here,

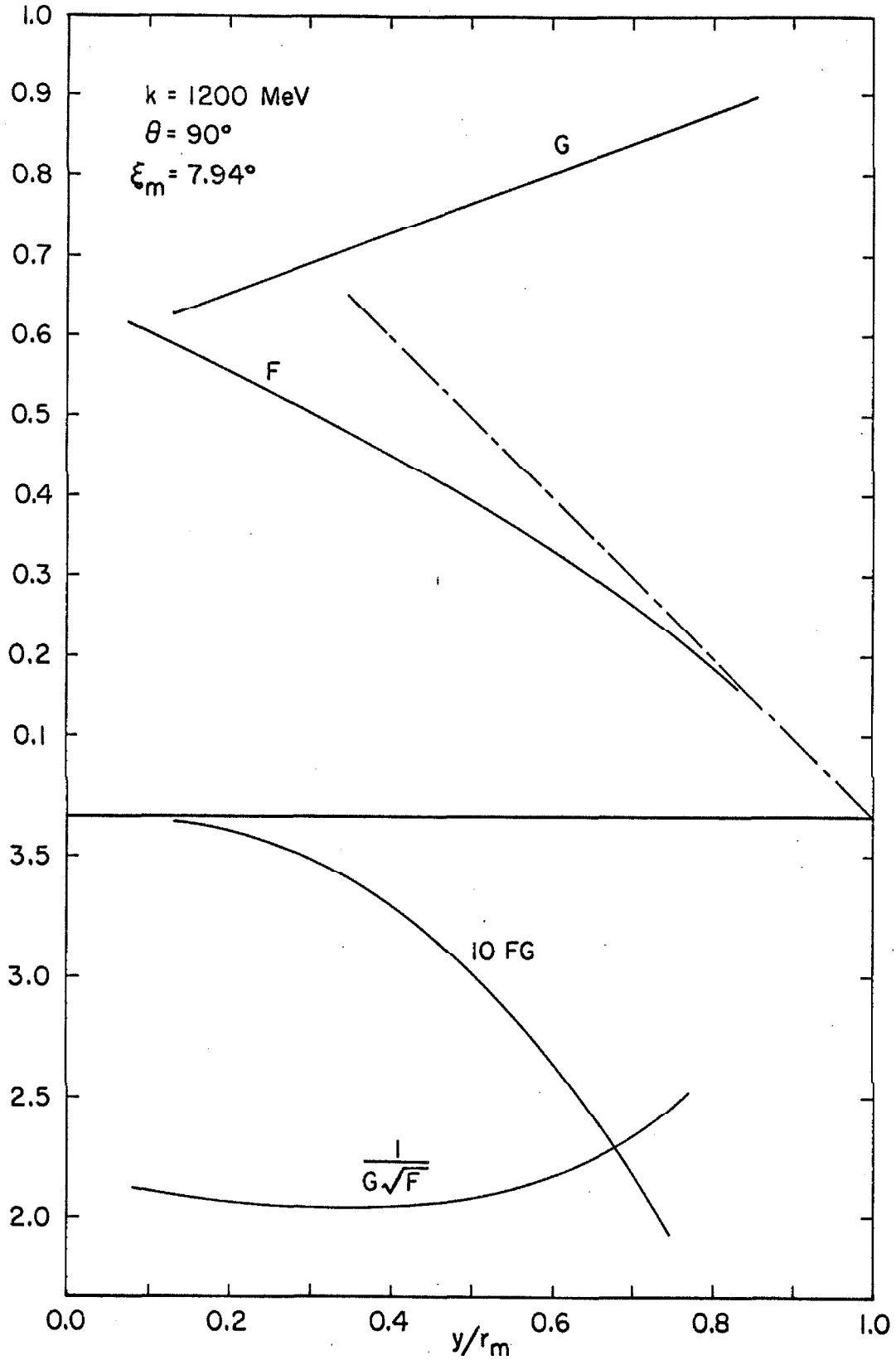

FIGURE 27. Dependence of Parameters Related to the Polarization Measurement upon Counter Position.

$$F = 0.451$$

$$G = 0.731$$

and thus

$$P = 2.21\, A_{+-} \pm \frac{2.21}{\sqrt{N}} \quad .$$

Evaluating the derivatives with respect to vertical position, we obtain

$$A_{+-}' = A_{+-} + 2.2\ \delta y(2.68 + 0.32\, P^2)$$

for the sensitivity to a vertical positioning error δy. If, for example, $\delta y = 0.1''$, we have

$$A_{+-}' = \alpha G(P + 0.05) \ .$$

The actual alignment errors found and their effect upon the polarization measurement were discussed in section 3.3.

4.4 The Distribution of the Sum of Squares of Normal Variables about a Point Other than the Mean.

In the analysis of this experiment, we have discriminated against unwanted particles by placing an upper limit S' on the parameter

$$S = \sum_{i=1}^{n} \left(\frac{L_i - L_{io}^K}{0.1\, L_{io}^K} \right)^2 .$$

S was approximately χ^2 distributed for the desired events, and the fraction satisfying the condition $S < S'$ could be estimated. But to obtain the discrimination efficiency against unwanted particles, we must know something about the distribution of S when the L_i are chosen from another distribution, e.g. one whose means are $L_{io}^P \neq L_{io}^K$.

The pulse height distributions were sufficiently normal that we may replace the problem with that of finding the probability distribution of

$$\rho^2 = \sum_{i=1}^{n} \left(\frac{y_i - a_i'}{\sigma_i} \right)^2$$

where y_i is normal (a_i, σ_i), and $a_i \neq a_i'$. We redefine the variables so that

$$\rho^2 = \sum_{i=1}^{n} (x_i - \delta_i)^2 ,$$

where x_i is normal $(0,1)$. It will also be useful to introduce the quantity

$$\delta^2 = \sum_{i=1}^{n} \delta_i^2$$

since as it will turn out, only this combination of the δ_i or its square root will enter. We also define the required probability distribution as

$$L_n(\rho^2, \delta)$$

and note that

$$L_n(\rho^2, 0) = K_n(\rho^2) ,$$

the familiar χ^2 distribution.(30)

The characteristic function of the required distribution is easily found to be

$$\varphi(t) = (1 - 2it)^{-\frac{n}{2}} \exp\left(\frac{it\delta^2}{1 - 2it}\right) .$$

The inversion problem is formidable, but from the function we can obtain the mean and variance of the distribution:

$$\mu_1 = n + \delta^2$$

$$\mu_2 = 2n + 4\delta^2$$

We proceed to find the explicit form of $L_n(\rho^2, \delta)$ by noticing a geometrical interpretation for the problem. Let $\vec{x} = \{x_i\}$ be a point in an n-dimensional space. The probability of a measurement giving $\vec{x}$ in a volume $dV = \prod_{i=1}^{n} dx_i$ is then

$$\prod_{i=1}^{n} \left(\frac{1}{\sqrt{2\pi}} e^{-x_i^2/2} dx_i \right) = (2\pi)^{-n/2} e^{-r^2/2} dV$$

where

$$r^2 = \sum_{i=1}^{n} x_i^2 .$$

Thus, the frequency function is simply $(2\pi)^{-n/2} \exp\left(-\frac{r^2}{2}\right)$. To find the appropriate probability distribution we need only to integrate the frequency function over the appropriate volume. In the usual χ^2 case, we obtain

$$K_n(\chi^2) = \int (2\pi)^{-n/2} e^{-r^2/2} dV ,$$

where the integral is over a sphere of radius χ centered at the origin. Noting that $dV \propto r^{n-1} dr$ and normalizing so that $K_n(\infty) = 1$, we obtain

$$K_n(\chi^2) = \int_0^{\chi} \frac{r^{n-1} e^{-r^2/2}}{2^{(n/2-1)}\Gamma(n/2)} \, 2 \, dr .$$

The problem at hand is similar, except that the appropriate volume is the sphere of radius ρ, centered at $\vec{\delta} = \{\delta_i\}$. This time, it is convenient to use as a volume element the cap whose thickness is dr and whose area is that portion of the spherical surface with radius

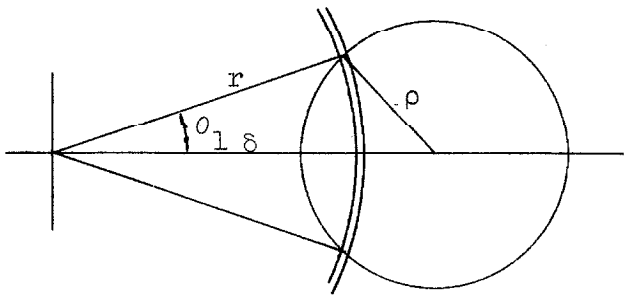

r centered at the origin which is contained within the sphere of radius ρ centered at $\vec{\delta}$. Choosing $\vec{\delta}$ along the polar axis of a generalized spherical polar coordinate system, we find

$$dV \propto r^{n-1} \int_o^{\theta_1} \sin^{n-2}\theta \, d\theta$$

for $|\delta - \rho| < r < (\delta + \rho)$ and integral $n \geq 3$.

Here

$$\cos \theta_1 = \frac{\delta^2 - \rho^2 + r^2}{2r\delta} \quad .$$

($n = 0$ and $n = 1$ may be treated as special cases.) We make use of the fact that

$$\int_o^{\pi} \sin^{n-2}\theta \, d\theta = \sqrt{\pi}\, \Gamma\left(\frac{n-1}{2}\right) / \Gamma\left(\frac{n}{2}\right)$$

and normalize as before. The result is

$$L_n(\rho^2, \delta) = \frac{1}{\sqrt{\pi}\, 2^{n/2-1}\, \Gamma\left(\frac{n-1}{2}\right)} \int_{\delta-\rho}^{\delta+\rho} e^{-r^2/2} r^{n-1} \int_o^{\theta_1} \sin^{n-2}\theta \, d\theta \, dr$$

for $(\delta - \rho) > 0$, and

$$L_n(\rho^2, \delta) = K_n((\rho - \delta)^2) + \frac{1}{\sqrt{\pi}\, 2^{n/2-1}\, \Gamma\left(\frac{n-1}{2}\right)} \int_{\rho-\delta}^{\rho+\delta} e^{-r^2/2} r^{n-1} \int_o^{\theta_1} \sin^{n-2}\theta \, d\theta \, dr$$

for $(\delta - \rho) < 0$.

For even n, the angle integral can be eliminated by integrating by parts over r, but the resulting integral is still difficult. For odd n, the angle integral is trivial, and we obtain

$$L_n(\rho^2, \delta) = \frac{1}{2}\left[K_n((\rho+\delta)^2) + \left(\frac{\rho-\delta}{|\rho-\delta|}\right) K_n((\rho-\delta)^2)\right] + \frac{1}{\sqrt{\pi}\, 2^{n/2-1}\Gamma\left(\frac{n-1}{2}\right)} \sum_{i=0}^{n-2} \Gamma(i+1) 2^i f_i(\rho^2, \delta)\left[K_{2i+2}((\rho+\delta)^2) - K_{2i+2}((\rho-\delta)^2)\right]$$

The f_i may be written explicitly for the general case, but they are sufficiently messy that it is easier simply to integrate the case of interest.

The case n = 7, for instance, is of use in the analysis problem. We obtain:

$$f_o = (\delta^2 - \rho^2)^5 f_5$$

$$f_1 = (\delta^2 - \rho^2)^3 f_4$$

$$f_2 = (\delta^2 - \rho^2) f_3$$

$$f_3 = -\frac{1}{28}\left(1 - \frac{(\delta^2 - \rho^2)}{2\rho^2} + \frac{(\delta^2 - \rho^2)^2}{8\delta^4}\right)$$

$$f_4 = \frac{1}{4\delta^3}\left(\frac{1}{3} - \frac{(\delta^2 - \rho^2)}{8\delta^2}\right)$$

$$f_5 = -\frac{1}{160\ \delta^5}$$

The function $L_7(\rho^2, \delta)$ is plotted in Figure 28 for several different δ. The frequency function $\ell_7(\rho^2, \delta) = \frac{d}{d\rho^2} L_7(\rho^2, \delta)$ is plotted in Figure 29.

We are now in a position to apply these results to the problem of particle discrimination. For a proton event fit under a kaon hypothesis, we may rewrite S as

$$S = \sum \left(\frac{L^p_{io}}{L^K_{io}} \frac{r_p}{0.1} \right)^2 \left(\frac{(L_i - L^p_{io}) + (L^p_{io} - L^K_{io})}{r_p L^p_{io}} \right)^2$$

$$S \approx \left[\left(\frac{L^p_{io}}{L^K_{io}} \frac{r_p}{0.1} \right)^2 \right]_{ave} \rho^2$$

where

$$\delta^2 = \sum \left(\frac{L^p_{io} - L^K_{io}}{r_p L^p_{io}} \right)^2 .$$

Here the superscripts label the particle assumed in calculating the L_{io}.

For our 1100 MeV point seven $\frac{dE}{dx}$ counters were used, and the above analysis is applicable. We find

$$S \approx 0.60\ \rho^2$$

and

$$\delta^2 = 74 .$$

Then

$$\mu_1 = 81$$

$$\sqrt{\mu_2} = 17.5$$

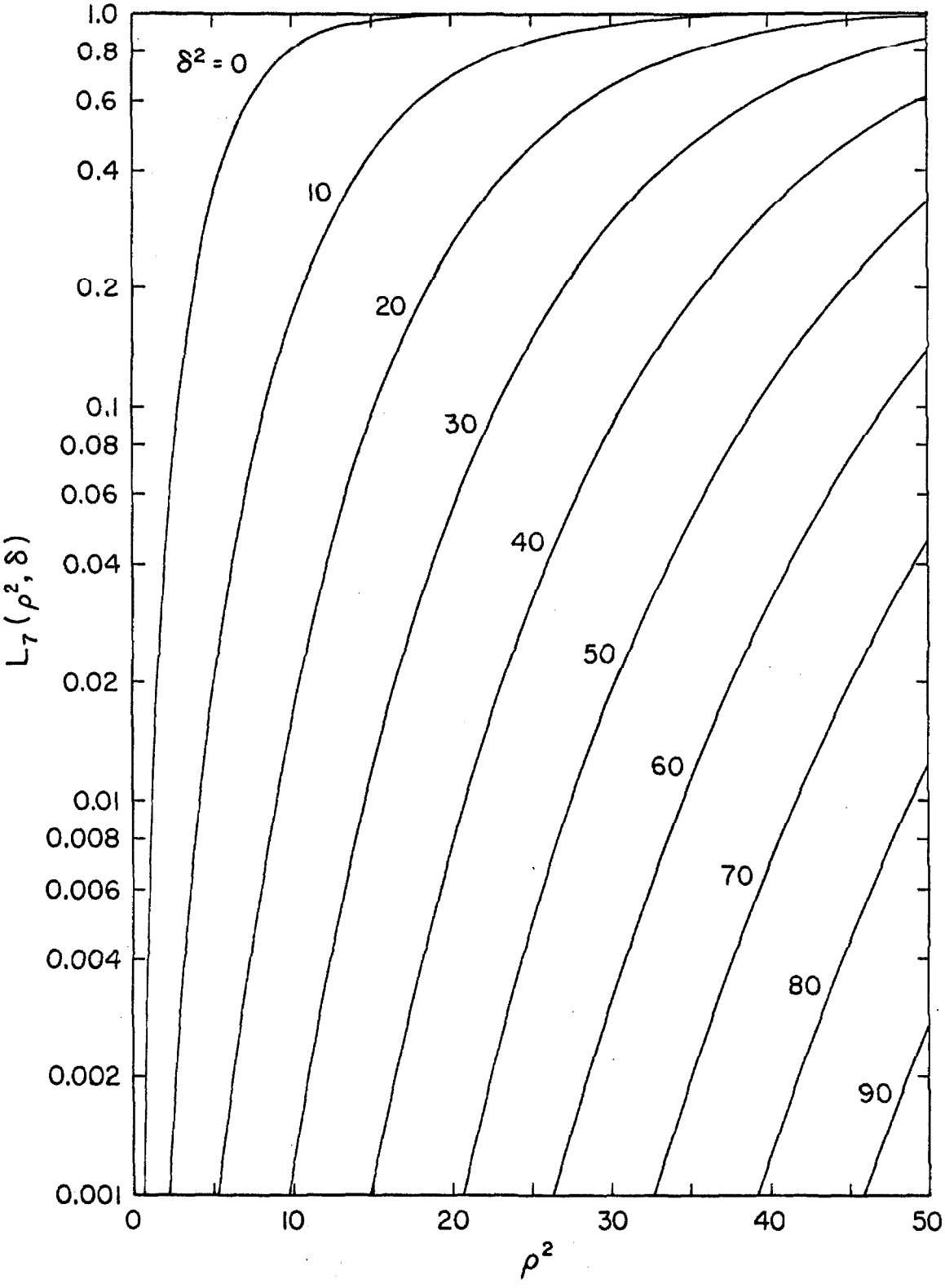

FIGURE 28. The Distribution Function $L_7(\rho^2, \delta)$.

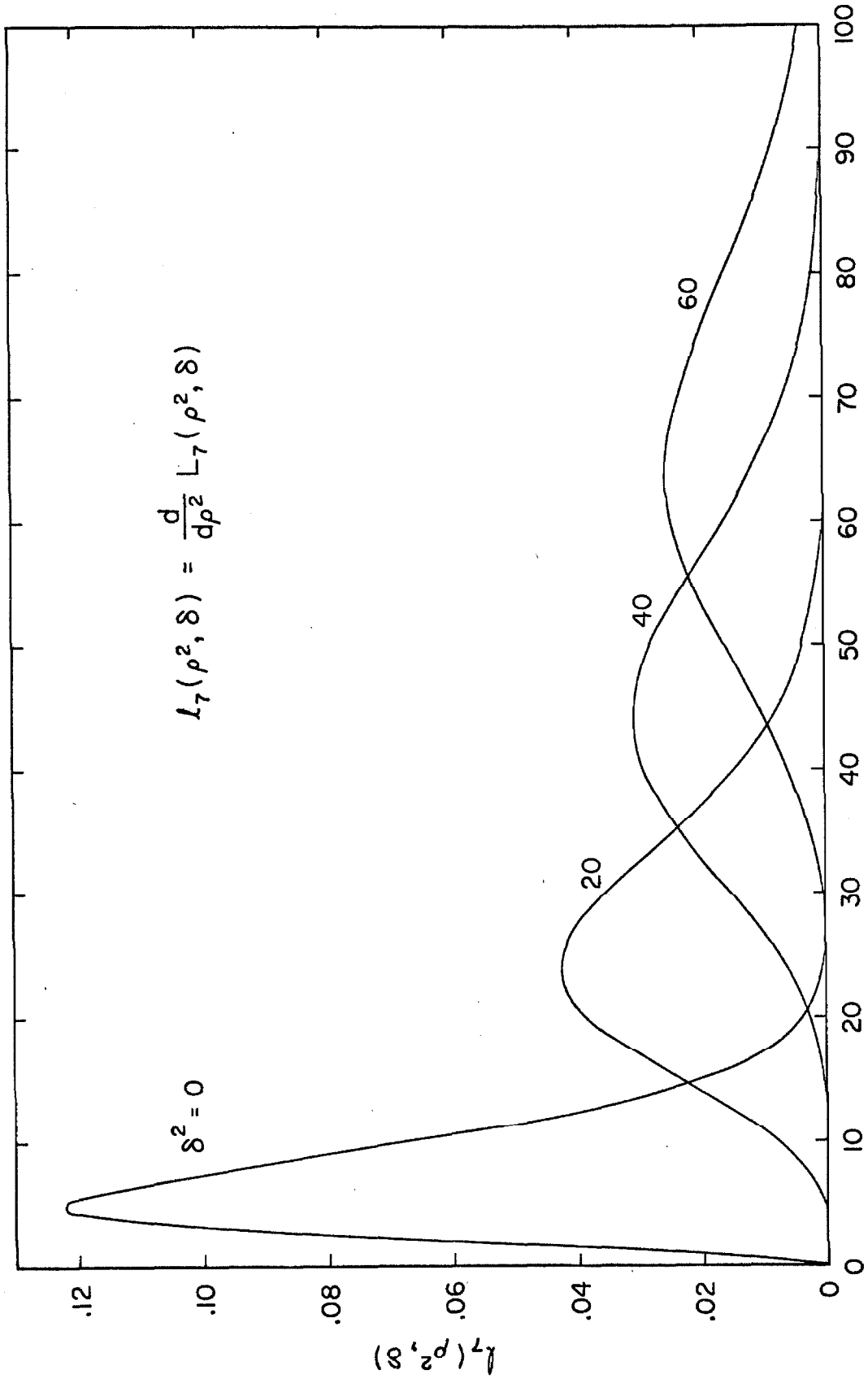

FIGURE 29. The Frequency Function for the Distribution $L_7(\rho^2, \delta)$.

Hence, the proton distribution has its mean at $S = 48$ and has standard deviation $\Delta S = 10.5$.

A bias of 25 in S is equivalent to a bias of 41 in ρ^2. From Figure 28, we then see that 0.4% of the protons lie in the region $0 < S < 25$. However, the dependence on δ^2 is quite strong. If the quantity $(L_{io}^{p} - L_{io}^{K})$ were in error by 10%, the proton acceptance would rise to 4%. Such an error corresponds to an underestimate of only 1.5 g/cm^2 in the range.

4.5 Range, Energy, and Light Output

4.5.1 Computational Procedure

The analysis programs required frequent access to the quantities L_o, $\frac{dL}{dx}$, R, and $\zeta = \frac{d}{dR}(\log \frac{dL}{dx})$. The arguments of these functions varied, but in addition to particle mass and counter thickness, any one of the first three could appear as an argument of the others. Therefore, the functions R/m, L/m, $\frac{dL}{dx}$, and $D = \frac{R}{m} \frac{d}{d(R/m)} \left(\frac{dL}{dx} \right)$ were tabulated over the useful range, and the functions required were obtained by interpolating and scaling. Tabulation intervals were approximately evenly spaced on a logarithmic scale, and a linear or quadratic Aitkins interpolation scheme was employed.

Since range-energy-light output tables for plastic scintillator ($C_1H_{1.10}$ for both Pilot B and NE-102) could not be found, integrations were performed to obtain the required tables. For the rate of energy loss, the formula given by Rossi[28] (2.5.7) was used.

Many investigators have observed that the light output of a scintillator is not proportional to the energy lost by a traversing particle, but that saturation effects occur at high rates of energy loss[31]. Birks[32] expresses the saturation in the form

$$\frac{dL}{dx} = \frac{A \frac{dE}{dx}}{1 + B \frac{dE}{dx}}$$

while Wright[33], using a different mechanism, derives the expression

$$\frac{dL}{dx} = \frac{C}{a} \ln \left(1 + a \frac{dE}{dx} \right) .$$

Here dL and dE are the light output and energy loss of a particle traversing dx of material. Experimentally, there is little reason to prefer one form over the other. We used the second, and followed the computational procedure of Gooding and Pugh[11].

Both Gooding and Pugh and Evans and Bellany[34] made measurements on NE-102 and obtained results which were well fit by

$$a = (0.025 \pm 0.002)(\text{MeV/g/cm}^2)^{-1} .$$

We therefore used this value. In the next section, we will present evidence that the saturation parameter $\underline{a}$ was actually about half this size for our sample of scintillator.

The two equations

$$\frac{dE}{dx} = f(\beta)$$

$$\frac{dL}{dx} = \frac{C}{a} \ell n \left(1 + a \frac{dE}{dx}\right) = g(\beta)$$

were treated as simultaneous and integrated by a Runge-Kutta method, using power law starting conditions. Following Sternheimer[35], the ionization constants

$$I_H = 1.40 \text{ Ry}$$

$$I_C = 5.74 \text{ Ry}$$

were used. Integrations for CH and Cu ($I_{Cu} = 27.7$ Ry) were also made for comparison purposes. The ranges calculated were about

2% higher than those obtained by Rich and Madey[36]. The results for Cu are very close to those published by Sternheimer in 1959[37], but a later erratum[38] reduces his results nearly to those of Rich and Madey report. We conclude that the tables of Rich and Madey are as accurate as any available, and that our integrations, while probably about 2% high, are about as accurate as the theory.

4.5.2 The Value of the Saturation Parameter a

The spectra observed in the three counters of the K^+ telescope stopping section were sensitive to the light output-energy loss relationship, and were used to obtain an estimate of the saturation parameter a. The data were not of such nature as to justify exhaustive fitting to the saturation models of various authors, but the "eyeball" fits obtained did preclude a nonlinearity as great as that reported in the literature.

Let us consider the spectrum N(L') observed in one of the counters, for instance δR2, when particles stop with a uniform range distribution in δR2 and δR3. We take the total light output L, the light output L' produced in δR2, and the rate of light output $\frac{dL}{dx}$, as functions of the particle's range x as measured from the front of δR2. The counter is of thickness t. Then for those particles which stop in δR2 ($x < t$)

$$L' = L(x)$$

$$N(L') = \frac{1}{\left.\frac{dL}{dx}\right|_{x(L)}}$$

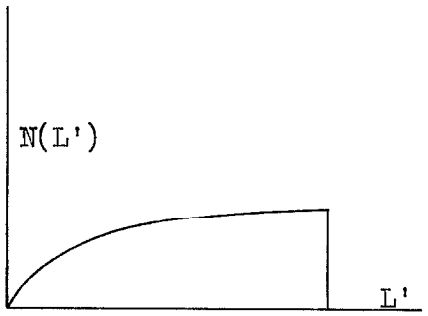

and for those particles which stop in $\delta R3$ $(t < x < 2t)$,

$$L' = L(x) - L(x - t)$$

$$N(L') = \frac{1}{\left.\frac{dL}{dx}\right|_{x(L)} - \left.\frac{dL}{dx}\right|_{x(L)-t}}$$

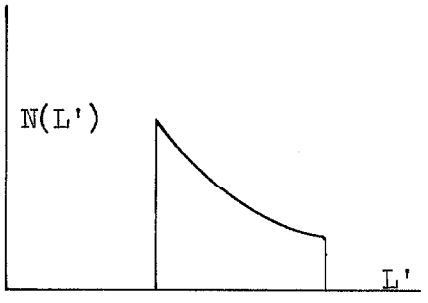

The net distribution is thus characterized by a sharp rise at light output

$$L_1 = L(2t) - L(t)$$

and a cutoff at

$$L_2 = L(t)$$

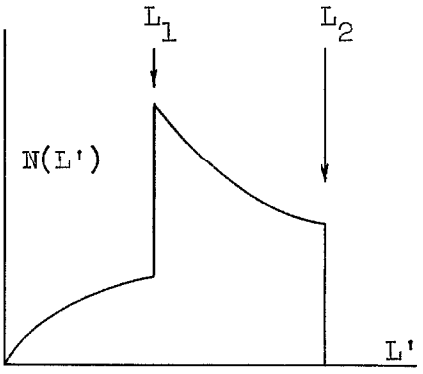

The ratio of the two break points in the spectrum, L_1/L_2, is independent of the counter gain, but it is sensitive to the saturation

parameter. In addition, the counter gain is independently known by the scheme discussed in section 2.9 of this thesis, so that L_1 and L_2 are known in absolute terms. L_2 is particularly sensitive to the saturation parameter, while L_1, by virtue of the calibration procedure, is nearly insensitive to it.

For comparison with experiment, the distribution function N(L) must be folded with the counter resolution function. A satisfactory fit to the data was obtained if this resolution function was taken as normal, with width proportional to the square root of the pulse height and equal to 12% of the pulse height at minimum ionization.

Experimental distributions for stopping protons were obtained by re-analyzing several of the 1100 MeV kaon runs to find the protons in the data. Runs were selected whose δR calibration data agreed to within 1.5%. The spectra for $\delta R1$, $\delta R2$, and $\delta R3$ are given in Figure 30.

The requirement that counter 12 not saturate the analyzer effectively placed a bias at about channel 30 in $\delta R1$. The large peaks near the origin in the $\delta R2$ and $\delta R3$ distributions are due to those particles which stopped in an earlier counter. (Channels 1 and 2 were zeroed before plotting.)

The statistical error in the calibration data is about 1.5%, but systematic errors, such as uncertainty in the position of the zero reference, could lead to errors as large as 5%. Since the protons used for calibration were about 3 times minimum ionizing in the stopping section, the calibration results depend upon $\underline{a}$. For later

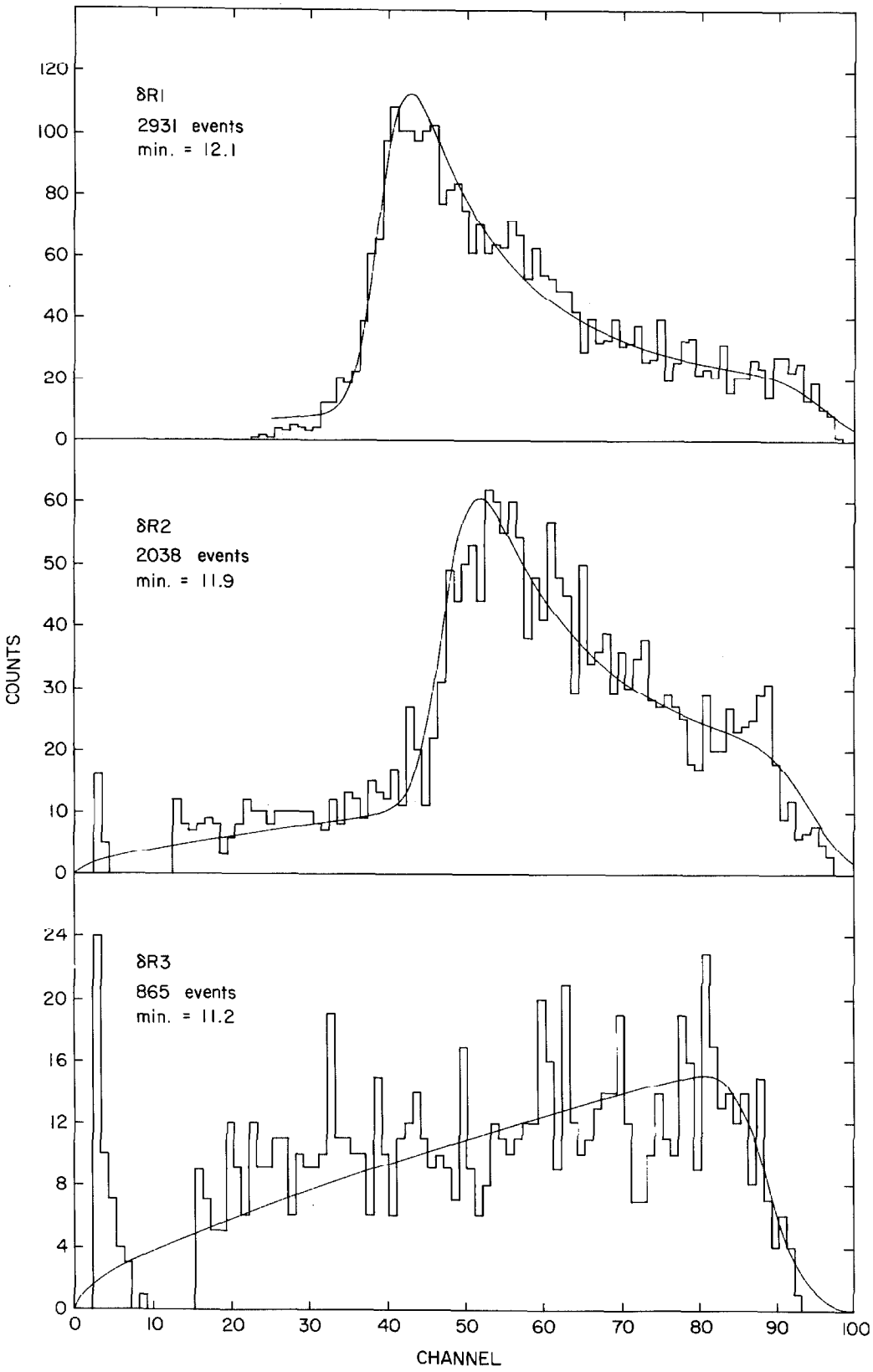

FIGURE 30. Proton Pulse Height Spectra in the δR Counters.

comparison with the gain required for a given fit, we list the calibration results obtained with different values of a in the table below. The data are expressed as the mean pulse height, in channels, to be expected of a minimum ionizing particle.

GAINS OF THE δR COUNTERS

	a =					
Ctr.	0.0	.007	.010	.015	0.02	.025
δR1	11.5	11.6	11.7	11.8	11.8	11.9
δR2	11.6	11.7	11.8	11.8	11.9	12.0
δR3	10.8	10.9	10.9	11.0	11.1	11.2

In Figure 31 are shown the results of four attempts to fit the δR2 data, with the gain in each case adjusted to give a decent fit at the spectrum cutoff. The $a = 0.007$ case gives the most reasonable fit to the calibration data, while the $a = 0.015$ case fits the spectrum best. This case would involve a 5% error in the calibration. Besides fitting the peak badly, the $a = 0.025$ case requires an 11% calibration error, which is unreasonable.

Similar results follow from the δR1 and δR3. Uncertainties in the data are such that a more detailed fit is not justified, but it is at least clear that a is in the range 0.007 - 0.015, with both 0.0 and 0.025 leading to very bad fits.

The smooth curves of Figure 30 are drawn for $a = 0.007$, with the gain in each case adjusted to give a reasonable looking overall fit.

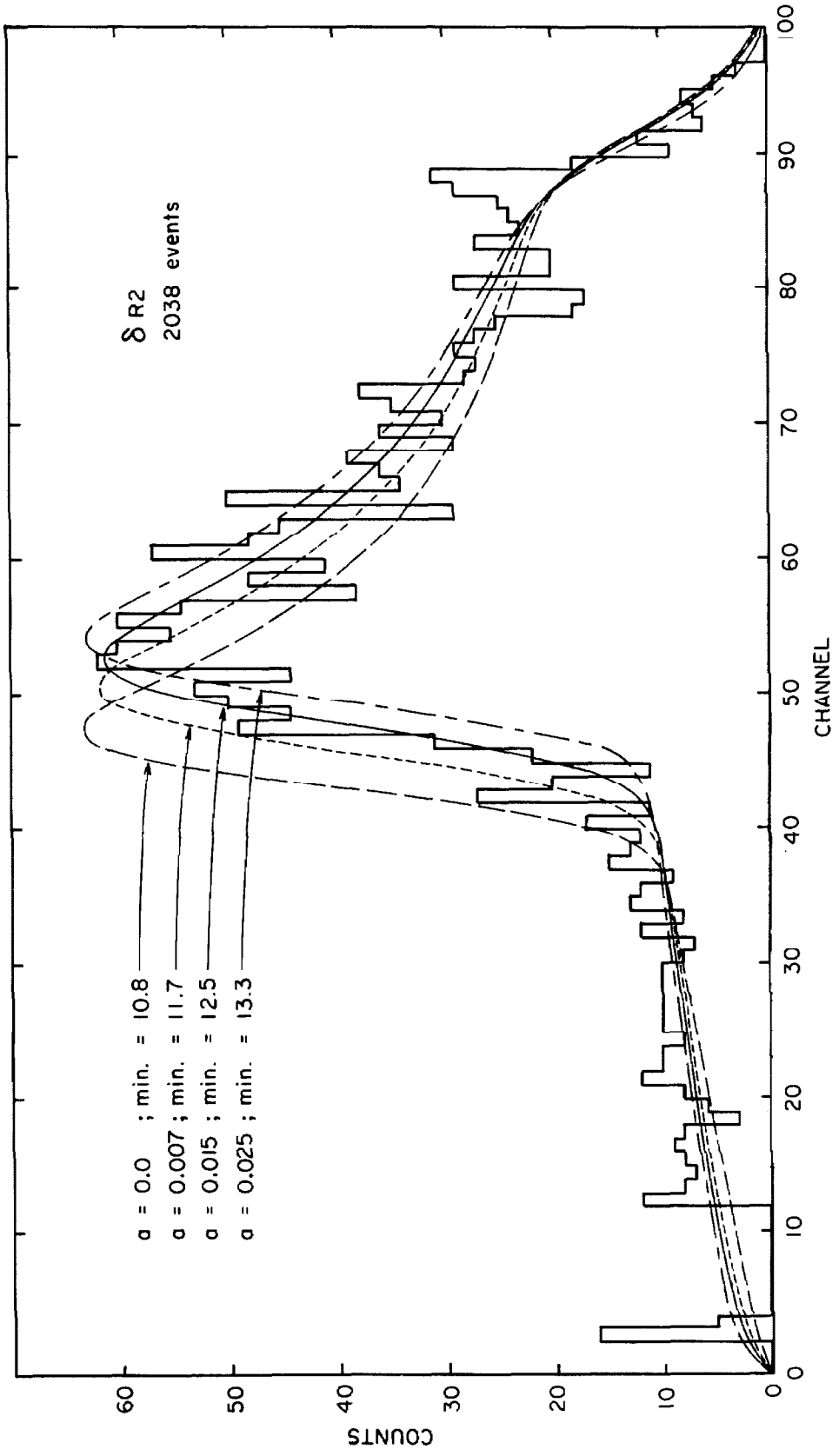

FIGURE 31. Fits with Different Values of the Saturation Parameter to the Proton Spectrum in δR2.

It should be emphasized that any phototube or other electronic saturation would produce exactly the opposite effect; we are observing a result more linear than expected.

We definitely observe a saturation effect in NE-102, but it is less extreme than that reported in the literature. The other experiments have been such that there is no reason to question them; perhaps we should instead question the uniformity of the scintillator plastic. Other properties, such as the light attenuation in the plastic, are known to vary considerably among different samples.

As was mentioned above, the value $\underline{a} = 0.025$ was used by the analysis program throughout this experiment. Because of an accident, the effect of this error is negligible. The range of the protons used for calibration was chosen, for different reasons, in such a way that the mean pulse height of calibration protons was nearly that of the data kaons in the front sections of the telescope. Hence, the saturation error cancels. In the stopping section, the effect is to yield higher values for the penetration depth δ than might otherwise be found. This is reflected in the occurrence of a large number of events in which δ is found to be an integral number of counter thicknesses. The error induced by this effect in the parameters S and U is unimportant.

4.6 Decay Particle Corrections and Side Counter Efficiency

4.6.1 Introduction

The use of a range telescope to define a K^+ beam was complicated by the fact that the stopped particles decay. The kaon lifetime is short enough that electronic rejection of pulses from the decay particles was difficult. Rather than to even attempt this, we chose to use an acceptance gate wide enough that most decay particle pulses were accepted.

A number of questions were then to be answered. One of these concerned the probability that the decay particle vetoed the event, either by going back into the system or by going through the end counter. (See Figure 3.) Related to this problem was that of computing the detection efficiency of the side counters. Another question concerned the effect of the decay particle on the pulse heights of the stopping section and the consequent effect on the goodness of fit criteria used by the analysis programs.

The proper way to solve these problems would be to do a detailed Monte Carlo calculation, choosing for each event not only an origin and direction for the decay, but also the time delay and the decay mode. However, the present problem hardly justified this treatment. As can be seen from Table 7, the kaon decayed in a two-body mode about 85% of the time. (The quantities h_i, g_i, and g_i' which are listed in this table are discussed later.) In this case, the charged particle was nearly minimum ionizing and had sufficient range to penetrate any counter near the stopping section. The pulse

TABLE 7

K^+ Decay Modes

Decay Mode	Branching Ratio (b_i)[14]	Energy of Charged Particle	Range in Scintillator	h_i	$g_i = h_i\, b_i$	g_i'
$K_{\mu 2} \rightarrow \mu^+ + \nu$	$(63.1 \pm 0.5)\%$	152.6 MeV	52 g/cm^2	1	0.631	0.565
$K_{\pi 2} \rightarrow \pi^+ + \pi^\circ$	21.5 ± 0.4	108.65	31	1	0.215	0.184
$K_{\mu 3} \rightarrow \mu^+ + \pi^\circ + \nu$	3.4 ± 0.2	0 - 134.1	0 - 47	$0.77 \pm .20$	$0.026 \pm .007$	0.021
$K_{e3} \rightarrow e^+ + \pi^\circ + \nu$	4.8 ± 0.2	0 - 228.0	> 25	1	0.048	0.043
$\tau^+ \rightarrow \pi^+ + \pi^+ + \pi^-$	5.5 ± 0.1	0 - 48.2	0 - 8.3	$0.53 \pm .25$	$0.029 \pm .014$	0.023
$\tau^{+\prime} \rightarrow \pi^+ + \pi^\circ + \pi^\circ$	1.7 ± 0.1	0 - 53.3	0 - 10.0	$0.12 \pm .06$	$0.002 \pm .001$	0.002

$\Sigma g_i = 0.951 \pm 0.016$

$\Sigma g_i' = 0.838$

height produced by such a particle was then proportional to the particle's path length in the counter. We have solved the problem in this more restricted form, and have used the results to estimate the results for the more general problem.

4.6.2 Detection and Side Counter Efficiencies for Minimum Ionizing Particles

Computer-generated particles were permitted to decay in random directions from random positions in the volume defined by the shadow of the aperture counter in the stopping section. An event was vetoed if the decay particle intersected the end counter, counter 11, or counter 12 (aperture). Barring a veto, the path lengths intersecting all counters hit were "pulse height analyzed." The total path length in all δR counters was also "pulse height analyzed," as was the penetration depth distribution. The calculation was done for 30,000 events.

Penetration depth and stopping section path length distributions are illustrated in Figure 32. The shape of the penetration depth spectrum is due to the higher veto probability of a kaon decaying near the front or back of the stopping section. It is sufficiently flat that we have made no corrections to the energy resolution function for this effect.

For these events, the overall detection efficiency was

$$E = 0.6258 \pm 0.0028$$

while side counter pulses were present in a fraction

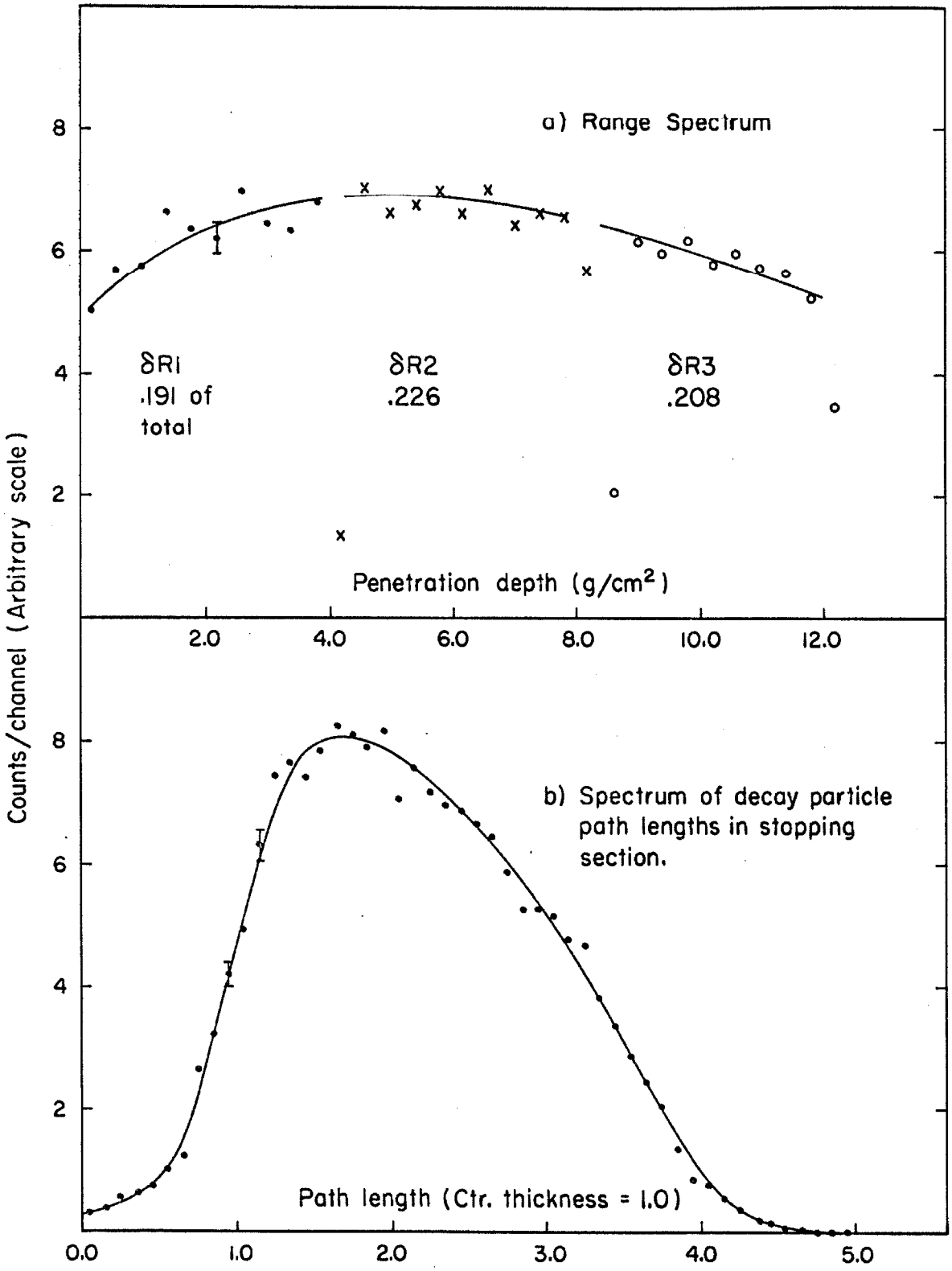

FIGURE 32. Range and Decay Particle Path Length Spectra for Non-Vetoed Monte Carlo Events.

$$E_s = 0.3018 \pm 0.0027$$

of the events.

4.6.3 Tests of the Analysis Program

Modifications of the program were used to generate entire particle-like events, which in turn were used to study the operation of the analysis program. Kaons which stopped and decayed with the emission of a minimum ionizing particle, kaons which stopped without decaying, and stopping protons and pions were generated. Pulse heights were generated for all counters, using the 1200 MeV configuration of the telescope. Contributions from decay particles were added where relevant. The pulses were then "randomized" by replacing each pulse height L_i by a number chosen from the set normal $(L_i, 0.12\sqrt{L_i})$. Since the analysis program could not distinguish these events from real events, we concluded that both the analysis program and the Monte Carlo program were working properly.

Several results of the analysis of these events have been discussed in section 3. Other results are listed in Table 8. The most striking feature is the frequent saturation of the pulse height analyzer by counter 12. For historical reasons, no absorber was placed between counter 12 and δR1; particles of small range in δR1 could therefore saturate counter 12. The cross section data have been corrected for this effect on the basis of a more careful calculation of its size. The other entries under "rejected events" reflect legitimate analysis program inefficiencies. The efficiencies k_I and k_O (for

TABLE 8

Summary of Analysis of Monte Carlo Events

	Decay particle present	Decay particle not present
Number of kaons	2400	300
Number not vetoed by decay particles	1484	300
Number not rejected by analysis program	1376	284
Rejected events	108	16
Ctr. 12 saturated[(a)]	78	15
δR ctr. saturated	14	0
Side ctr. saturated	5	0
$1-\delta > 0.35$[(b)]	5	0
$U > 2.0$	4	1
$S > 25.0$	2	0
Total, other than ctr. 12 saturated	30	0
Efficiency, neglecting losses due to ctr. 12 saturation	$k_I = 0.980 \pm .004$	$k_0 = 0.997 \pm .003$

(a) The pulse height was sufficiently large that the pulse height analyzer was saturated.

(b) A rough event preselection was made by requiring

$$\left|\frac{L_i - L_{io}}{L_{io}}\right| \leq 0.35$$

in the front section, where the L_{io} were computed under the assumption that the particle stopped in the last counter to show a pulse. Kaon loss could occasionally occur if the kaon stopped in δR1 but the decay particle gave pulses in δR2 and δR3, so that an incorrect set of L_{io} were used.

kaons decaying inside and outside of the linear gate, respectively) are incorporated into an overall efficiency in the next section.

The analysis program imposed an upper limit of 3.5 times minimum ionization in one δR counter and 4.0 minimum in all δR counters for the contribution of a decay particle. From our calculation, we obtained

Total contribution	≥ 4.0	1.18% of accepted events
Single Counter Contribution	≥ 3.5	2.13% of accepted tries.

The fact that the pion from the $K_{\pi 2}$ mode is perhaps 1.2 minimum ionizing would raise these numbers somewhat, as would the τ decay. But usually the effect of the restriction upon these extreme events would be to somewhat increase the range calculated by the program, which probably would not cause the event to be lost.

4.6.4 Efficiency for Detecting Real Kaons

We are now in a position to use the results of section 4.6.2 to calculate a realistic decay particle correction to the telescope detection efficiency.

The counters involved were gated on for a time T after the kaon pulse, and this number is known to within δT. Then a fraction

$$f = 1 - e^{-T/\tau \pm \delta T/\tau}$$

decay inside the gate, where $\tau = 12.5$ ns., the kaon lifetime. Gates were set so that $T = 20$ ns. $\pm$ 5 ns., giving us

$$f = 0.80 \pm 0.04 .$$

Of the kaons decaying inside the gate, a fraction g decay in such a way that the decay particles can leave the stopping section. Of these, a fraction E escape electronic veto and are accepted by the analysis program with an efficiency k_I. This group of particles is thus detected with an efficiency $k_I f g E$. Similarly, a fraction $(1 - g)$ of those decaying inside the gate do not produce decay particles which leave the stopping section. The analysis program efficiency for such events should also be close to k_I, for a net detection efficiency of $k_I f(1 - g)$. Finally, $(1 - f)$ of the events decay after the gate has closed and pass the analysis program with an efficiency k_O. Combining all of these possibilities, we obtain

$$e = k_O(1 - f) + k_I f((1 - g) + E g)$$

for the kaon detection efficiency.

By a similar argument, we may calculate the side counter efficiency. A fraction f of the particles decay inside the gate; of these, a fraction E_s produce particles heading for a side counter, and of these, a fraction g' are of the proper energy and direction to be accepted by the side counter. Finally, such events are accepted by the analysis program with efficiency k_I. We thus obtain

$$e_s = k_I f g' E_s .$$

There remains only the problem of computing g and g'. We may write

$$g = \sum b_i h_i$$

where b_i is the fraction decaying in the i^{th} mode, and h_i is the fraction which escapes the stopping section. This assumes an isotropic distribution from the stopping section, which is not the case for low energy particles. However, the contribution to g is so small in these cases that a large error in h_i is relatively unimportant. In fact, we take the length distribution of particles escaping from the stopping sections as that given by Figure 32b, even though particles destined for veto have a somewhat different distribution.

In Figure 32b, 1.0 counter thicknesses = 3.92 g/cm^2 of plastic scintillator. Thus, from Table 7 we see that for the $K_{\mu 2}$ and $K_{\pi 2}$ modes, $h_i = 1.00$. From phase space considerations[39], we find that about 98% of the electrons from the K_{e3} mode escape the stopping section, so we may take $h_{e3} = 1.0$ also.

The $K_{\tau+}$, $K_{\tau+'}$, and $K_{\mu 3}$ cases are more difficult. Let P(R) be the probability distribution in range for the charged decay particles, and let F(R) be the frequency distribution in range as given in Figure 32b. Then

$$h_i \approx \int P(R)\, F(R)\, dR .$$

P(R) was taken from a phase space calculation[39] for the $K_{\mu 3}$ case and from experimental distributions for the $K_{\tau+}$[40] and $K_{\tau+'}$[41] cases. By doing very rough hand integrations, we obtain

$$h_{\mu 3} = 0.77 \pm 25\%$$

$$h_{\tau +'} = 0.12 \pm 50\% ,$$

where the errors reflect a pessimistic guess as to the badness of the isotropy assumption.

The $\tau +$ case is confused by the fact that if one charged particle does not escape, another one might. We roughly correct for this by multiplying $\int P(R)\, F(R)\, R\, dr$ by 3. This gives

$$h_{\tau +} = 3(0.175) = 0.53 \pm 0.25 .$$

The above results are summarized in Table 7. The final result is

$$g = 0.95 \pm 0.02 .$$

The calculation of g' for the side counter efficiency case is identical except for the added complication that pulse height windows were set on these counters. Side counter pulses were counted only if the pulse height fell between 0.65 and 2.1 times minimum ionizing. The Monte Carlo program gave us the expected pulse height spectra in these counters for the minimum ionization case; 0.896 fell within the window. Thus,

$$g_{\mu 2}' = g_{\mu 2} \cdot 0.896$$

$$g_{e3}' = g_{e3} \cdot 0.896 .$$

Similarly, about 0.85 of the pions from the $K_{\pi 2}$ mode fall within the window, and for the remaining modes the figure is about 0.8. We then calculate

$$g' = 0.84 .$$

Finally assembling all of this, we obtain

$$e = 0.716 \pm 0.016$$

$$e_s = 0.198 \pm 0.013 .$$

The number which is really measured, of course, is the ratio

$$e_s' = e_s/e = 0.278 \pm 0.023 .$$

The uncertainty δT is the largest contribution to the error in these results.

4.7 Programs

4.7.1 Introduction

The most severe limitations on program organization were imposed by the generality of the input data format and by the fact that the Burroughs 220 memory consists of only 5000 words. (A word is 10 BCD characters plus an 11^{th} which is normally interpreted as a sign.) Data strings usually consisted of about 10,000 words, and the programs as they appeared in their final form totaled about 7000 words. The primary input was paper tape. The procedure adopted to bypass the memory length difficulties was to read in everything from paper tape and write it onto magnetic tape, at the same time building a dictionary of control words found in the input string so that random recall was possible. A given analysis function was performed by a subprogram which occupied memory only while it was in use.

A governor program, designed to facilitate these manipulations, occupied the first 2200 words of memory. It contained the input-output buffering mechanisms, format routines, and service routines. Much of it was modeled after the system routine organization provided for the larger computers by systems such as FORTRAN.

Since it was anticipated that the experimenter would operate the computer, programs were designed to leave many subjective decisions to him. There were a great many programmed halts, at which the operator was to make an entry into a register or set a switch before proceeding. The system was made as "idiot proof" as possible by providing that if the operator or the data did something nonsensical the program would return to the halt after printing a

diagnostic message. The operator could also interrupt the program by setting switches. These program control switches (PCS) were interrogated by commands; the program would continue or branch, depending upon the result.

The subprograms which proved to be useful were Pulse Height Print, Kicksort, Calibrate, and K Analysis. Pulse Height Print simply printed out specified input data event by event, and was for the most part useful in understanding strange effects. The others will be discussed in the following sections.

A numeric assembler[42] written by L. J. Fretwell permitted the programmer to use floating address and to insert, delete, and modify commands. It was an invaluable aid in terms of programming time and convenience.

4.7.2 Data Format

The pulse height analyzer[10] accepted up to 25 pulse heights ("analog inputs"), each of which resulted in a two digit BCD number (aa). One pulse height input was grounded so that the zero offset zz could also be recorded. Alternatively, a two-digit position in the pulse height analyzer's memory could be treated as eight bits which could be set, e.g., by coincidence circuit outputs. Let d be a digit used in this "digital input" mode. The output consisted of from one to five words in Burroughs 220 format, which could either be punched onto paper tape or transmitted via a direct data link to the computer.

To make things definite, the event format

$$4\ (aa)_1(aa)_2(aa)_3(aa)_4(aa)_5$$
$$0\ (aa)_6\ .\ .\ .$$
$$.$$
$$.$$
$$.$$
$$0\ .\ .\ .\ (aa)_n\ zz\ d_1d_2d_3\ .\ .\ .$$

was chosen. The first word of the event had a 4 in the sign position; the others, zero. The number of analog and digital inputs present were specified in a control word which prefaced the unit of data. This word also contained digits which specified the run and data unit within the run.

4.7.3 The Governor Program

The governor program was read into memory either from paper tape or from the system library, where it was filed. Its operation is outlined in Figure 33.

In the first phase of normal operation, the data and program were written onto magnetic tape and a dictionary compiled. Normally, PCS 1, 2, 3, 6, and 7 were in the off (F) position. After the appropriate initialization of memory, magnetic tape was prepared and the subprograms copied onto it, again either from paper tape or from the system library. The subprogram material included tables describing the telescope configuration which would be required in the analysis. Control words and the corresponding tape addresses were filed in a dictionary. Then data was read into a buffer 90 words at a

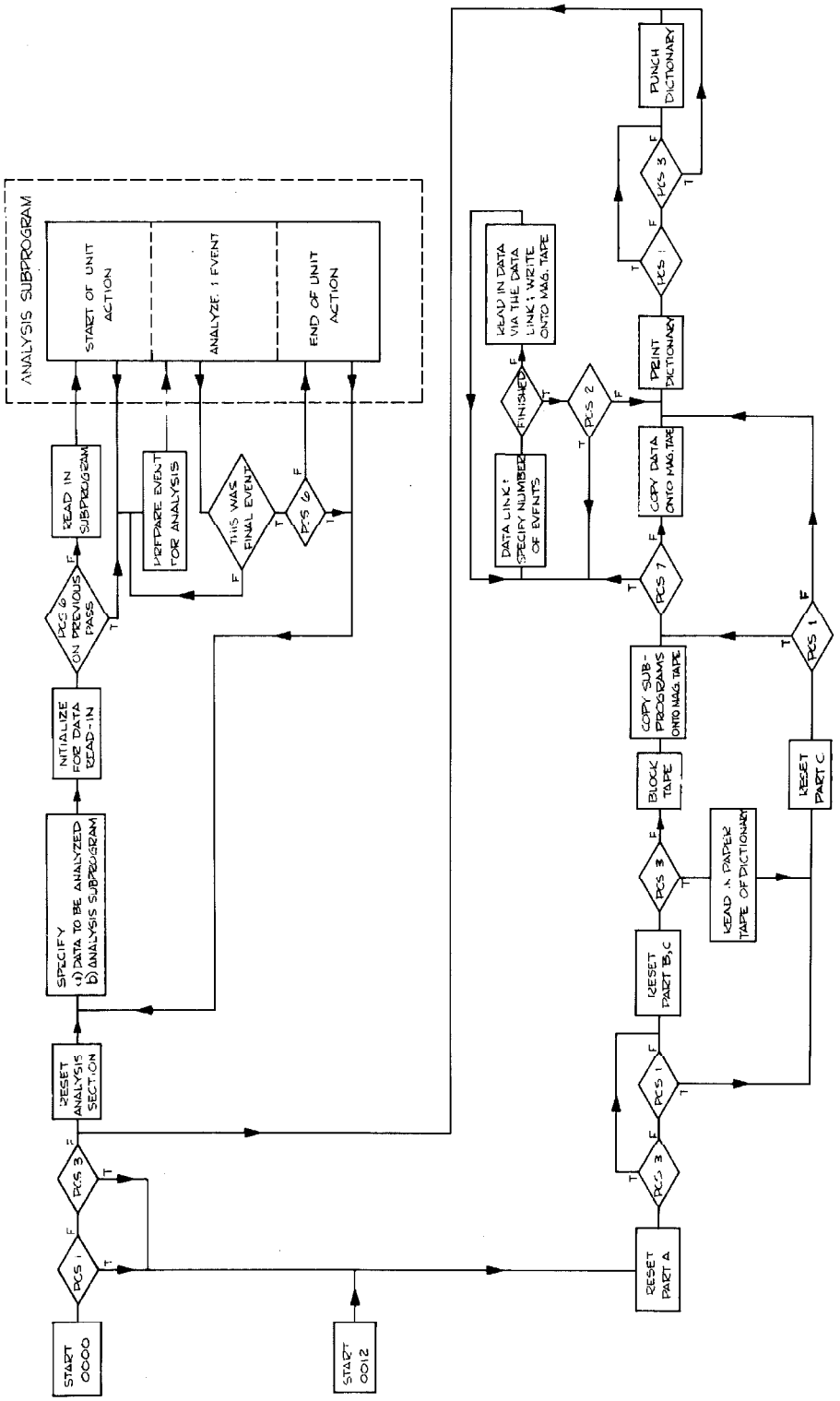

FIGURE 33. Flow Diagram of the Governor Program.

time, inspected for errors and control words, and written onto tape. The procedure was interrupted by a control word at the end of a reel of tape; another reel could be loaded or the read-in procedure terminated. When this occurred, the dictionary was printed and punched and control was transferred to the analysis mode.

If PCS 7 were true, data was received over a data link instead of being read from paper tape. The operator specified the number of events desired, and the system was sensitive until that number had been received or the experimenter transmitted a terminating control word. No external interrupt signal could be accepted by the computer; nor could it warn the pulse height analyzer to "hold" when it could no longer accept data. Thus, no computing during data reception was possible. These hardware restrictions made it impossible to use the computer in any truly "on-line" sense. The data link mode of operation was occasionally used for calibration data, but for the most part it was not useful.

In the analysis phase of operation, the computer halted for instructions after the necessary initialization. The operator specified the data unit to be analyzed, the subprogram to be used, the mode of the subprogram if more than one existed, and, if desired, which events within the data unit were to be analyzed.

The analysis program was called from magnetic tape if it was not already in memory, and control was transferred to it for initialization. Then a section of the specified data was read into a buffer. An event was "unpacked"; i. e. from each two digit input aa the zero

reference zz was subtracted, and the resulting number converted to a floating point word. The digital inputs were converted to binary. Control was transferred to the analysis program so that it could process the event. Upon return of control, the governor program unpacked the next event, and so on, until the specified data had been analyzed. Then control was returned to the analysis program for whatever final data reduction or printout was necessary.

Several units of data could be analyzed as one, if desired, by setting PCS 6 true before or during analysis.

Even after terminating the read-in phase and doing part of the analysis, more data could be accepted. PCS 1 was set true and the program started. The read-in proceeded as before except that certain parts of the initialization were bypassed.

By mischance or design, the dictionary of tape locations was often destroyed. In this case, the paper tape version could be read in and the previous state reconstructed. PCS 3 controlled this logic.

The tape write, tape read, and input-output portions of the program were also available to the analysis subprograms as subroutines.

4.7.4 Kicksort

This routine enabled the apparatus to be used as up to 25 independent 100 channel pulse height analyzers. To each possible number for each input was assigned a cell of memory; when this number occurred the contents of the cell were incremented. After analyzing all events in this way, the accumulated pulse height spectra were

printed. Alternatively, they could be plotted by means of an on-line Moseley plotter. Examples of the plotter output are given in Figures 30 and 31.

4.7.5 Calibrate

The technique used to calibrate the counters of the telescope has been discussed in section 2.9; it was applied in a completely straightforward way. Most of the complications of the calibration program had to do with the many possibilities open to the operator at the conclusion of the analysis.

The tables describing the telescope which were available to the program listed the range from the front of each counter to the front of the stopping section, the thickness of each counter, the nominal calibration for each counter, the number of counters to be taken for the front section, and the range from the front of the stopping section to the center of the calibration section. In the subprogram initialization procedure, a table of expected proton pulse heights was constructed using these data and with the aid of the range-energy routines discussed in section 4.5. As everywhere in the analysis, the calibration of a counter was stated as the mean pulse height, in channels, produced by a minimum ionizing particle.

Results were printed out at the conclusion of the analysis. These included the mean, r.m.s. deviation, and skewness for the data of each counter, and the r.m.s. deviation $\underline{e}$ of the means found for the front section counters from the assumed means. In addition,

the table of means was prefaced by two control words and written onto magnetic tape. There was opportunity for the operator to flag one of the control words if $\underline{e}$ was large enough that the results should not be considered final.

The quantity $\underline{e}$ was related to the δ introduced in section 4.4. For large $\underline{e}$ the proton acceptance efficiency was reduced; moreover, a biased sample of protons was lost. Application of the results of section 4.4 to this problem showed that $\underline{e}$ should be less than about 3% for the selection of an unbiased proton sample. If this was not the case, the control word was flagged and the analysis of the data repeated. On this pass, the results of the previous pass were used as the nominal means. The process converged in two or three iterations.

An example of the procedure is given in Table 9. The first iteration gave agreement with the assumed means to within 4%. In the next iteration a few more events were used and the agreement with the previous set was within 0.4%.

The skewness served chiefly as a measure of the number of strange events present. For example, the skewness listed for counter 12 in the table indicates one or two events with very small pulse heights, which in turn explains the large result for the width.

After all the units of calibration data for a given run were analyzed, the program formed the weighted average of their final results. The operator had control over whether or not a given set was included. The combined result was recorded on magnetic tape for use by the K analysis program and, at the operator's option,

TABLE 9

Example of Proton Calibration Results (Unit 064 0059)

Counter	$L_o(m_K)$[a]	$L_c(m_p)$[b]	0th[c,d] iteration	1st[d] iteration	2nd[d] iteration	σ/L[e]	μ[f]
1	1.46	1.61	36.00	36.60	36.61	9.37	.06
2	1.49	1.63	36.00	33.91	33.66	10.48	.39
3	1.53	1.66	36.00	38.14	38.36	8.80	.15
4	1.57	1.70	36.00	36.73	36.75	8.74	.38
5	1.65	1.75	36.00	33.49	33.42	8.65	.17
6	1.72	1.80	36.00	35.81	35.88	8.80	.06
7	1.80	1.85	30.00	30.91	31.04	8.98	.17
8	1.90	1.91	30.00	30.60	30.66	9.32	.12
9	2.18	2.04	30.00	30.99	31.03	6.75	-.10
10	2.32	2.09	20.00	21.77	21.81	8.69	-.03
11	2.50	2.14	20.00	23.41	23.43	9.30	.09
12	2.75	2.21	20.00	21.48	21.50	12.34	-3.92
δR1	3.49	2.31	12.00	11.72	11.73	7.94	.10
δR2	3.52	2.50	12.00	12.00	12.01	7.83	.08
δR3	- -	2.76	12.00	12.59	12.62	10.12	-.14
E	- -	3.01	25.00	25.54	25.58	9.63	.03
L	- -	1.54	40.00	49.56	49.50	19.45	-2.02
R	- -	1.55	40.00	38.06	38.04	20.52	-.35

Events satisfying proton criteria	117	122
r.m.s. deviation from previous iteration (for first 8 counters)	4.15%	0.36%

Total events recorded -- 268

(a) Kaons stopping in center of δR2. L_o = 1.00 at minimum ionization.

(b) Protons stopping between Cal.1 and Cal.2. L_o = 1.00 at minimum ionization.

(c) Input data.

(d) Reduced to mean pulse height expected of minimum ionizing particle.

(e) Standard deviation divided by the mean, in per cent.

(f) Third moment about the mean divided by the cube of the standard deviation.

punched onto paper tape. This tape could be spliced into the data tape so that if the data were re-analyzed at a later time the calibration stage could be deleted.

4.7.6 K Analysis

The selection techniques used by this program have been discussed in sections 2.7 and 2.8. The full-blown procedure took about 12 seconds per event. So to save time, the final version of the program did a fair amount of preselection. Most events could be rejected as uninteresting after a cursory inspection.

The selection proceeded in several steps, as follows:

a) An event was rejected if some pulse height saturated the analyzer (pulse height = 99).

b) A rough range was estimated as the range to the center of the last stopping counter to show a pulse. Expected mean pulse heights L_{io} for this range and a kaon mass were available from a table constructed during the initialization phase. An event was rejected if

$$\left| \frac{L_i - L_{io}}{L_{io}} \right| \geq 0.35$$

for some counter in the front section or if S as computed under this range hypothesis exceeded 40.

c) U_K was then calculated, and the event rejected for $U_K \geq 8$.

d) S_K was calculated. The event was rejected for $S_K \geq 25$. If a plot was specified when the subprogram was called, a point was added to the dot plot of U_K vs. S_K. Examples of this plotter output have been given in Figures 9, 10, 14, and 15.

e) If $U_K < 2$, the event was kept as a probable kaon. The event's contribution was added to an accumulating S spectrum such as those of Figure 12. Separate spectra were accumulated for Λ decay telescope logics $A\overline{B}$ and $\overline{A}B$ and for the combinations $A\overline{B}$ and $\overline{A}B$ with a telescope side counter pulse also present.

f) If the event was not rejected because of a saturated counter, an attempt was also made to fit it with a proton hypothesis. It was first checked as in b) above, except that a proton mass was assumed. It was kept if $U_p < 2$, and still kept if $S_p < 25$. If it satisfied all of these requirements, its contribution was added to one of two S spectra, depending upon whether the decay proton telescope logic $A\overline{B}$ or $\overline{A}B$ was satisfied.

g) If the kaon logic was satisfied, information about the event (event number, penetration depth hypothesis best fitted, U, etc.) was printed. In addition, data about the proton fit was printed if the event had also satisfied the proton logic.

Somewhere in this procedure, a tally was incremented to indicate the event's disposition by the program. At the conclusion of the analysis of a unit, these tallies were printed, as were the S spectra.

A paper tape of the S spectra was punched. Later, this tape was converted to cards so that the data of this unit could be combined with other data by an IBM 7094 program.

5 REFERENCES

1. P. L. Donoho and R. L. Walker, Phys. Rev. 112, 981 (1958); B. D. McDaniel, A. Silverman, R. R. Wilson, and G. Cortellessa, Phys. Rev. 115, 1039 (1959).

2. H. M. Brody, A. M. Wetherell, and R. L. Walker, Phys. Rev. 119, 1710 (1960).

3. R. L. Anderson, E. Gabathuler, D. Jones, B. D. McDaniel, and A. J. Sadoff, Phys. Rev. Letters 9, 131 (1962).

4. A. J. Sadoff, R. L. Anderson, E. Gabathuler, and D. Jones, Bull. Am. Phys. Soc. 9, 34 (1964).

5. C. W. Peck, Phys. Rev. 135, B830 (1964).

6. C. W. Peck, Ph. D. Thesis, California Institute of Technology (1964).

7. Although the linear dependence of the total cross section upon momentum is mentioned in many of the papers (1 - 5), it is explicitly demonstrated nowhere. For an s and p wave mixture, it is equivalent to the similar statement for the differential cross section data at 90°, given in ref. 3. The total cross sections are illustrated in Figure 11 of reference 6.

8. J. H. Marshall III, Ph. D. Thesis, California Institute of Technology (1965).

9. For the particular instrumentation used, see A. Barna, J. H. Marshall, and D. F. Torzewski, Rev. Sci. Instr. 36, 1666 (1965).

10. D. E. Groom and J. H. Marshall, Rev. Sci. Instr. 33, 1249 (1962).

11. T. J. Gooding and H. G. Pugh, Nuc. Instr. and Methods 7, 189 (1960).

12. K. R. Symon, Ph. D. Thesis, Harvard University (1948). The useful data is also given in reference 28.

13. J. H. Cronin and O. E. Overseth, Phys. Rev. 129, 1795 (1963).

14. A. H. Rosenfeld, A. Barbaro-Galtieri, W. H. Barkas, P. L. Bastien, J. Kirz, M. Roos, Rev. Mod. Phys. 36, 977 (1964).

15. W. C. Kaiser and J. A. M. deVilliers, I. E. E. E. Transactions on Nuclear Science, NS-11, 29 (1964)

16. B. J. Moyer, Rev. Mod. Phys. 33, 367 (1961).

17. G. T. Hoff, Phys. Rev. Letters 12, 652 (1964).

18. T. P. Wangler, A. R. Erwin, and W. D. Walker, Phys. Rev. 137, B414 (1965).

19. B. D. McDaniel, private communication.

20. T. K. Kuo, Phys. Rev. 129, 2264 (1963).

21. N. A. Beauchamp and W. G. Holladay, Phys. Rev. 131, 2719 (1963).

22. S. Hatsukade and H. J. Schnitzer, Phys. Rev. 128, 468 (1962), and Phys. Rev. 132, 1301 (1963).

23. Fayyazuddin, Phys. Rev. 123, 1882 (1961), and Phys. Rev. 134, B182 (1964).

24. M. Gourdin and J. Dufour, Nuovo Cimento 27, 1410 (1963), and J. Dufour, Nuovo Cimento 34, 645 (1964).

25. A. Kanazawa, Phys. Rev. 123, 993 (1961). See also G. T. Hoff, Phys. Rev. 131, 1302 (1963).

26. M. Rimpault, Nuovo Cimento 31, 56 (1964).

27. J. Dufour, private communication.

28. B. Rossi, High Energy Particles, Prentice-Hall, 1952.

29. Marshall P. Ernstene, Ph. D. Thesis, California Institute of Technology, 1959.

30. H. Cramér, Mathematical Methods of Statistics, Princeton University Press, 1958.

31. R. D. Brooks, Progress in Nuclear Physics, Vol. 5 (Pergamon Press, 1956) 252. On pages 267 ff. are discussed most references to that date.

32. J. B. Birks, Proc. Phys. Soc. A 64, 874 (1951).

33. G. T. Wright, Phys. Rev. 91, 1282 (1953).

34. H. C. Evans and E. H. Bellamy, Proc. Phys. Soc. 74, 212 (1959).

35. R. M. Sternheimer, Phys. Rev. 103, 511 (1956).

36. M. Rich and R. Madey, UCRL 2301 (1954). Reissued in 1960.

37. R. M. Sternheimer, Phys. Rev. 115, 137 (1959).

38. R. M. Sternheimer, Phys. Rev. 124, 2051 (1961).

39. California Institute of Technology, Synchrotron Laboratory unpublished curves SL-498 and SL-502, 1961.

40. S. McKenna, S. Natali, M. O. Connell, J. Tietge, and N. C. Varshneva, Nuovo Cimento 10, 763 (1958).

41. G. Gaicomelli, D. Monti, G. Quareni, A. Quareni-Vignudelli, W. Puschel, and J. Tietge, Physics Letters 3, 346 (1963).

42. L. J. Fretwell, Burroughs 220 Assembler II, November 1963 (revised edition), California Institute of Technology, unpublished.